THE DESIGN, MANUFACTURE AND VERIFICATION OF A HIGH CAPACITY FORCE AND MOMENT MEASUREMENT SYSTEM

JOHN R. TUCKER

The Design, Manufacture and Verification of a High Capacity Force and Moment Measurement System

By

John R. Tucker. P.Eng.

A thesis submitted to the school of Graduate

Studies in partial fulfillment of the

requirements for the degree of

Master of Engineering

Faculty of Engineering and Applied Science

Memorial University of Newfoundland

August 1998

St. John's Newfoundland

ABSTRACT

A series of tests was conducted to study the interaction of a multifaceted conical structure with multi-year ridges. The tests were conducted in three phases, one in Calgary, Alberta, one in Ottawa, Ontario, and the third at the Institute for Marine Dynamics in St. John's, Newfoundland. The St. John's phase of the program tested some of the largest ice features ever attempted at this facility, including an attempt at a one in one hundred year consolidated multi-year ridge. This thesis documents the design, manufacture and testing of the force and moment measurement system developed for use in the St. John's tests. A series of calibration tests were conducted in the Structures Laboratory of The Faculty of Engineering in which the global force measurement system was secured to the floor, and loads of known magnitude and direction were applied using a hydraulic ram with an in-line force transducer installed. Fourteen different orientations were tested and a fifteenth test was conducted in which one half of the loading system was chilled using ice to simulate the condition of having half of the force measurement system submerged in the IMD ice tank. Following this series of calibration tests, the equipment was taken to the Institute for Marine Dynamics and installed. Calibration tests were conducted there to verify the integrity of the force and moment measurement system, and a series of dynamic 'pluck' tests were carried out to determine the natural frequencies of the towing system and model. In this thesis, the results of these pluck tests are compared to the frequency of the forces observed during an ice test to ensure that resonance did not occur during testing, and that the data collected are sound.

ACKNOWLEDGMENTS

This thesis was compiled from research and work conducted at Memorial University of Newfoundland and the National Research Council's Institute for Marine Dynamics, with joint university/industry funding from the National Science and Engineering Research Council, the National Research Council, Esso Resources Canada Limited and Memorial University of Newfoundland. This, in addition to the departmental support within the Faculty of Engineering and Applied Science were essential to the success of this study.

I would like to sincerely thank my supervisor, Dr. D.B. Muggeridge, Dean of Science at Okanagan University College, B.C., whose support, encouragement, guidance and patience made this endeavor a reality. I would also like to thank Dr. A.S.J. Swamidas and Dr. L Lye, Professors of Engineering, Memorial University of Newfoundland the many individuals working in the laboratories of this faculty as well as the IMD for their assistance and advice.

The manufacture of the equipment outlined in this thesis and all of the equipment used in this test program including the models was conducted at Technical Services within the Faculty of Engineering and Applied Science. It is a testament to their superb craftsmanship, and I wish to thank them also for their generosity, time and patience.

Finally, I would like to express my sincere gratitude to the members of my family, especially my wife Cindy, for support, encouragement and affection provided during this trying period.

TABLE OF CONTENTS

TABLE OF CONTENTS (continued)

LIST OF TABLES

LIST OF FIGURES

LIST OF FIGURES (continued)

NOMENCLATURE

F_X	Total force in the X direction
$F_{X'i}$	Measured force in the X' axis direction on the i'th load cell
M_x	Total overturning moment about the X axis
X_i	X location of the i'th global load cell with respect to the defined coordinate system
$F_{applied}$	Force applied to the load measurement system
$F_{measured}$	Force recorded by the load measurement system
SAE	Sum of absolute prediction error
MAPE	Mean absolute percentage error
MAPE'	Mean absolute percentage error desensitized to the applied load
MMAPE'	The MAPE' desensitized to the system capacity
F_{nX}	Total neck force in the X direction
V	Model velocity during ice test
h	Ice sheet thickness
σ_{fu}	Flexural strength of the ice sheet
H	Ridge thickness
σ_{FU}	Flexural strength of the ridge tested
PSD	Power spectrum density

Chapter 1

1.0 INTRODUCTION

When conducting model tests to study such events as ice/structure interaction, it is important to perform the tests at a number of model scales to determine precisely what parameters should be accounted for in the analysis. This is of particular importance when studying events involving complex, anisotropic materials. A model test series was conducted to study ice/structure interaction between multi-year ice ridges and multi-faceted conical structures, with the goal in mind of testing at as large a scale as possible to facilitate the development of an algorithm to predict forces experienced in such an interaction at full scale.

1.1 Background

In the past two decades extensive research has been conducted to examine the feasibility of using smooth cones to protect offshore structures such as oil rigs and bridge piers from sheet

and multi-year ice. A recent state-of-the-art review of ice forces on conical structures (Wessels and Kato. 1988) describes ice failure modes around conical structures. and has summarized available model scale and full scale measurements. These tests showed the effectiveness of conical structures in ice defence. However. it was highly desirable from a manufacturing standpoint to replace the rounded conical surface with a flat faceted one.

This program was developed to study the different aspects of ice loading on a multi-faceted conical structure. The interaction loads with a multi-year ridge was of particular interest to designers as this would be the design ice condition for structures located in the Beaufort or Chukchi Seas.

Another point of interest was the effect of using a conical structure with a larger diameter neck than previously considered. This would have the obvious benefit of permitting a smaller cone to protect a larger piece of equipment such as bridge piers or structural members of offshore oil rigs.

Scale effects are also considered with a total of four model scales being examined. The 1:10 and 1:20 scale tests were conducted at ERCL's outdoor basin in Calgary. a 1:50 model was utilized at the tests in IME in Ottawa. and the 1:25 and 1:50 scale models were tested at the IMD's facility in St. John's.

and multi-year ice. A recent state-of-the-art review of ice forces on conical structures (Wessels and Kato, 1988) describes ice failure modes around conical structures, and has summarized available model scale and full scale measurements. These tests showed the effectiveness of conical structures in ice defence. However, it was highly desirable from a manufacturing standpoint to replace the rounded conical surface with a flat faceted one.

This program was developed to study the different aspects of ice loading on a multi-faceted conical structure. The interaction loads with a multi-year ridge was of particular interest to designers as this would be the design ice condition for structures located in the Beaufort or Chukchi Seas.

Another point of interest was the effect of using a conical structure with a larger diameter neck than previously considered. This would have the obvious benefit of permitting a smaller cone to protect a larger piece of equipment such as bridge piers or structural members of offshore oil rigs.

Scale effects are also considered with a total of four model scales being examined. The 1:10 and 1:20 scale tests were conducted at ERCL's outdoor basin in Calgary, a 1:50 model was utilized at the tests in IME in Ottawa, and the 1:25 and 1:50 scale models were tested at the IMD's facility in St. John's.

The test parameters that were varied in each of the test facilities are indicated in Table 1. The first two phases of the test program were completed and documented by Metge and Weiss, (1989), Metge and Tucker, (1990), and Irani et al, (1992). The third phase of the program was carried out at IMD and forms the basis of this thesis.

The test program conducted in IMD was a collaborative effort between Memorial University of Newfoundland (MUN) and the National Research Council (NRC) of Canada. The general concept of the test series as well as the execution was done jointly, and several individuals were involved in this project. The detailed design, fabrication and testing of the model and the load measurement assembly were done by J. Tucker of MUN under the supervision of D.B. Muggeridge. M. Lau of NRC had the responsibility of executing the test plan

Table 1.1: Test Parameters Varied in Test Facilities at ERCL, IME and IMD

Variation Tested	ERCL Calgary	NRC Ottawa	NRC St. John's
Model Scale	1:10, 1:20	1:50	1:25, 1:50
Structure Orientation	No	Yes	No
Neck Diameter	No	Yes	Yes
Ice Movement Rate	No	Yes	Yes
Ice Floe Thickness	Yes	Yes	Yes
Ice Floe Strength	Yes	Yes	Yes
Ridge Thickness	Yes	Yes	Yes
Ridge Strength	Yes	Yes	Yes
Ridge Orientation	Yes	No	No

Engineering Research Council of Canada (NSERC). The program involved a total of four test series conducted in three phases. The first phase consisted of tests conducted over two winter seasons (scales 1:10 and 1:20) at ERCL's outdoor ice testing basin in Calgary. The second phase consisted of model tests conducted at NRC's Institute for Mechanical Engineering (IME) in Ottawa (scale 1:50); and the final phase was a series of tests conducted at NRC's Institute for Marine Dynamics (IMD) in St. John's (scales 1:25 and 1:50). The St. John's test matrix had several features incorporated into it:

- The 54 kPa ridge was built using the 'brick layer' method whereas the lower strength ridges (28 and 14 kPa) were constructed using the 'dump truck' method (Spencer et al, 1990). These ridge building techniques were developed at the IMD in an attempt to produce consolidated ridges of appropriate strength and dimension to simulate a one in one hundred year, multi-year ridge.
- Tests from the phase conducted in Calgary with ERCL which were selected for comparison were incorporated into the matrix.
- A model speed of 0.06 m/s was used in both the ERCL and IME tests series and was used as a standard speed for this series as well.
- A number of extreme ice conditions were also simulated.

Smooth cones have been fairly widely used to protect bridge piers, caissons and offshore structures, and it is generally accepted that forcing ice to break in bending results in less force

being experienced by the structure than if the ice were to fail in crushing. The manufacture of large, smooth conical structures is inherently expensive due to the manufacture of rounded plates and internal supporting structures. An alternative to the smooth conical design is to approximate the surface with a multifaceted conical design. The interaction of ice features with these faceted conical structures was the subject of investigations that consisted of a combination of model tests and analytical studies. Loads associated with this interaction could not be accurately predicted, this required that tests be carried out on scaled models of a generic design in an effort to produce an appropriate numerical algorithm.

At present several methods are available to measure the forces and moments exerted by ice features. A newly developed method for the purposes of this study consisted of three six-component force and moment transducers sandwiched between two plates. Concerns over the inability to rigidly fix the three load transducers to two plates led to a design enhancement in which the load cells were rigidly fixed to one plate using a bolted connection while the connection to the other plate was achieved using flange-mounted spherical bearings.

To test this transducer arrangement, and to alleviate concerns about this new systems' ability to measure forces and moments accurately, a series of mock-up tests were performed on the load cell arrangement in the Engineering Structures Lab in the S.J. Carew Building at Memorial University of Newfoundland. The system was later used in the test program to

measure the ice forces experienced by a six faceted conical structure interacting with a multi-year ice pack consisting of embedded multi-year ridges.

1.3 Objectives and Scope of the Overall Program

The principle objectives of the program were:

(I) To understand how multi-year ice floes and ridges would interact with a multifaceted conical structure; and

(ii) To investigate the effects on ice interactions and forces of having the diameter of the above-water vertical 'neck' of the structure be almost as large as the waterline diameter.

Two scaled models, 1:25 and 1:50, of a prototype Beaufort Sea structure were used in the tests, and two neck sizes were tested at the 1:25 scale.

Two ridge targets were used. The first ridge target was one that would represent approximately the yearly average multi-year ridge size and strength tested at the 1:15 scale. This was chosen because it is a more commonly encountered ice condition in which full scale

data might be available in the near future. Furthermore, this ice condition was also tested in Esso's '89-'90 test series from which a direct comparison was possible. The second target was a 1 in 100 year multi-year ridge to be tested at the 1:50 scale. This was tested as part of the grant mandate.

The ridge construction techniques used in the tests conducted in Calgary and Ottawa were employed in the present test series. This permitted examination of the effects of ridge construction techniques on ice failure mechanisms and loads. It also helped correlate the test results from the three phases of the test program. Ridge strength and thickness as well as sheet ice strength and thickness were varied throughout the five weeks of tests conducted.

A transducer system had to be designed, manufactured and calibrated which would permit the measurement of global (total overall) forces and moments on the model. Due to the model scale being used and the ice features being tested, the predicted global forces and moments would be greater than any previously measured in a test program at the IMD, and would be close to the capacity of the towing carriage. For this reason, use of a single six component load transducer was ruled out.

1.4 Thesis Objectives

The major objectives of this thesis were:

(i) To outline a new design of a transducer system intended for use in the multifaceted conical structure program outlined above.

(ii) To record a series of calibration tests conducted at the S.J. Carew Building in which a known load was applied to the load cell system and its outputs recorded, resolved into meaningful data and compared with the recorded applied loads

(iii) To develop a meaningful method for comparing the results of these calibration tests with the known applied load

(iv) To examine the performance of the test equipment in the IMD phase of the multifaceted conical structure program.

The equipment designed, constructed and verified was an essential component to the success of the program.

Chapter one is the introduction to the thesis, outlining the rationale behind the project and the background behind the multifaceted conical structure project and chapter two is a review of relevant literature. Chapter three discusses the design of of the force measurement system, and details a set of calibration tests conducted in the Structures Laboratory of the S.J. Carew building. A set of two indices are also developed and presented which can be used to indicate the degree of error in the calibration tests. Chapter four describes the entirety of the test equipment and the installation of it in the IMD ice testing facility. A discussion of the multifaceted conical structure test program is also included which describes the test parameters varied throughout the series. Chapter five is an evaluation of the equipment's performance in the test series. Calibration data gathered during the program is analysed and discussed and a dynamic analysis is performed comparing the natural frequency of the test structure with the frequency of the loading function during an ice test. Chapter six presents an overview of the thesis as well as findings and suggested directions for future work.

Chapter 2

2.0 LITERATURE REVIEW

Physical testing, be it of model structures in a simulated environment or of full scale structures in nature, requires the accurate measurement of all important parameters. The modeling of physical environments and objects for testing purposes is necessary for the maintenance of controlled environments, but the use of modelling and similitude laws for scaling purposes then becomes necessary. In the ideal situation, one would test a full scale structure in a controlled environment. This is of particular interest when developing algorithms for predicting events on full scale structures based on model tests. The repeated testing of the same conditions through a variety of scales would then optimize the algorithm, and enhance our understanding of modeling and similitude laws.

Ice-structure interaction testing has been carried out by researchers for decades with the motive of reducing the risk to offshore structures from such threats. Strain gauged proving

rings were among the first of the precise ice force measurement devices (Saeki, 1977), used by a variety of researchers to measure forces acting on a structure in a single axis. Devices such as this were used in conjunction with plates to infer pressure or to permit the use of multiple sensors to measure multi-axis measurements, but their implementation and validation is difficult and cumbersome.

Indeed, there have been tests conducted on actual structures where they have been instrumented to measure the loads on them resulting from interaction with ice. In 1975, the Kemi I lighthouse (Määtänen, 1977) was constructed and instrumented for the measurement of forces acting upon it from ice forces. The total ice load was measured by monitoring and recording the bending deformation of the lighthouse (5.8 m diameter) underwater structure. Four 7.4 m long rods were mounted vertically inside shielded tubes so that they were free to move relative to the concrete structure. Strain gauge transducers were used to measure the relative movement of the rods. The notion was that output would be directly proportional to the bending moment or the total ice load on the structure. It was stated by the author that the total ice load measurement accuracy was reduced as a consequence of "mechanical signal to noise ratio" and the vertical situation or location of the ice load.

The JZ20-2-1 platform was instrumented in Liao Dong Bay (Fan and Jin, 1990)to measure the total ice force on the jacket or platform in October of 1987. They used three types of sensors, viz., strain gauges, accelerometers and load panels which were used together to

determine the total ice force on the structure resulting from what was termed severe ice conditions. The load panels measured the forces on the structure only at the location of ice-structure interaction, and had to be mounted such that they could be adjusted to accommodate the tide levels.

A study was performed (Masroor and Zachary, 1991) on the use of applying strain gages to structures, using the structure itself as the force measurement device for a physical test. In this study, the authors demonstrated the viability of this technique, but cautioned that one should be careful in locating the position of the strain gages. Errors may be propagated through structural members, resulting in significant errors. They recommend that different combinations of strain components could be studied and evaluated on the basis of error-propagation, and that the best among these could be selected for the placement of strain gages. Their study, however, was restricted to linearly elastic structures with small strains where the principle of superposition retained its validity.

In 1990, a joint Sino-German project to explore the correlation between model and full scale ice forces on a jacket platform was conducted (Wessels and Jochmean, 1991) in which research was conducted in two phases. In the first stage, one of the four legs of a jacket platform in Bohai were instrumented using custom designed ice force measuring panels. Five such panels were mounted on the surface of the leg and adjacent to each other so as to cover the entire front sector (180°) of the leg in the direction of ice impingement at rising

tide. For the scale model tests, a single force dynamometer was positioned at the top of a frame to which the test structure was mounted and driven through the model ice. In this case, only sheet ice was tested and the vertical structure used tended to promote failure of the ice in crushing, which resulted in very little movement of the line of action of the force experienced by the test structure relative to the axis of measurement of the load transducer.

Structures which are bottom founded and which interact with ice in nature experience extraordinarily large forces. The ice failure on and about the structure could result in large overturning moments also being experienced during these types of interactions. This is particularly the case where the walls of the structure have a slope, permitting the ice to slide up or down the surface prior to failure. Such conical structures have been used to protect offshore platforms, lighthouses and bridge piers. These structures often have a sloped surface at the waterline which would either lift the ice interacting with it up, or force it down in order to cause the failure of the ice in bending as opposed to crushing. Many of these structures have more than one inclination of sloping surface, and a vertical wall or pillar beyond the sloped surfaces. The net affect is that as the ice slides up the inclined surfaces, the line of the action of the force relative to some datum is constantly changing. In their book, "Ice Interaction with Offshore Structures", Cammaert and Muggeridge (1988) present a number of algorithms which may be used to predict the forces experienced by an inclined structure experiencing ice. These algorithms extend from two dimensional to three dimensional analysis and include both elastic and plastic limit failure modes (Nevel, 1972;

Ralston, 1977). The location of the forces and the resulting overturning moment experienced by the structure would be a consequence of the location of the centre of mass of the ice.

During the physical test of a structure in which the line of action of the force moves about the location of the force/moment sensors, it is not inconceivable for very large moments to be experienced by the force transducers being used. One method used by researchers to instrument structures which are to experience this type of loading is to use single axis load transducers and install them with couplings that are rigid in only the axis of measurement. Using these, only forces in the load bearing axis of this coupling unit will be transferred to the force sensor. Instrumentation such as this was used in the second phase of the multifaceted conical structure program (Irani, 1992), as well as a number of other tests including a series of tests of impact forces on a flat jacket deck (Murray, 1997). This method of instrumentation is effective, but does not lend itself to quick modification of the test equipment due to the large number of components required for the setup.

In the book "Vibration and Testing - Theory and Practice" (McConnel, 1995), the issue of the effects of bending moments on measured forces is addressed. Using an example of the measurement of the dynamic response of a steel bar rigidly attached to a force transducer and struck with an impulse hammer, ghost resonances appeared in the measured experimental frequency response functions. This issue is principally the one being addressed in this thesis, and more specifically a method to reduce the moment being applied to the force transducers

used in an experimental setup. He goes further to state that force transducers are sensitive to bending moments and shear forces, and there is little known of the definition of bending moment sensitivities, let alone the prescription of methods of correction.

Nonlinearity in force transducers is defined as the amount by which the transducer output deviates from between a straight line zero load and the rated load outputs (Antkowiak and Rencis, 1994). This percentage of the rated output can be used to classify the performance of a transducer (setup). In their paper, they evaluate the linearity of a small strain gage force transducer and compare their experimental calibration results with a finite element analysis of the same structure. In their study, they found that small discrepancies occured between the FE and test results. They theorized that these could be the result of nonlinear material behaviour, machining tolerances or residual stresses due to machining. Such issues as these would certainly be compounded in a complex transducer setup like that examined in this thesis.

For accurate force measurements and to simplify analysis of the forces being measured, it is beneficial to attach the transducer systems base to an ideal or 'rigid' foundation (McConnell, 1995). In such a case, the mass of the foundation is considered infinite, and the transducer/model configuration acts like a single degree of freedom system where the transducers may be considered as very stiff springs.

A two dimensional mathematical model for simulating the behaviour of a force transducer when subjected to bending moments was developed in 1993 (McConnell and Varoto, 1993). The analysis was verified with experimental results and it was demonstrated that bending moment sensitivity affected the transducer's overall sensitivity, and that this may cause large measurement errors depending on how the transducer is employed in a test.

From the above review, it can be seen that a force measurement system should be: (i) rigid; (ii) linear in response; (iii) should not respond dynamically to the applied forces; (iv) have low signal to noise ratios, and (v) be able to measure forces and moments in a repeatable manner. The following pages outline the design, fabrication and verification of a system to measure the ice loads exerted on a faceted conical structure.

Chapter 3

3.0 THE DESIGN, FABRICATION, CALIBRATION AND ASSEMBLY OF THE FORCE MEASUREMENT SYSTEM MOCK-UP

To measure the high forces and moments experienced by the test structure and maintain as rigid a test structure as possible, three large capacity six-component dynamometers were utilized simultaneously and the global forces and moments were resolved from the recorded data streams. The dynamometers were rigidly attached to an upper load cell plate using spherical bearings in flanged housings (Figure 3.1). This was done for ease of assembly and to reduce the moment pre-load on the dynamometers due to imperfections in the manufacture of the instrumentation assembly. For the test series in the IMD, the upper load cell plate was attached to a tow post and the model was rigidly secured to the lower load cell plate. The load cell details and specifications are given in Appendix A.

Rigidly attaching several multi-axis force transducers together with rigid, reinforced plate

system. For the installation to be successful in the case where three load cells would be attached between two plates, the six surfaces on the plates which will contact the load cells must all be perfectly parallel, and in the same plane. This is a difficult construct to manufacture given the size of the plates in question. If any irregularities exist between two mating surfaces or in one or another of the plates, the result upon installation is that the force

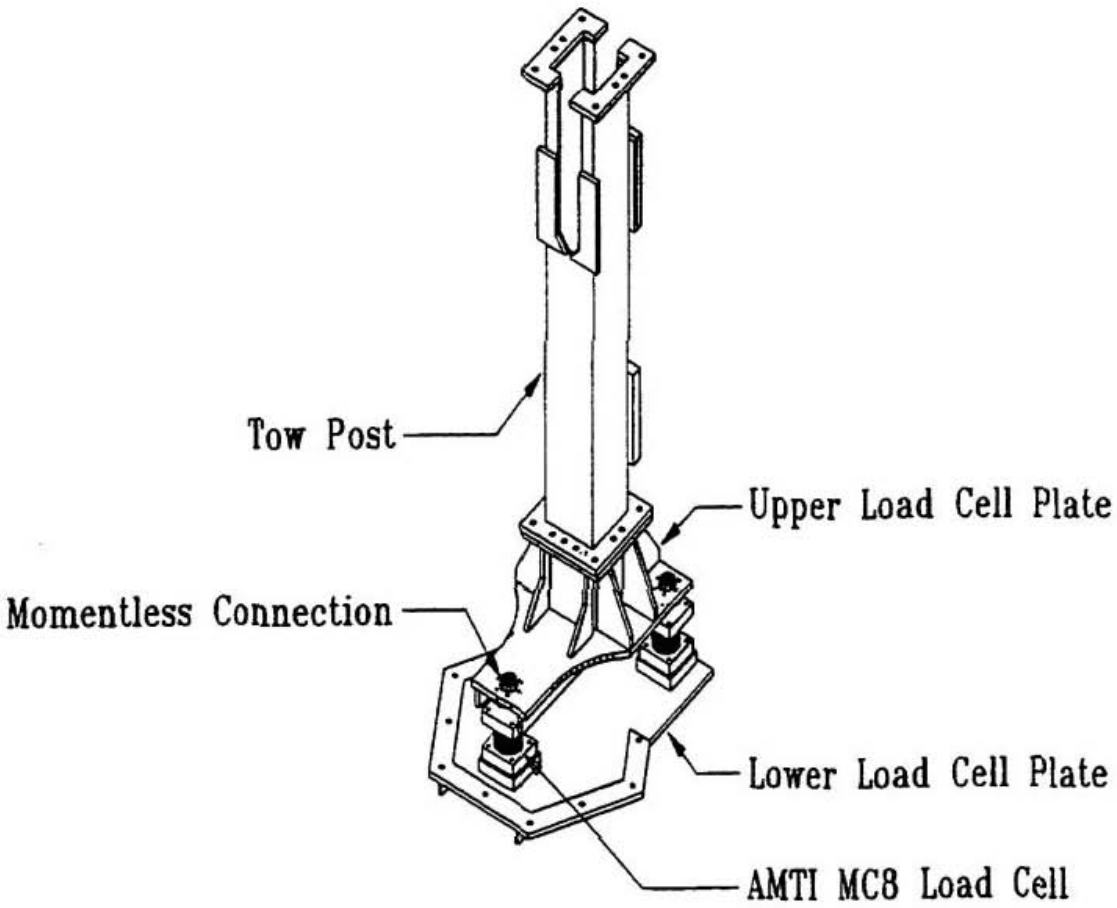

Figure 3.1: Global Load Measurement Assembly

transducer would be pre-loaded with a force equal to that required to deform the plates such that their surfaces mate with the end plates of the transducers.

Another issue is that any deformation in one or another of the plates would result in a moment being applied to the load cells in the area of the setup. It has been found that large moments applied to a multi-axis load cell will introduce errors in measurements obtained on other channels of that transducer. To alleviate these concerns, a novel concept was introduced.

3.1 Design And Fabrication Details

The IMD maintain five tri-axial force transducers, three of which were used in the global force measurement system (Figure 3.2) [produced by Advanced

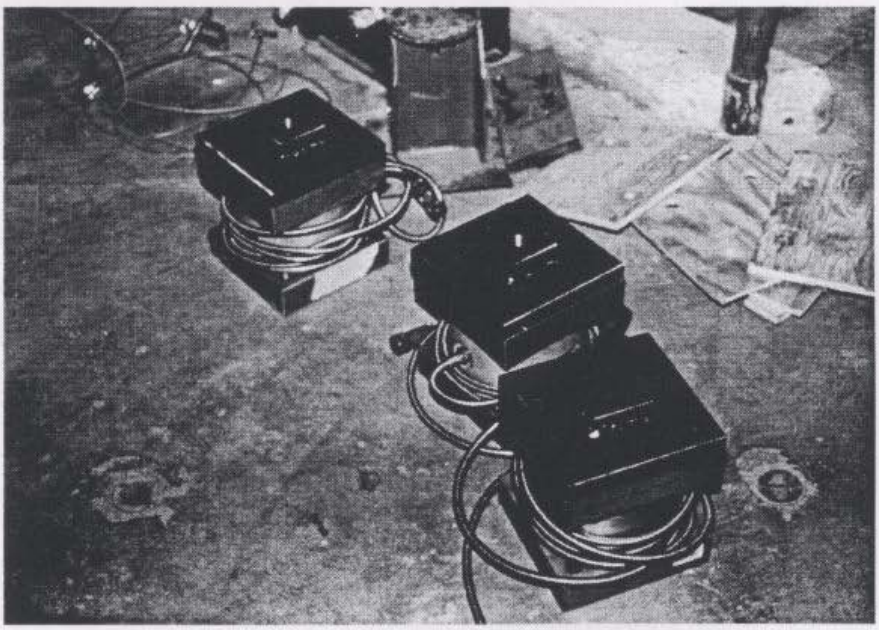

Figure 3.2: AMTI 6 Component Force Transducers

Mechanical Technology Inc. (AMTI)] of the MC8 series (1 X 89 kN capacity and 2 X 44.5 kN capacity). These are splashproof, six component load cells designed to measure forces in each of the X, Y and Z directions as well as moments about each of these axes. If these three force transducers were placed in series in the newly designed transducer setup, they would have a combined force capacity in the Z direction of 178 kN and 89 kN in each of the X and Y axes. These load cells are strain gage transducers, structural members with strain gages attached to them which, when loaded register a precise and consistent amount of strain on any of a number of sets of strain gages installed on them. The gages are positioned strategically to avoid any strain being measured on them when off-axis loading is taking place by fixing them on the neutral axes of the two non-sensing axes. A problem arises when sufficient plastic or elastic deformation of the structural member takes place to alter the geometry and shift the neutral axis of the member. In this instance, errors will be registered on the unloaded axes. This scenario most often occurs when large moments are being applied to the force transducers. To alleviate this problem, a mechanism was devised to minimize the moments experienced by the individual load cells during loading.

The load cells were attached to a rigid 25.4 mm thick steel plate with gussets applied to the underside for additional rigidity. This mounting plate was the one to be used in the actual test program (Lower Plate in Figure 3.4). Plate thicknesses and appropriate reinforcement was determined using plate bending theory and forces anticipated from the maximum forecasted testing conditions. All plates and mounting fixtures were manufactured by the

welding and machining technicians of Technical Services in the S.J. Carew building, at MUN. The load transducers were bolted to seating pads on this plate (called the 'lower load cell plate') which had been ground and polished flat. The purpose of the polishing was to reduce the chance of any surface irregularities causing a deformation in the mounting plate of the load cell, resulting in a moment applied to the *load cells during assembly in the system.*

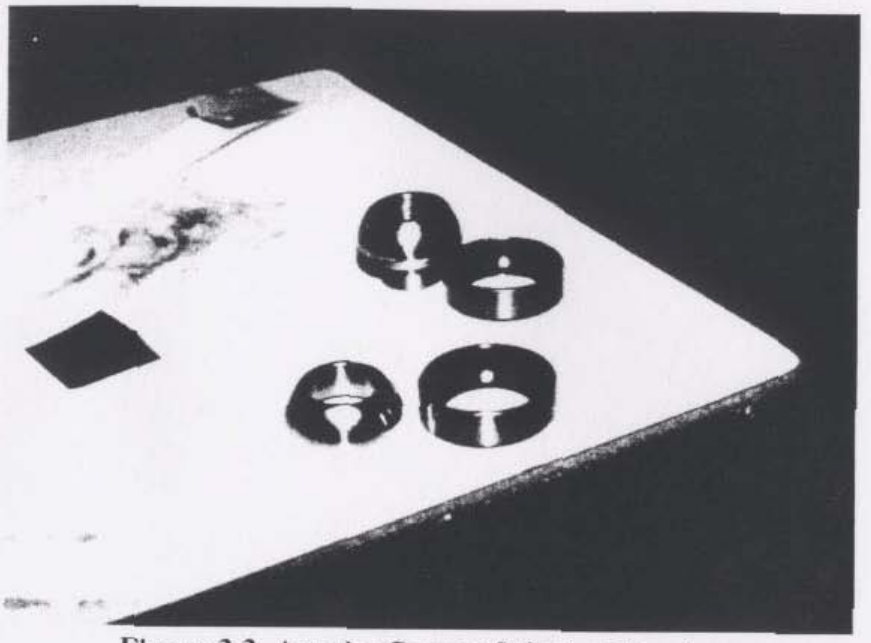

Figure 3.3: Angular Contact Spherical Bearings

Two teflon lined, angular contact spherical plain bearings (Figure 3.3) were mounted in each of three flanged cups and separated by a spacer. The spacer was designed such that the centre of rotation of each of the spherical bearings would coincide, resulting in a 'ball joint' type arrangement. The flanged

Figure 3.4: Angular Contact Spherical Bearing and Flanged Housing

cup was bolted to its mating flange, and a 1.0 mm spacer was installed to permit preloading of each of the bearing assemblies preventing vibration and any movement other than rotation. The flanged assemblies were attached to the second of the two mounting plates (Figure 3.5), and provided the coupling mechanism for attachment of the load cells.

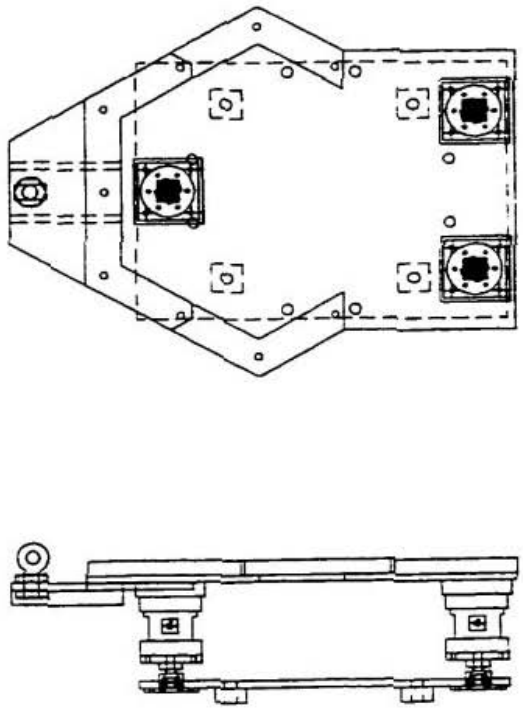

Figure 3.5: Test Assembly

One of the two plates were to be attached to a rigid surface (the floor of the Structures Laboratory in the case of the calibration, and the tow post in the case of the model tests), while the load was applied to the second plate. Assuming that the bearings were ideal, the effect of this arrangement was to remove any moment application to the load cell by the mounting fixtures. The only moments experienced by the individual load transducers would be a result of the axial forces applied at each of the respective spherical bearings. Physical limitations of the bearings resulted in friction along the sliding surfaces and a net moment being observed at the centre of rotation/connection points between the load cells and the bearings. The amount of friction observed and the amount of moment applied to each load cell was directly proportional to

the amount of axial load applied to bearing at that instant in time. Subsequently, an effort was made in the design to minimize the distance between the centres of the bearings and the mounting plate of the load cell.

3.2 Global Load Cells

One AMTI model SRMC8-6-20000 and two AMTI model SRMC8-6-10000 six component load cells, manufactured by Advanced Mechanical Technology Incorporated (AMTI), were used in this configuration. The measurement axes (X', Y', Z') for the individual load cells (Nos 1, 2 and 3) were oriented as shown in Figure 3.5, and the forces and moments were resolved to a global X, Y, Z coordinate system. The origin of the global coordinate system was located along the centerline of the cone at the water level. The X-axis was positive in the direction of ice motion, the positive Z-axis was directed vertically upwards, and the direction of the Y-axis was such that X, Y, Z form a right handed, orthogonal coordinate system.

The global forces in the X, Y and Z directions were obtained using a simple algebraic summation approach:

$$F_X = \Sigma_{i=1,2,3} F_{X'i} \quad (3.1)$$

$$F_Y = \Sigma_{i=1,2,3} F_{Y'i} \quad (3.2)$$

$$F_Z = \Sigma_{i=1,2,3} F_{Z'i} \quad (3.3)$$

where:

F_X - Total force in the X direction

F_Y - Total force in the Y direction

F_Z - Total force in the Z direction

$F_{X'i}$ - Measured force in the X' axis direction on the i'th global load cell

$F_{Y'i}$ - Measured force in the Y' axis direction on the i'th global load cell

$F_{Z'i}$ - Measured force in the Z' axis direction on the i'th global load cell

Global overturning moment induced on the test structure was the result of the F_{Xi}, F_{Yi} and F_{Zi} forces observed and their respective application points and directions of action with respect to the global axes.

Due to different water levels that changed with test scales, the relative location of the

global origin to which all moments were resolved changed. Consequently, the moment arms changed with varying water level.

The global moments were calculated using the following equations:

$$M_X = \sum_{i=1,2,3} F_{Z\,i} * Y_i + F_{Y\,i} * Z_i \quad \textbf{(3.4)}$$

$$M_Y = \sum_{i=1,2,3} F_{X\,i} * Z_i + F_{Z\,i} * X_i \quad \textbf{(3.5)}$$

$$M_Z = \sum_{i=1,2,3} F_{Y\,i} * X_i + F_{X\,i} * Y_i \quad \textbf{(3.6)}$$

where:

M_X - Total overturning moment about the X axis

M_Y - Total overturning moment about the Y axis

M_Z - Total overturning moment about the Z axis

X_i - X location of the i'th global load cell with respect to the defined axis system

Y_i - Y location of the i'th global load cell with respect to the defined axis system

Z_i - Z location of the i'th global load cell with respect to the defined axis system

The moment arms for each of the three axes used for each of the calibration test setup

variations are given in the respective spreadsheets and are dependent on the location of the transducer setup as well as the location of the hydraulic ram (or ice ridge/floe level) used to load the apparatus.

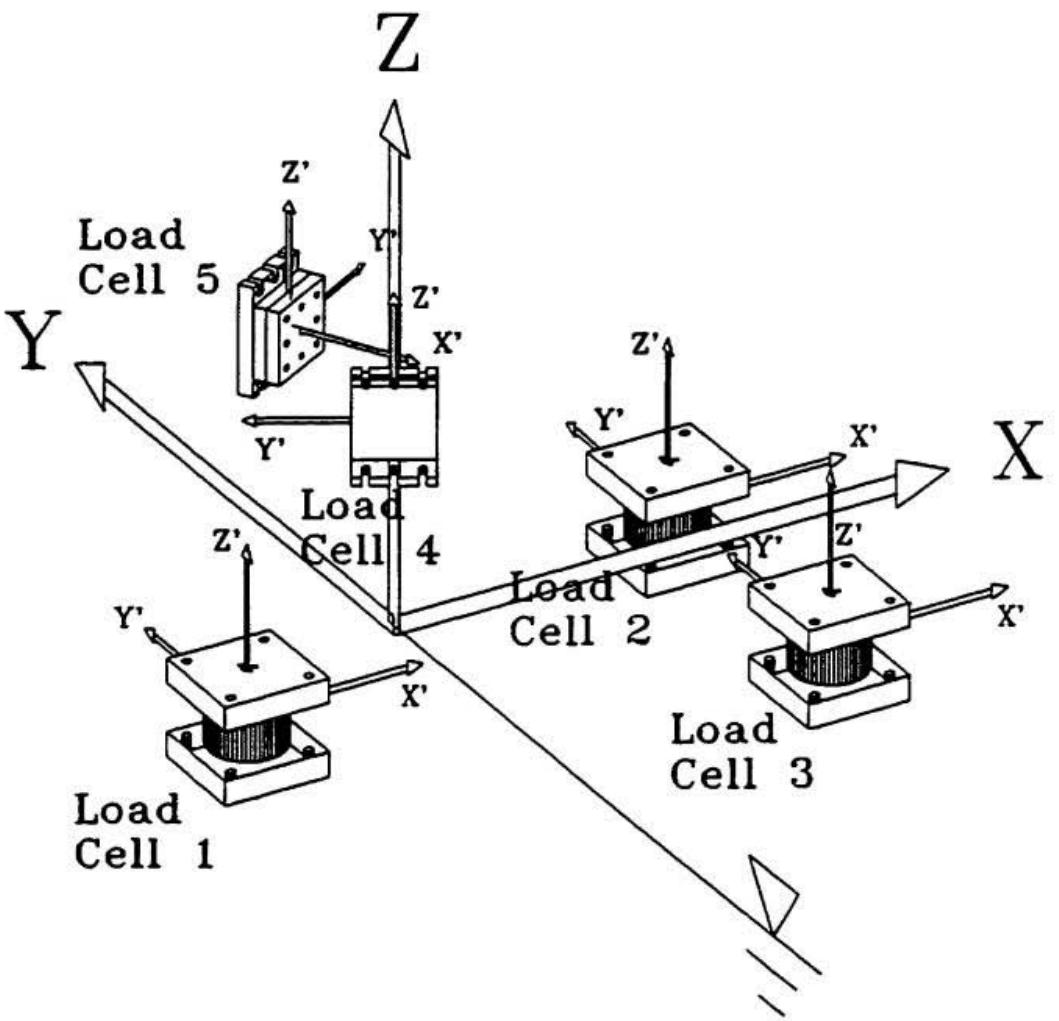

Figure 3.6: Orientation of load cell coordinate axes with respect to global coordinate axis

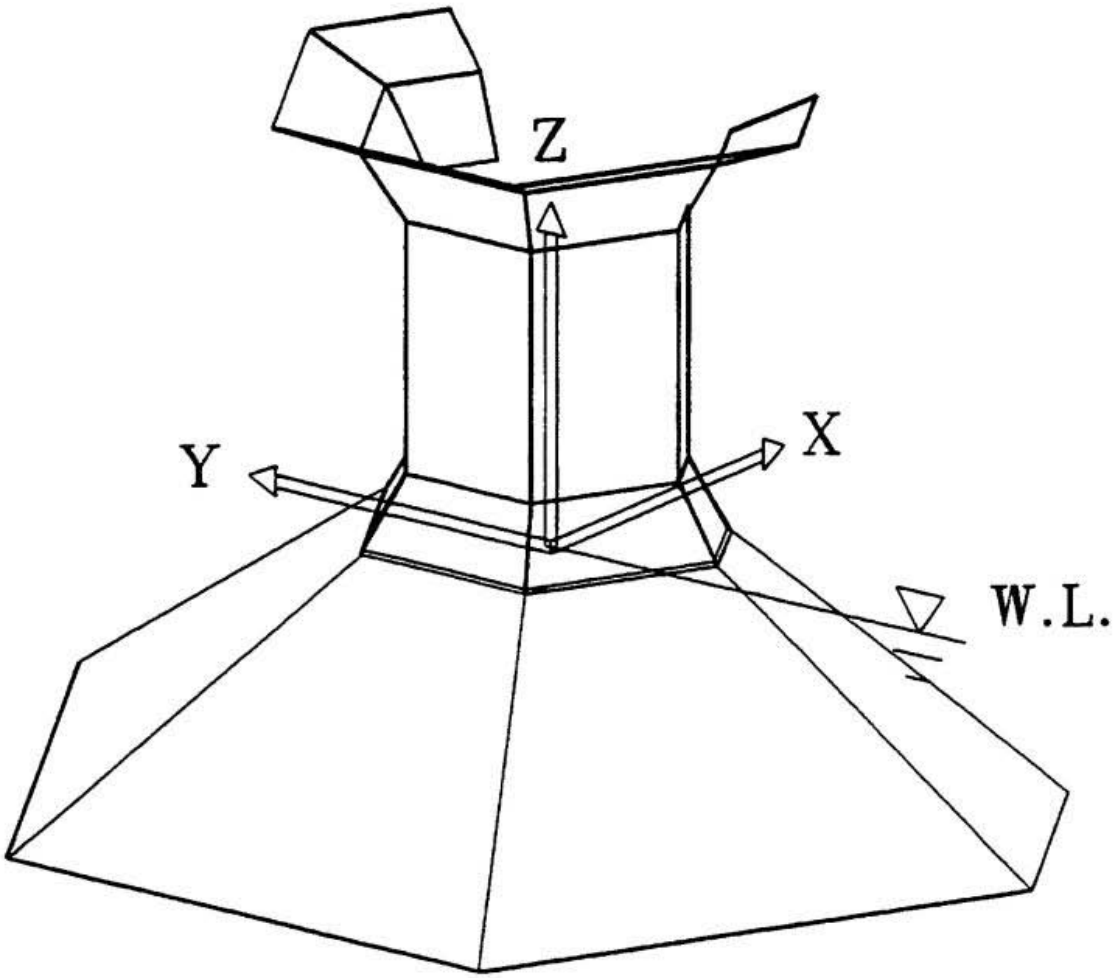

Figure 3.7: Orientation of global coordinate axis with respect to model structure

3.3 Calibration of Test Setup

Prior to the test series in the IMD, a mock-up of the test structure and support system was created in MUN's Structural Engineering Laboratory. An in-depth series of calibration checks were performed on the force measurement systems.

For mock up and calibration purposes, the flange/bearing assemblies were bolted to a 25.4 mm thick mild steel plate (test plate)(Figure 3.3). A plate thickness of 25.4 mm was used to reduce the amount of deflection during loading to a minimum and was additionally stiffened with 50 mm x 250 mm low carbon steel flat bars running lengthwise and laterally, and attached to

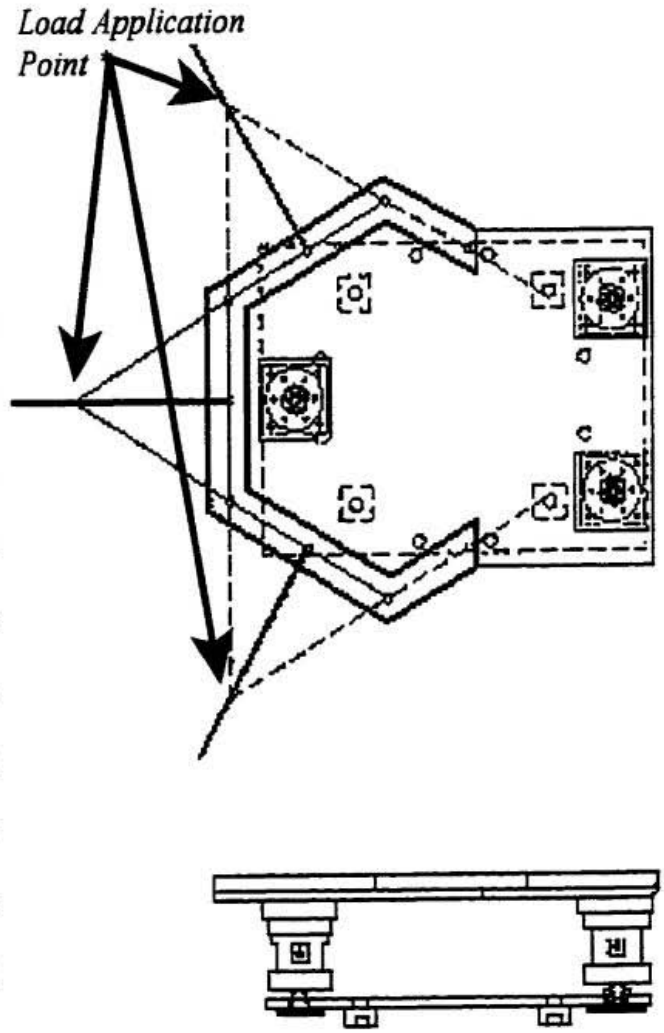

Figure 3.8: Calibration and Mock-up equipment

the plate with stitch welds. This plate had 12 bolt holes flame cut in it to permit fastening of the entire transducer setup to the structures laboratory floor. There were a total of 3 sets of 4 holes cut in a 600 mm by 600 mm square, each set of holes rotated 30° from the other such that the setup could be fastened to the floor in a total of 12 configurations. This test plate was separated from the floor by cylindrical spacers to permit a safe separation distance from the flanges to the floor surface. The spacers were fashioned as bushings, aligning the floor bolts and the test plate. The entire transducer assembly was attached to the Structures Laboratory 900 mm thick reinforced concrete floor using the floor bolts and bushings, and restraining the assembly in all axes.

The loading arm shown in Figure 3.8 was also manufactured from 25.4 mm thick steel plate and had a bolt pattern matching that of the lower cone model to be attached to the transducer assembly. The mating surfaces of the loading arm and model plate were also milled to a fine tolerance (±0.05 mm) to ensure a proper fit when attached and reduce residual stresses during the test.

The manufacturer's specified transducer calibrations were verified prior to the start of the test series and used to compute the calibration coefficients for the individual force channels throughout the test program.

3.4 Test Setup and Assembly

The test apparatus described above and the procedure listed below were designed to compare the forces and moments measured about the X, Y and Z axes by the transducer configuration and compare these measurements to the actual loads applied to the plates. The objective of this test was to prove conclusively that the three tri-axial or six component load cells sandwiched together between two rigid plates with spherical bearings, to eliminate the moments, would accurately measure large triaxial forces and moments .

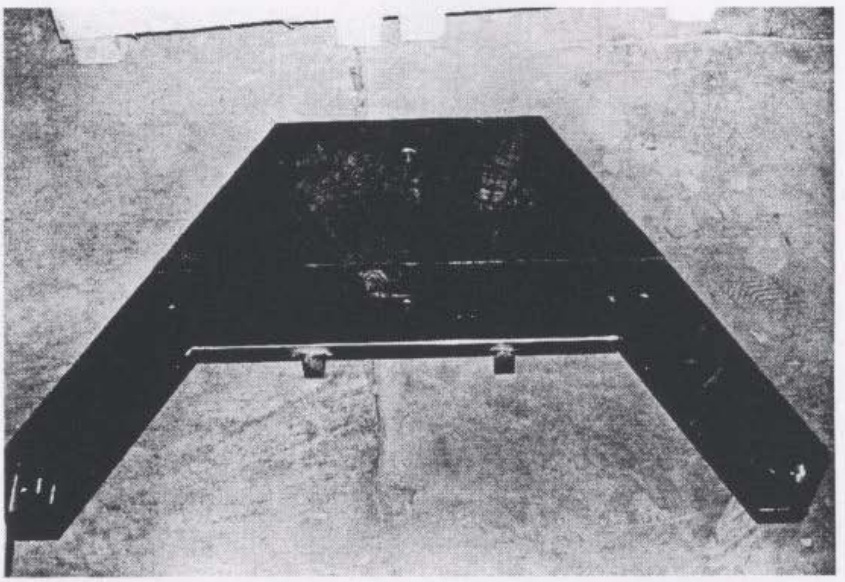

Figure 3.9: Loading Arm

Loads were transmitted to the test jig using a 50 kN hydraulic ram. The ram was mounted in a test frame constructed for this program using structural steel members available in the Structures Laboratory and had a load cell attached in series with the loading arm to monitor the applied forces. The applied load was tensile in nature, and was delivered to the loading arm through an eye bolt located near its front, using a braided steel cable and steel shackles.

To change the angle of loading with respect to the Z axis, there were three options: (i) Change the lateral position of the hydraulic ram; (ii) Change the orientation of the test plates (12 variations possible); or (iii) Change the position of the loading arm on the front of the model plate (3 positions). In this test program, variations of all 3 options were used.

The test consisted of two phases, the first was the application of known loads at known distances from the load cell defined origin after the transducer setup was zeroed. The resultant loads and moments on the loadcell plate were calculated and compared to the loads and moments measured by the three six-component load transducers. Forces were applied at each of three points (Figure 3.7) and varied through a range of 0 to 23 kN.

The second phase of the test consisted of electronically zeroing the transducer setup, and then reducing the temperature of one of the load cell plates by a known amount. This was achieved by placing approximately fifty kilograms of ice on the upper plate and monitoring the plate's temperature. The shift in the zeroes on all the transducer channels was noted as a consequence of irregular thermal expansion and contraction, and the equipment was rezeroed. The procedure outlined in phase one was then repeated. This test was referred to as the ice test.

All tests were conducted in the Structures Laboratory of the S.J. Carew Building, Memorial University of Newfoundland. In all tests, the test frame was loaded and permitted to 'settle'

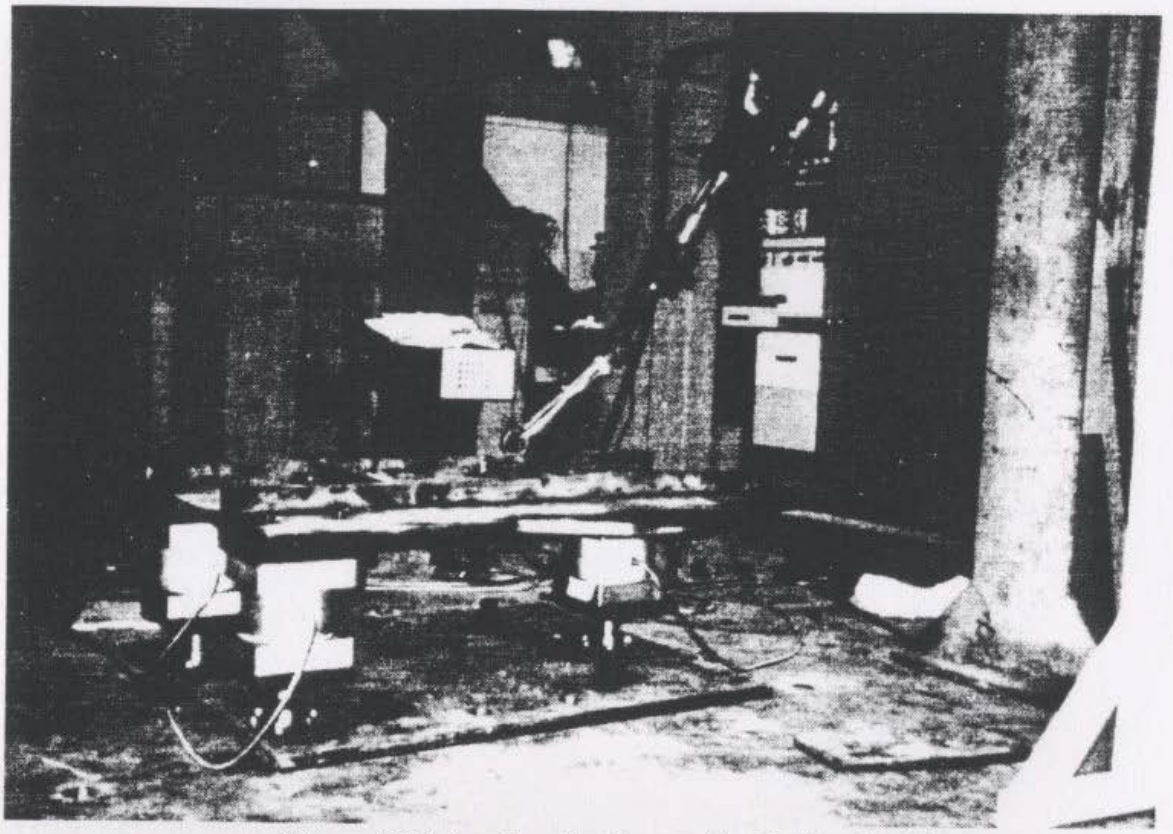

Figure 3.10: Loading Equipment for Calibration Tests

or allow for any relaxation of the loading system, and the channels of all transducers were scanned using a Hewlett Packard 3497A Data Acquisition/Control Unit and recorded.

3.5 Method of Comparison of Results

To determine an evaluation process for the performance of this system, we should first consider what features an ideal force measurement system would have. Plotting the observed data from the transducer setup against a known standard, perfect correlation between the new

system and the standard would be indicated by a perfect fit of this line with the linear equation of

$$F_{Applied} = a + b\ F_{Measured} \tag{3.7}$$

where a = 0, and

b = 1

A perfect fit would be indicated by linear regression with an R^2 value of 1, and a slope of 45° as shown in Figure 3.10, assuming that intercept of this plotted line is zero.

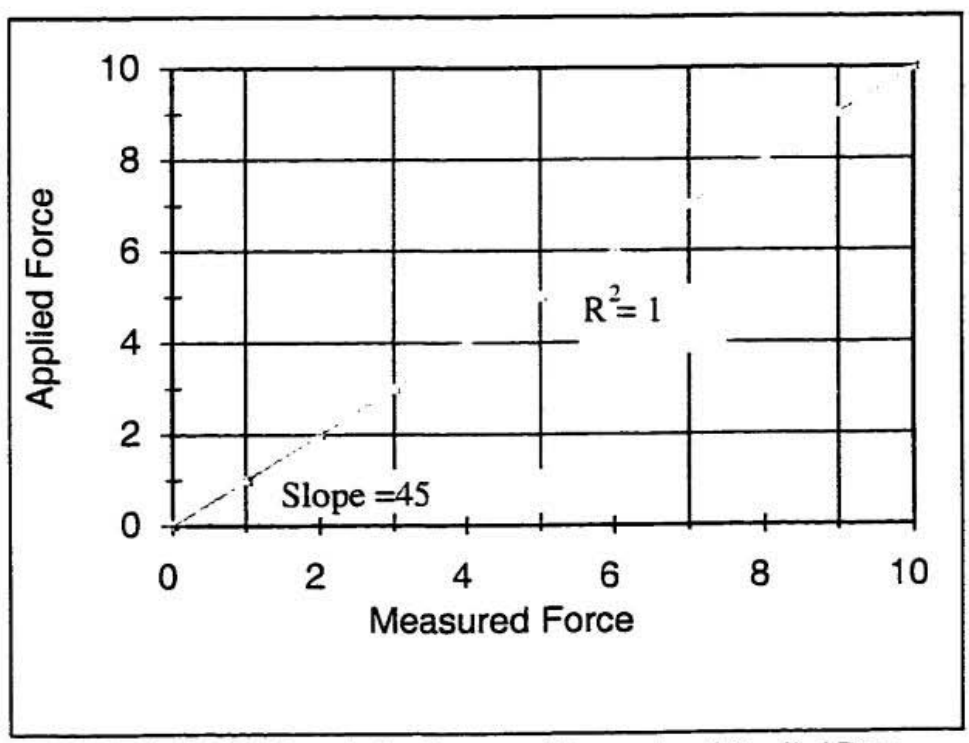

Figure 3.11: Perfect Correlation Between Measured and Applied Data

The value of R^2 and the slope alone are not good indicators of goodness of fit with the line of perfect agreement. It is conceivable that the line of Applied Force vs. Measured Force plotted could have an R^2 value approaching one, but that its slope and intercept could vary greatly from the values of one and zero. It has been recommended that the Sum of Absolute Prediction Error (SAE) (Castillo et al, 1997) would be a good goodness of fit criterion. This is given as:

$$SAE = \sum_{i=1}^{n} \left| F_{Applied_i} - F_{Measured_i} \right| \qquad \textbf{(3.8)}$$

where n = the number of samples

If the value of the SAE for a given set of measurements is equal to zero, then the values of a and b given in equation (3.7) are equal to zero and one respectively. Slight modification of this measure desensitizes it to the number of samples, resulting in a criterion called the Mean Absolute Percentage Error (MAPE):

$$MAPE = \frac{1}{n} \sum_{i=1}^{n} \left| F_{Applied_i} - F_{Measured_i} \right| \times 100 \qquad \textbf{(3.9)}$$

The MAPE is a finite measure of the magnitude of error observed through a series of measurements. To present the error as a percentage of the applied load, the MAPE' could be presented as:

$$MAPE' = \frac{1}{n} \sum_{i=1}^{n} \frac{F_{Applied_i} - F_{Measured_i}}{F_{Applied_i}} * 100 \qquad (3.10)$$

The MAPE' is a good measure of the performance of the system overall. but to examine and compare the performance of the system between each axis of measurement. there comes into play the issue of resolution. The system being examined here has a 89 kN capacity in the X and Y axes, and a 178 kN capacity in the Z axis of measurement. These electrical transducers (as are all electrical transducers) are designed such that they produce a maximum output of, typically, 10 volts when they are subjected to the peak loads for which they are designed with the manufacturers prescribed excitation voltage being applied. The resolution of the system is determined by the tools that are used to measure the voltage output of the transducer. A measurement tool which has 12 bit resolution would take the range of voltage that it is designed to measure within and divide it into 2^{12} discrete units, registering a detected change in voltage whenever a change in voltage of at least one of these units has been detected.

As an example, a system measuring 10 volts with 12 bit resolution would register that a change in

$$Discrete\ Unit = 10/(2^{12} - 1) = 0.002442\ Volts \qquad (3.11)$$

the output from the sensor 0.002442 volts. If we have, as is the case for two of the three

load transducers used in the setup. a capacity of 44.5 kN for which we would have an output of 10 volts at maximum load, then we would require a load of 10.867 N to be applied to the transducer before a change would be registered on the system. In the case of the 89 kN load cell, a load of 21.734 N would be required before a change in load was detected.

Based on this example, it is obvious that the capacity of the measurement system cannot be ignored when evaluating the errors of the system. Given two load transducers, one with a high capacity and one with a low capacity, if both have equivalent outputs and are connected to similar data acquisition systems, it would be expected that errors in measurements for low loads would be greater for the larger capacity system. Dividing the MAPE by the capacity of the system and multiplying it by 100 will result in the MMAPE being presented as a percentage of the total capacity of the system in this axis. This will not only desensitize it to the capacity of the system, but also result in the Modified MAPE' (MMAPE) being a number that may be considered more universally.

$$MMAPE = \frac{100}{n * SystemCapacity} \sum_{i=1}^{n} \frac{F_{Applied_i} - F_{Measured_i}}{F_{Applied_i}} \qquad (3.12)$$

The larger the capacity of the system, the more conservative will be the value of the MMAPE, a direct result of the system capacity divisor in Equation 3.12. The global force applied to the system may be defined as the vectorially summed forces in the X, Y and Z axes being applied to the system. The global force capacity will vary depending on the

direction of loading, but will be a maximum when a load is being applied along the Z axis of the system only. Subsequently, calculated values of the MMAPE for the global force component use the same capacity as that of the Z axis, 178 kN. The system moment capacities may be determined from the axial load capacities of the load cells multiplied by the moment arms or the distance from bearing centre to bearing centre about the appropriate axes. System capacities are given in Table 3.1.

Table 3.1: System Capacities

Component	Capacity	Component	Capacity
F_x	89 kN	M_x	25 kN m
F_y	89 kN	M_y	89 kN m
F_z	178 kN	M_z	57 kN m
F_g	178 kN		

The values of the MMAPE and MAPE factors obtained for this set of calibration tests are given in Tables 3.2 and 3.3 and graphical comparison of the forces and moments for each test with the line of perfect agreement is given in Appendix B.

Table 3.2: MAPE' and MMAPE Factors for Force Measurement During the Calibration Tests

Test	Fx		Fy		Fz		Fg	
	MAPE'	MMAPE	MAPE'	MMAPE	MAPE'	MMAPE	MAPE'	MMAPE
Orientation 1	0.76	0.0008	3.63	0.0041	4.16	0.0023	0.97	0.0011
Orientation 2	0.50	0.0006	0[1]	0[1]	4.05	0.0023	1.09	0.0012
Orientation 3	0.74	0.0008	6.33	0.0071	2.08	0.0012	0.56	0.0006
Orientation 4	0.54	0.0006	13.94	0.0156	3.41	0.0019	1.37	0.0015
Orientation 5	2.04	0.0023	104.60	0.1174	6.10	0.0034	1.49	0.0017
Orientation 6	1.73	0.0019	21.20	0.0238	3.16	0.0018	1.42	0.0016
Orientation 7	4.81	0.0054	11.00	0.0123	1.68	0.001	1.03	0.0012
Orientation 8	4.50	0.0050	2.29	0.0026	1.72	0.0010	0.39	0.0004
Orientation 9	5.55	0.0062	3.40	0.0038	2.25	0.0013	1.69	0.0019
Orientation 10	3.86	0.0043	1.32	0.0015	2.90	0.0016	0.82	0.0009
Orientation 11	0.50	0.0006	6.32	0.0071	5.35	0.0030	1.06	0.0012
Orientation 12	0.81	0.0009	5.24	0.0059	3.88	0.0022	0.81	0.0009
Orientation 13	0.91	0.0010	0.85	0.0010	4.63	0.0026	0.81	0.0009
Orientation 14	0.63	0.0007	2.11	0.0024	3.60	0.0020	0.66	0.0009
Ice Test	0.93	0.0010	1.05	0.0012	4.16	0.0023	1.59	0.0018

NOTE: 1. Due to the direction of loading, there is no error measure possible for this direction.

Table 3.3: MAPE' and MMAPE Factors for Force Measurement During the Calibration Tests

Test	MX		MY		MZ	
	MAPE'	MMAPE	MAPE'	MMAPE	MAPE'	MMAPE
Orientation 1	4.08	0.0165	1.54	0.0017	4.84	0.0076
Orientation 2	0[1]	0[1]	1.80	0.0020	0[1]	0[1]
Orientation 3	4.34	0.0175	1.06	0.0012	0.60	0.0010
Orientation 4	1.14	0.0046	2.06	0.0023	15.16	0.0266
Orientation 5	9.65	0.0389	3.13	0.0035	6.92	0.0122
Orientation 6	22.40	0.0905	1.06	0.0012	26.02	0.0457
Orientation 7	1.86	0.0075	1.28	0.0014	5.59	0.0098
Orientation 8	2.81	0.0113	2.06	0.0023	1.85	0.0033
Orientation 9	2.56	0.0103	1.79	0.0020	0.61	0.0011
Orientation 10	0.92	0.0037	1.42	0.0016	1.30	0.0023
Orientation 11	6.89	0.0278	1.40	0.0016	3.59	0.0063
Orientation 12	2.48	0.0100	2.61	0.0029	3.24	0.0057
Orientation 13	0.24	0.0010	2.83	0.0032	4.46	0.0078
Orientation 14	11.57	0.0467	1.20	0.0013	8.00	0.0141
Ice Test	8.45	0.0341	1.70	0.0019	7.10	0.0125

NOTE: 1. Due to the direction of loading, there is no error measure possible for this direction.

3.6 Discussion of Results

For the entire series of tests, the system generally performed well. Global force measurement errors had a MAPE' value of less than 2% in all cases, including the ice test. Orientation 1 had a direction of global loading such that the force was largely in the X and Y (1300 N and 8000 N, respectively) directions, and some loading in the Z direction (approximately 4000 N). The MAPE' values for all three measurement axes were less than 5% for both force and moment measurements.

Orientation 2 was a pull in the X and Z directions only, theoretically resulting in zero force along the Y axis of measurement and no moment about the X or Z axes. For this reason, no error analysis is available for these channels of measurement. In actual fact, small forces and moments were recorded along these zero load axes which were typically less than 10% of the recorded values along and about the intended axes. Imperfections of the orientation of the loading and measuring equipment during loading most likely resulted in some off-axis *loading for this test.* Global and axial errors MAPE' error values were all well below 2%.

Orientations 3 to 14 inclusive were a series of pulls along a variety of directions, and all with the exceptions of orientations of 4, 5 and 6 resulted in good MAPE' values along all axes of measurement of less than 5.55%.

Orientation 4 was a pull in which the Y load was less than half of that recorded in either the X or Z directions. The MAPE' index for the global force of this test was 1.37%, and the MAPE' for the X and Z directions were 0.54% and 3.41% respectively. The MAPE' for the force in the Y direction, however, was 13.94%, more than three times the error recorded on any other axis. Similarly, the moment about Z axis was unusually high, with a MAPE' value of 15.16%. Since the global errors are quite small, and inspection of the loading curves demonstrates that the percentage error is consistent throughout the loading range, it is theorized that once again, the equipment either shifted when being loaded or the direction of the applied load was incorrectly recorded. Similar observations may be made for tests conducted along Orientations 5 and 6. Orientation 5, in particular, was a loading scenario which was intended as extreme. The line of action of the force resulted in very little force being applied along the Y axis of the system, but it was significantly off centre, resulting in a very large moment about the Z axis. The transducer setup would never be subjected to this type of extreme loading scenario under regular loading conditions in the upcoming test program. Still, the global force measurements for orientations 5 and 6 had MAPE' values of 1.49% and 1.42% respectively.

MMAPE values were consistent as well. Again, the error indices were higher for tests on Orientations 4, 5, 6 and 7, as were the MAPE' indices, but this is expected. The global force values of the MMAPE were consistently very low (0.0004 - 0.0019), and the forces in the X and Z axes were also quite good. The MMAPE index for the force in the Y direction,

however, was the highest of the four calculated indexes in most cases (9 out of 14 tests). In all of these cases, the loading frame was positioned relative to the transducer setup such that loads being applied to it were mostly in the X and Z axes, resulting in small loads being measured with a high capacity system and consequently larger errors being recorded than on the other sensing axes. This example is demonstrated in the extreme by examining the loading direction and subsequent errors for Orientation 5, in which the transducer setup is loaded almost exclusively in the X and Z axes, but off-centre of the setup.

The Ice Test conducted was intended to simulate the effect on the transducer setup of having one plate submerged in ice water during the test program, while the other was in the open air during testing. With one of the loading plates chilled to approximately two degrees Celsius and the other at room temperature, the equipment was again loaded. The transducer setup performed well within specifications for this loading scenario, with MAPE' values for the global forces and the forces in the X, Y and Z directions of 1.59%, 0.93%, 1.05% and 4.16%, respectively, but the MAPE' values for the moment measurement axes were a little higher with values for the measurements about the X, Y and Z axes being 8.45%, 1.70% and 7.10% respectively.

Chapter 4

4.0 THE IMD TEST EQUIPMENT

The objective of the test program was to perform a series of ice structure interaction tests at a variety of scales. The equipment used in the program had to be structurally sound and simple enough that it would be possible to switch from one model to another in minimal time. A finite window of opportunity was available when equipment modifications could take place. This typically occurred after the ice sheet had been grown and the ridges manufactured, and while the ice was being tempered or its strength lowered. Working on the equipment was not possible during ice growth as it would have an effect on the crystal structure of the ice to be tested, affecting its material properties at the time of testing.

4.1 *The Model Test Structure*

Two model scales, 1:25 and 1:50 with three configurations were tested in this program. *Figure 4.1 is a photograph of the 1:25 scale large neck model mounted in the IMD tank.* Due to the nature of the geometry of the cone, it was possible to manufacture a model that could be converted from one scale to the other. This was done by manufacturing various sizes of necks and collars which could be attached to a universal lower cone. By changing the neck and collar of the model as well as the waterline diameter of the lower cone, the scale of the model structure could be altered. Dimensions of the three model configurations are shown in Figures 4.2, 4.3 and 4.4.

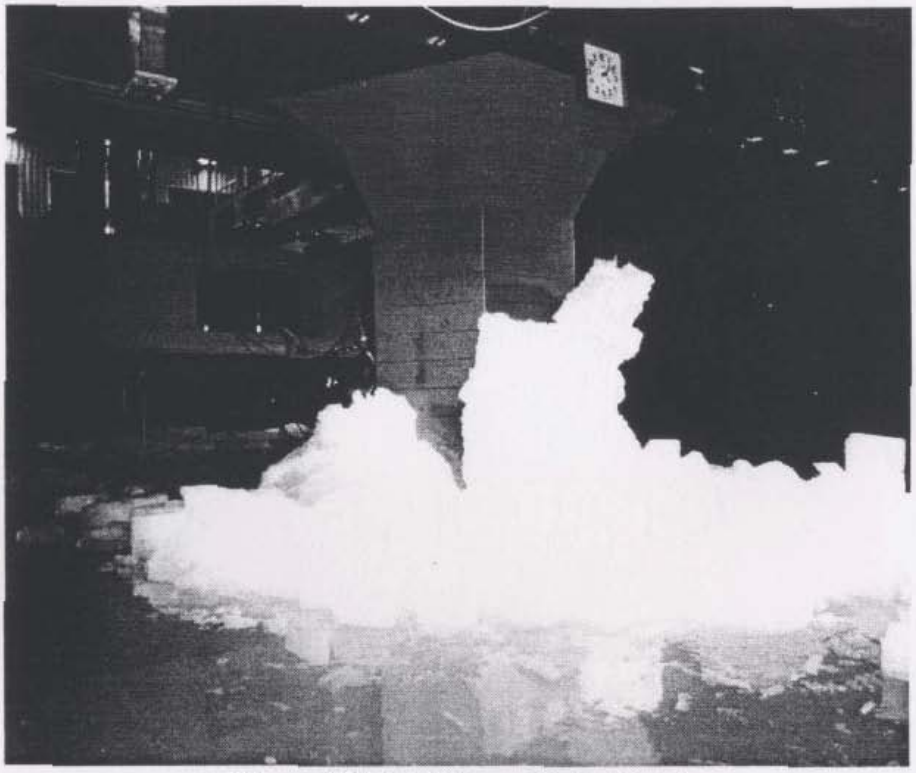

Figure 4.1: 1:25 Large Neck Model

The model was constructed of 6.35 mm thick marine grade aluminum plates welded to a rigid frame of 50 mm x 200 mm aluminum channel. It was designed to be as rigid as possible and of a modular construction to speed the change over of the model when testing two different neck sizes and two scales in a limited time period. The main component of the model was the lower cone structure to which various necks and collars could be attached to facilitate these changes.

Due to rigidity considerations, it was decided to attach the model directly to the IMD carriage as opposed to a model test frame. The model was attached to the underside of the IMD carriage

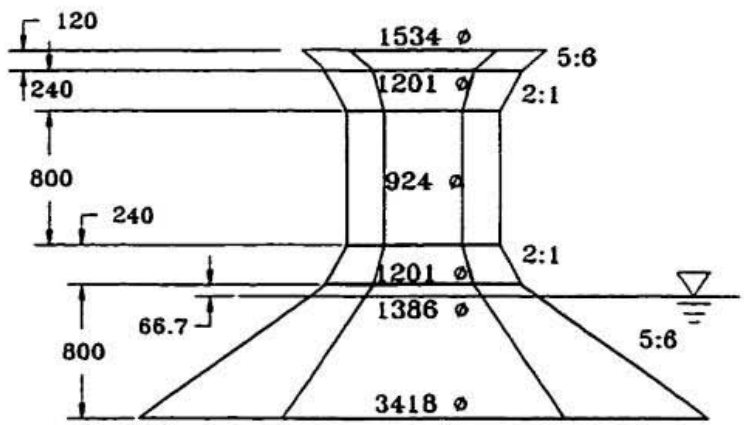

Note: All diameters are corner to corner;
All slopes are of the facet centers and given as a ratio of vertical:horizontal; and
All dimensions are in millimeters.

Figure 4.2: 1:25 Large Neck Model Dimensions

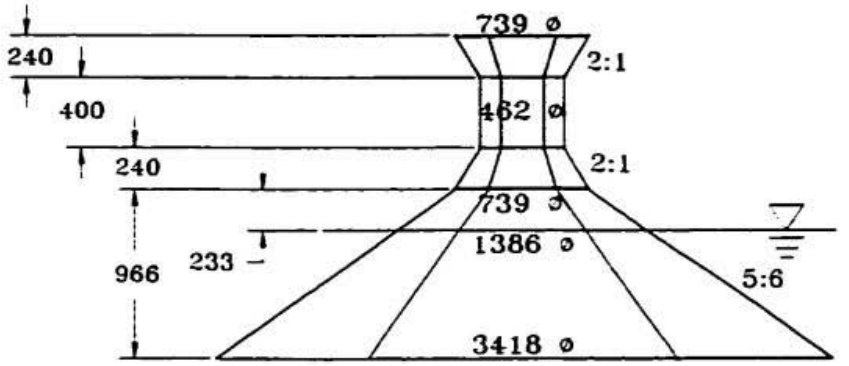

Note: All diameters are corner to corner;
All slopes are of the facet centers and
given as a ratio of vertical:horizontal; and
All dimensions are in millimeters.

Figure 4.3: 1:25 Small Neck Model Dimensions

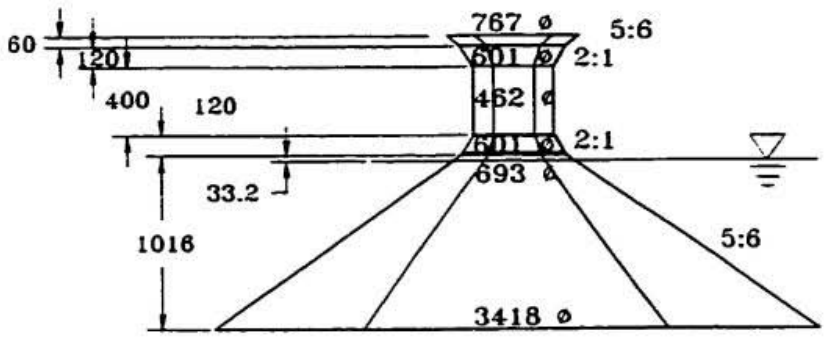

Note: All diameters are corner to corner;
All slopes are of the facet centers and
given as a ratio of vertical:horizontal; and
All dimensions are in millimeters.

Figure 4.4: 1:50 Large Neck Model Dimensions

using a specially designed towing post constructed from 300 mm x 300 mm x 12.7 mm steel box beam (Figure 3.1), and was instrumented to measure the global forces and moments on the entire structure as well as the forces on the vertical neck portion of the model.

Some of the equipment used in the calibration and verification of the load cell setup at the S.J. Carew Building was reused in the final test setup for the program. The load cell plate which had a truncated hexagonal bolt pattern was designed such that the model multi-faceted conical structure would be able to be mounted on it. In the final test program, this was the lower load cell plate.

4.2 Instrumentation and Data Acquisition System

The waterline was stationary relative to the scale model cone, but changed relative to the force measurement system when the model was changed (Figures 4.2, 4.3 and 4.4). Subsequently, the moment arms used for computations varied from one scale to another. The values of X_i, Y_i and Z_i for the 1:25 and the 1:50 scale models are given in Table 4.1.

The global force load cells located in the lower cone were partially submerged in one model configuration and completely submerged in the others. The load cells were waterproofed by the manufacturer and fitted with a water proof rubber 'boot' prior to installation to ensure

Table 4.1: The values of X_i, Y_i and Z_i for the 1:25 and the 1:50 scale models

1:25 Scale			
Load Cell I	X_i (m)	Y_i (m)	Z_i (m)
1	-0.293	0	-0.082
2	0.707	-0.278	-0.082
3	0.707	0.278	-0.082
1:50 Scale			
Load Cell I	X_i (m)	Y_i (m)	Z_i (m)
1	-0.293	0	-0.332
2	0.707	-0.278	-0.332
3	0.707	0.278	-0.332

that no water leaked into the transducer housings.

The force and moment instrumentation for the model set up had to be designed and manufactured especially for the program. No existing equipment had both the force and moment capacities for the expected loading scenarios of this program.

4.2.1 Neck Load Cells

Due to the three model configurations tested, two vertical neck sections were utilized in this test program. The large diameter neck was used in the 1:25 large neck model configuration (Figure 4.5) and was equipped with two AMTI model SRMC6-6-4000 dynamometers of capacity 17.8 kN (Nos. 4 and 5). A mounting unit for these load cells was rigidly attached to the cone and the vertical neck was rigidly attached to the dynamometers. The manufacturers specification sheets of the load cells are given in Appendix A.

The local axes for the individual neck load cells were oriented such that the Z' axes were parallel to the global Z axis, and the X' axes were out of phase with the global X axes by ± 30°, and the Y' axes were such that X', Y' and Z' formed a right hand coordinate system (Figure 3.5).

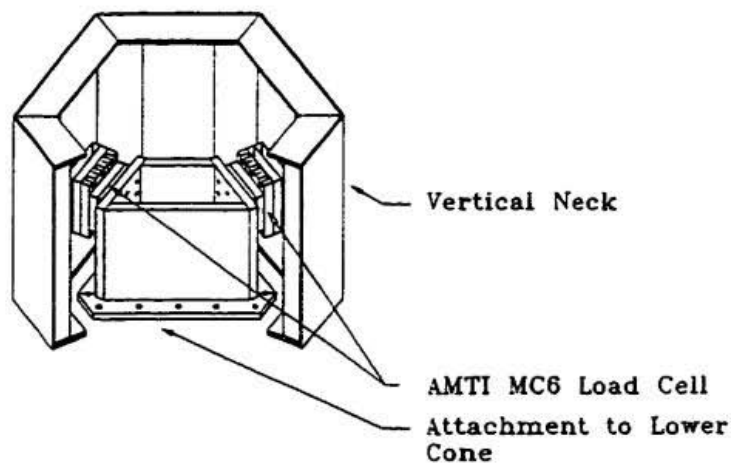

Figure 4.5: Neck load cell arrangement for the 1:25 large neck model

Using the known geometry of the system, the forces experienced by the neck were resolved to the global origin of the model. The following equations resulted:

$$F_{nX} = (F_{X'4}+F_{X'5}) \cos(30^o) + (F_{Y'5}-F_{Y'4}) \cos(60^o) \quad \textbf{(4.1)}$$

$$F_{nY} = (F_{Y'5}+F_{Y'4}) \cos(30^o) + (F_{X'4}-F_{X'5}) \cos(60^o) \quad \textbf{(4.2)}$$

$$F_{nZ} = F_{Z'4}+F_{Z'5} \quad \textbf{(4.3)}$$

where:

F_{nX} - Total neck force in the X direction

F_{nY} - Total neck force in the Y direction

F_{nZ} - Total neck force in the Z direction

$F_{X'4}$ - Measured force in the X' axis direction on load cell 4

$F_{Y'4}$ - Measured force in the Y' axis direction on load cell 4

$F_{Z'4}$ - Measured force in the Z' axis direction on load cell 4

$F_{X'4}$ - Measured force in the X' axis direction on load cell 5

$F_{Y'4}$ - Measured force in the Y' axis direction on load cell 5

$F_{Z'4}$ - Measured force in the Z' axis direction on load cell 5

Moments on the neck portion of the test structure were not to be measured in this test series.

The full scale structure would be made of welded steel plates with moments being applied to the neck portion of the structure only being an impossibility.

The small diameter neck was used in both the 1:25 small neck and 1:50 large neck model configurations. Due to size constraints, the models were fitted with only one of the SRMC6-6-4000 dynamometers. In a similar manner, the dynamometer was the connection point between the neck of the model and the lower cone (Figure 4.6).

The axis of the local coordinate system of the load cell used in the small diameter neck of the model was oriented such that the X', Y' and Z' axes were oriented in the same direction as the X, Y and Z axes of the global coordinate system. Consequently, the forces on the small diameter neck could be read directly from the transducer output.

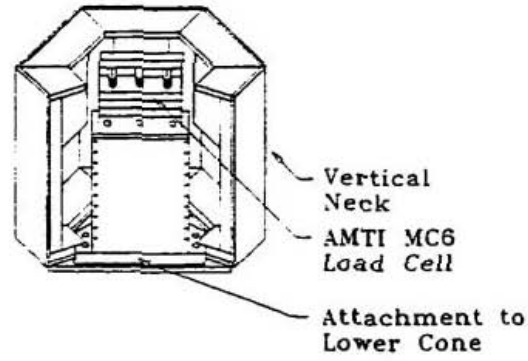

Figure 4.6: Neck load cell arrangement for the 1:50 large neck and 1:25 small neck models

4.2.2 Accelerometers and LVDT

Accelerations of the model in the three principal axes were measured using three Systron Donner accelerometers. The deflection of the tow pole and the

model were measured by two Schaevitz linear voltage displacement transducers (LVDT). The particulars of the accelerometers and displacement transducers, along with their specification date are given in Appendix A.

4.2.3 Data Acquisition System

A schematic arrangement of the data acquisition system is given in Figure 4.7. The data acquisition hardware was mounted in the towing carriage operators' room and was connected to appropriate transducers mounted on the model via cables passing under the floor. Excitation for the transducers was provided by a NEFF System 620 Series 300 signal conditioner available in the Ice Tank towing carriage. The transducer outputs from the load cells and the LVDT's were filtered by a 10 Hz analog low pass filter and digitized at a rate of 50 Hz whereas the accelerometer outputs were filtered by a 100 Hz analogue low pass filter and digitized at a rate of 200 Hz by a NEFF system 620 Series 100 amplifier/multiplexer and stored on a Vax 11/750 computer for analysis. The analog outputs of the transducer were recorded by a KYOWA RTP-600B 14 channel tape recorder as backup.

Data collected were down-loaded to the faculty's VAX cluster via ETHERNET for further analysis.

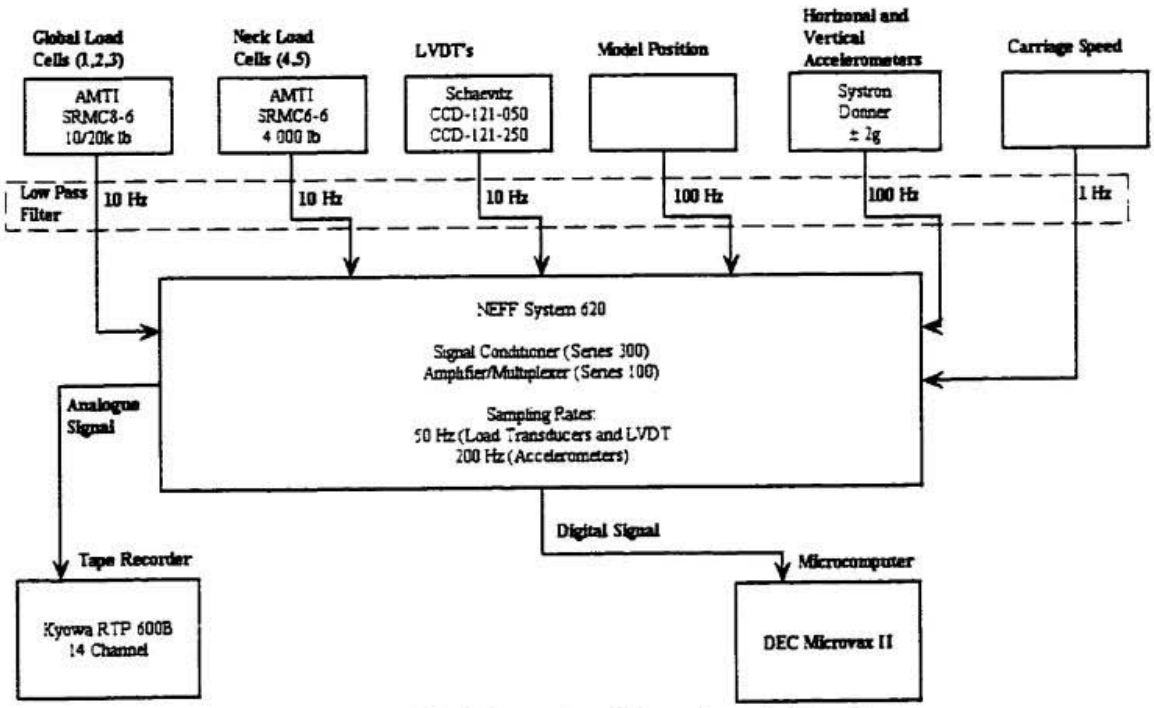

Figure 4.7: Schematic of Data Acquisition System

4.3 Test Program with Results

The test matrix, with details of the test program, is given in Table 4.2. It was developed to accommodate the testing of two scales (1:25 and 1:50) of model, two sizes of neck at one scale (1:25), and a variety of ridge and sheet ice strengths and thicknesses over a five week period. The models were tested in the face on orientation.

Five tests were performed on 14 model ridges in 5 ice sheets. In each test, level ice tests were performed at model velocities of 0.01 m/s, 0.04 m/s and 0.06 m/s to assess the effect

of different interaction rates. All ridge tests were performed at a velocity of 0.04 m/s.

Two types of ridge construction techniques were developed for this test program. The Dump Truck (DT) ridge was constructed by dropping slabs of sheet ice in a given location and breaking it up into smaller pieces. The result was a ridge made of sheet ice rubble with randomly oriented crystals. The Split Layer (SL) ridge was constructed by gently placing one layer of sheet ice atop another until the desired thickness of ridge was achieved. The material properties of the ice were adjusted by allowing them to temper by placing thermal blankets over the top of them and allowing them to warm while the sheet ice continued to freeze in the cold -20° C air. Typically, 1 DT ridge and 2 SL ridges were tested per ice sheet.

All DT ridges tested in this program simulated the 1 in 100 year multi-year ridge at the 1:50 scale (i.e. 54 cm thick and 14 kPa flexural strength); while, the SL ridges tested were designed to model conditions comparable to yearly average ice conditions found in the Canadian Arctic. It should be noted that the DT ridge tested with the model at the 1:50 scale (i.e. Test MUNCONE7_007, ridge thickness - 50 cm, ridge flexural strength - 23.8 kPa) specifically simulated the design loading condition for the Beaufort Sea.

The degree of variation in the model ice parameters throughout the St. John's test program permits the extrapolation of the test data to other scales by modifying the geometric scale of the model structure.

Table 4.2: Test Matrix for the Multifaceted Cone Tests - IMD

Test	Test Type	V (cm/s)	h (cm)	σ_{fu}^{-} kPa	H (cm)	σ_{FU}^{-} kPa	Ridge Type
Test Model: 1:25S; Sheet No. 1							
MUNCONE3_001	L	1	15.8	44.4			
MUNCONE3_002	L	6	15.8	44.1			
MUNCONE3_003	L+R	4	15.8	43.6	42.0	99.3	SL
MUNCONE3_004	R	4	15.8	42.5	32.0	48.7	SL
MUNCONE3_005	L	4	14.8	29.4			
MUNCONE3_006	R	4	14.8	29.3	50	16.2	DT
MUNCONE3_007	R	4	14.8	28.9	50	32.5	DT
Test Model: 1:25L; Sheet No. 2							
MUNCONE4_001	L	1	16.0	41.1			
MUNCONE4_002	L	6	16.0	40.6			
MUNCONE4_003	L	4	16.0	40.4			
MUNCONE4_004	R	4	16.0	40.2	43.5	112.2	SL
MUNCONE4_005	R	4	16.0	39.7	32.7	69.2	SL
MUNCONE4_006	L	4	16.4	19.7			
MUNCONE4_007	R	4	16.4	19.6	50	26.5	DT
Test Model: 1:25L; Sheet No. 3							
MUNCONE5_001	L	1	9.5	30.7			
MUNCONE5_002	L	6	9.5	30.2			
MUNCONE5_003	L+R	4	9.5	29.9	36.8	80.5	SL
MUNCONE5_004	R	4	9.5	27.3	50	10.9	DT
Test Model: 1:25L; Sheet No. 4							
MUNCONE6_001	R	4	12.4	22.5	33.4	65.5	SL
MUNCONE6_002	L	4	12.4	22.5			
MUNCONE6_003	L	1	12.4	22.5			
MUNCONE6_004	L	6	12.4	22.5			
MUNCONE6_005	R	4	12.4	22.5	50	12	DT
Test Model: 1:50L; Sheet No. 5							
MUNCONE7_001	L	1	16.0	33.7			
MUNCONE7_002	L	6	16.0	33.2			
MUNCONE7_003	L	4	16.0	32.8			
MUNCONE7_004	R	4	16.0	32.5	32.9	135.5	SL
MUNCONE7_005	R	4	16.0	32.0	32.9	135.5	SL
MUNCONE7_006	L	4	16.3	18.7			
MUNCONE7_007	R	4	16.3	18.4	50	23.8	DT

NOTES:
1. L - level ice test; R - ridge ice test
2. Ice flexural strength - Bottom in tension
3. SL - Split layer ridge; DT - Dump truck ridge
4. All tests run in face-on orientation.

Chapter 5

5.0 PERFORMANCE OF THE EQUIPMENT

The test equipment was installed in the IMD ice testing facility and verified prior to actual testing. Modifications, adjustments and checks of the setup had to be completed prior to the start of growth of the ice sheet. Any disturbance of the water during the formation of the ice crystals would have disturbed the ice crystal structure and significantly affected the sheets physical properties.

5.1 Load Cell Calibration

The manufacturer's specified transducer calibrations were again verified prior to the start of

the test series by applying known loads to the individual load cells, and used to compute the calibration coefficients for the individual force channels throughout the test program.

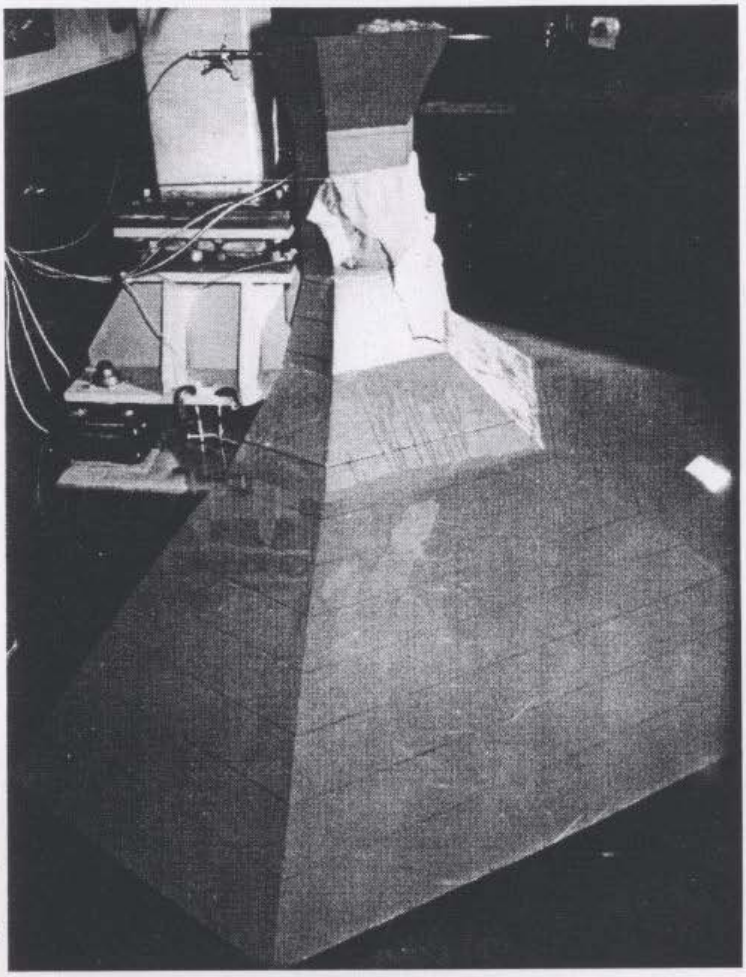

Figure 5.1: Load Cell Calibration Setup

In-situ calibrations of the load cells along all three principle axes were conducted both immediately after each model was installed and prior to each test to ensure that all force measurement systems were working properly. The origin of the coordinate system used was located in the appropriate place for the model configuration as presented in Chapter 4.

All force measurement systems were calibrated at the same time using the method shown in Figure 5.1. A steel cable was anchored to the IMD tow tank and wrapped around the neck portion of the model. Pads were placed between the cable and the model to protect the paint finish, essential to the friction characteristics of the model. A hand winch and calibration

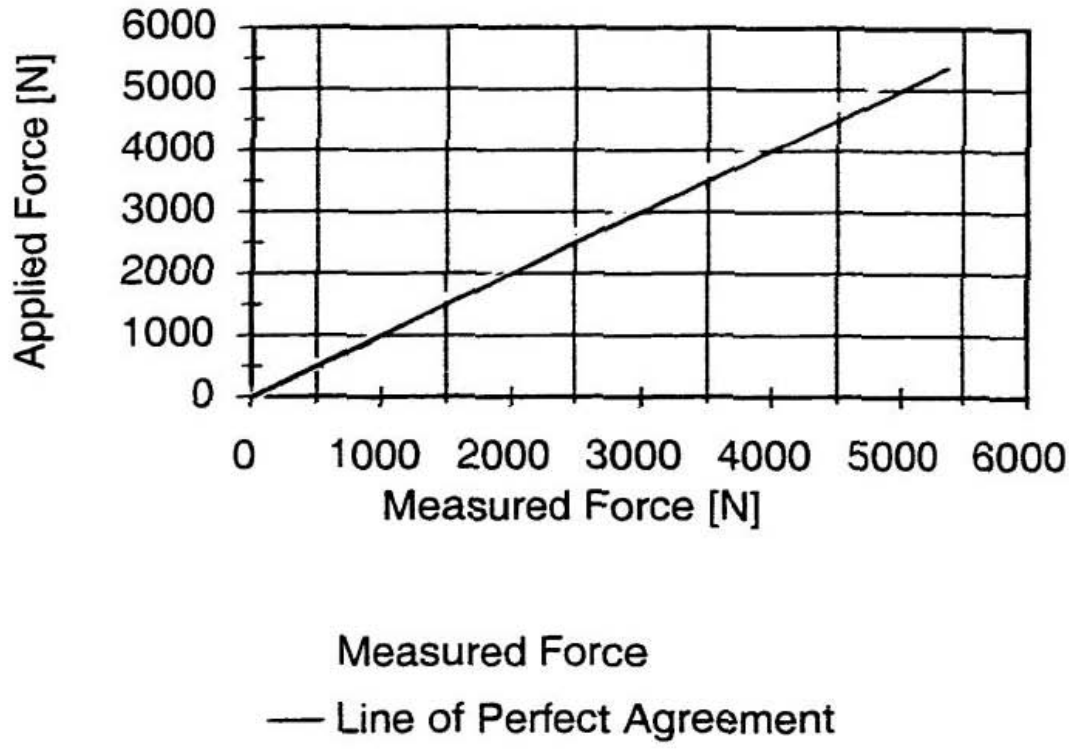

Figure 5.2: Global Force Calibration Data from Test Conecal 4

load cell were placed in series between the point where the cable was anchored and the model. Varying loads were applied to the structure using the hand winch and the reference force for comparison with the test equipment outputs was obtained from the in-line load cell.

Measurement of the precise line of action of the applied force was difficult in the tow tank with the equipment installed. For this reason, the forces in the X, Y and Z directions resolved from the test setup were vectorially summed and compared to the applied force as measured from the in-line load cell. A sample of the data from one of these calibration tests

is given in Figure 5.2. The test shown has a MAPE' of 4.40% and a MMAPE of 0.0049.

5.2 Natural Frequency of the Test Structure

For model testing purposes, it was essential that the natural frequency of the test structure be significantly higher than the ice breaking frequency during testing. This was to ensure that resonance in the model structure and force measurement equipment did not occur and interfere with the recorded force data.

In-situ free vibration tests were performed on each model configuration (Figure 5.3). In each test, the model was loaded up to 500 kg in the along-tank direction, and the loading cable was

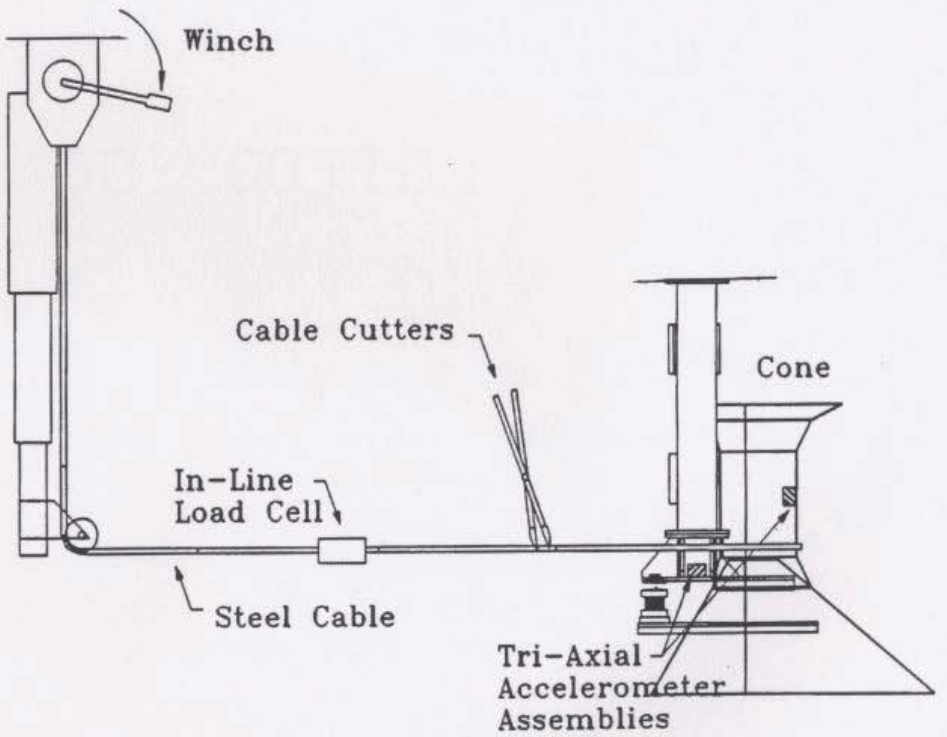

Figure 5.3: Setup for Dynamic 'Pluck" Test

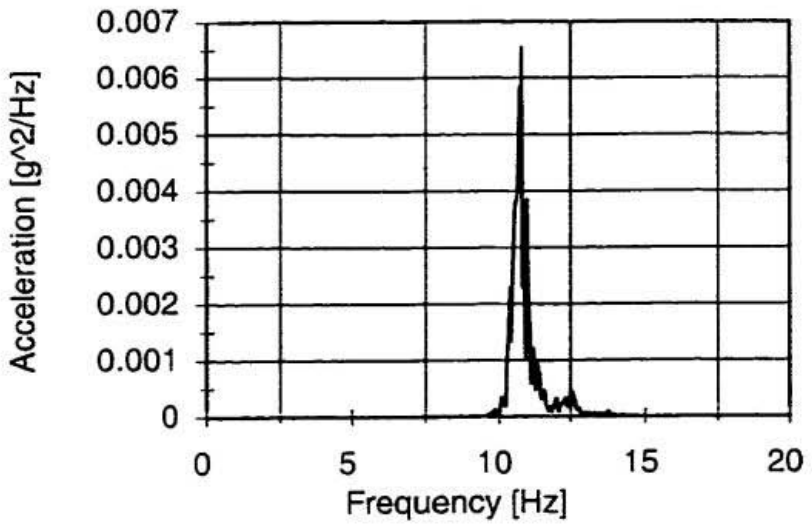

Figure 5.4: PSD analysis of acceleration data in the X direction

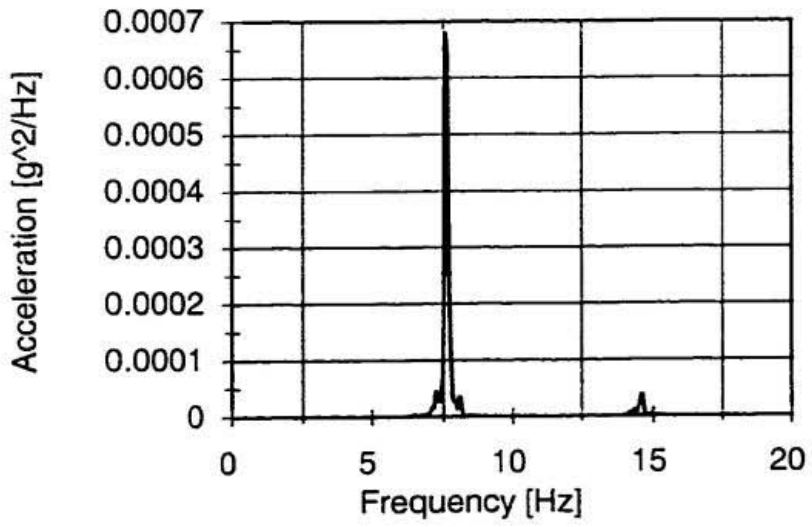

Figure 5.5: PSD analysis of cone acceleration in the Y direction

abruptly cut. All instrumentation and data acquisition systems, as well as real-time monitoring was operated during the test. Power Spectrum Density (PSD) analysis of the accelerometer signals (Figure 5.4, 5.5 and 5.6) showed a dominant frequency of the cone in the X direction at about 11 Hz, and two resonant frequencies of the cone in the Y

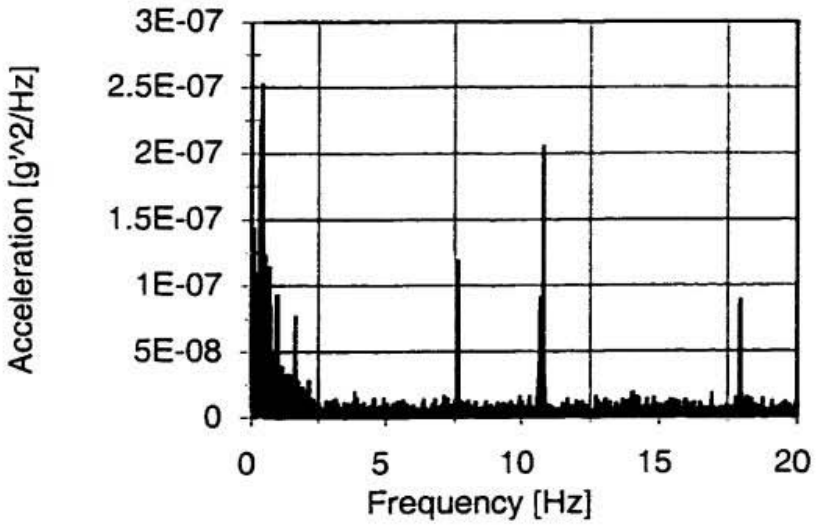

Figure 5.6: PSD analysis of post acceleration data in the X direction

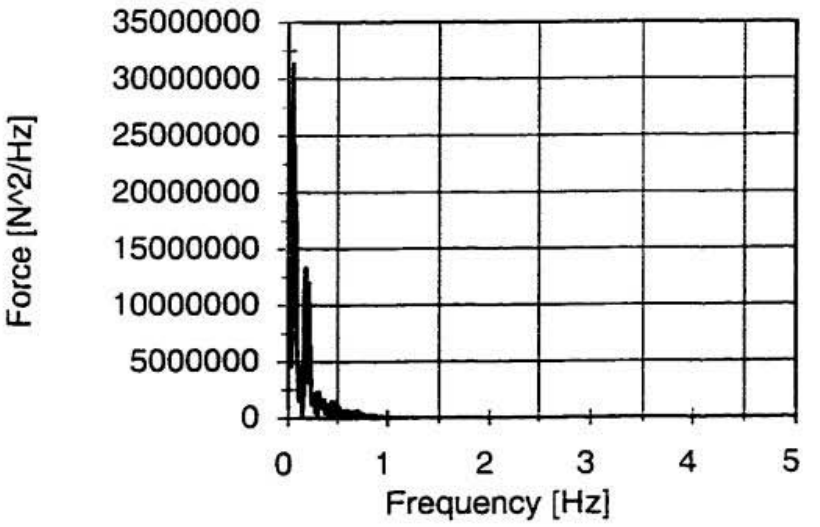

Figure 5.7: PSD analysis of ice force data in X direction

direction at approximately 8 and 14 Hz. The post alone was instrumented along the X axis only, and demonstrated resonant frequencies at 8, 12 and 17 Hz, with a resonance also being observed at slightly greater than one Hz as a consequence of resonance of the towing carriage itself. Acceleration data were also collected along the Z axis for the cone,

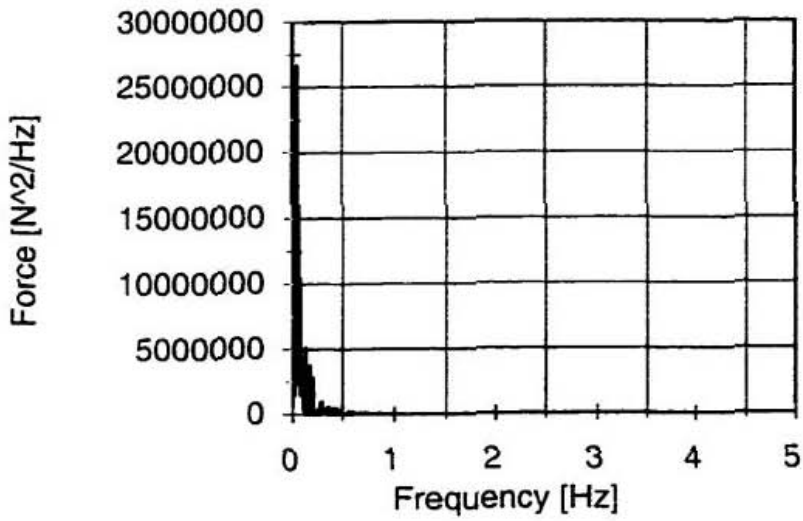

Figure 5.8: PSD analysis of ice force data in Y direction

but no distinct low frequency resonance was obvious, demonstrating the high stiffness of the towing system in this axis. The 8 Hz resonant frequency observed was due to the rigid and relatively heavy towing pole and model structure undergoing a rotational motion about the connection to the carriage while the higher frequencies were due to the model structure undergoing rotational motion about the centre of stiffness of the global load cell assembly.

The ice breaking length for the IMD's 1:25 scale model has been analyzed and was found to be approximately 0.1 characteristic length or 1 times the ice thickness. This is the case for test thicknesses ranging from 0.09 to 0.16 m independent of test velocity (from 0.01 to 0.06 m/s). The corresponding ice breaking frequency for the test velocity range (0.01 to 0.06) is less than one Hz for all tests with the 1:25 scale model. (i.e. 0.06m/s / 0.09 m = 0.666 m is the estimated higher limit.)

PSD analysis of the force data collected (Figures 5.7 and 5.8) demonstrated that only very low forcing frequencies on the order of 0.1 Hz were observed. The significant differences between the frequency of the forces on the model and the natural frequencies of the structure and towing system validate the effectiveness of the system for this test series.

5.3 Test Results

Test data were acquired using the equipment outlined in section 4.2.3 and were digitally filtered with an upper cutoff frequency of 2.75 Hz before plotting. The data for MUNCONE7_007 are presented in Figures 5.9, 5.10 and 5.11. This test was of the most extreme ice feature tested in this program, the one in one hundred year ridge, and resulted in the highest forces recorded as well.

For the test program, analysis of the force and moment data were broken into two sets. The level ice tests were studied separately from the ridge test data in an attempt to isolate the extreme ice feature tests. Peak forces and moments acquired during the ridge tests of the program are presented in Table 5.1.

The ridge test data had significantly higher peak loads. Forces in the X direction had a maximum value of approximately 25 kN and forces in the Z axis peaked at approximately 23 kN (MUNCONE4) while Y forces had a maximum value of approximately 2.5 kN (MUNCONE7). Y forces would only be significant in the cases where a large piece of ice cleared around one side or the other of the cone. For this same reason, moments about the Y axis were significantly greater than moments about the Z or X axes. Y moment had a peak value (MUNCONE3) of approximately 27 kN·m, while moments about the X and Z axes had a peak value of approximately 5.5 kN·m.

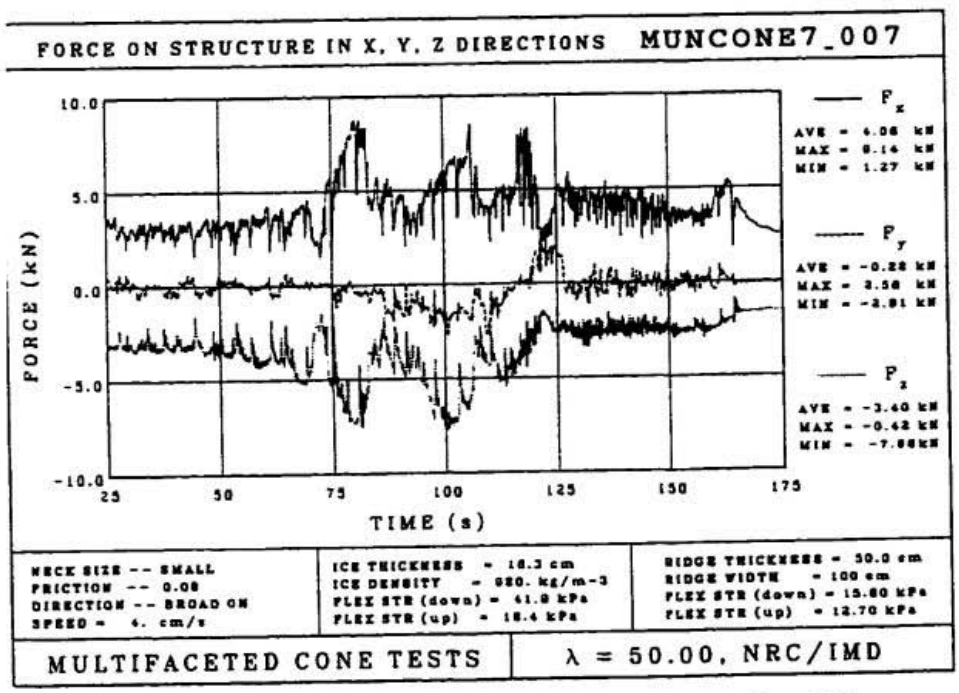

Figure 5.9: Time series trace of global forces in the X, Y and Z directions for test MUNCONE7_007

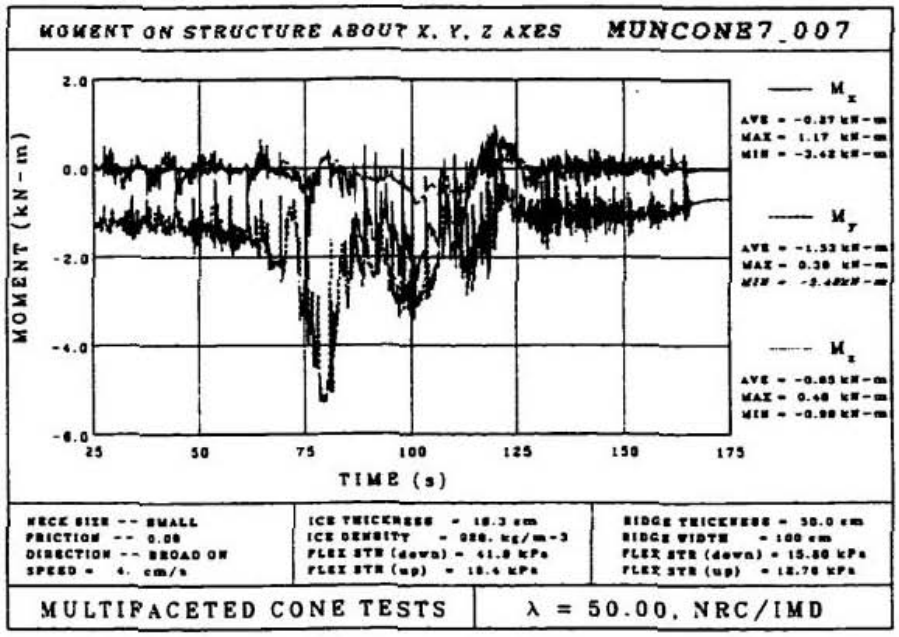

Figure 5.10: Time series trace of global moments about the X, Y and Z axes for test MUNCONE7_007

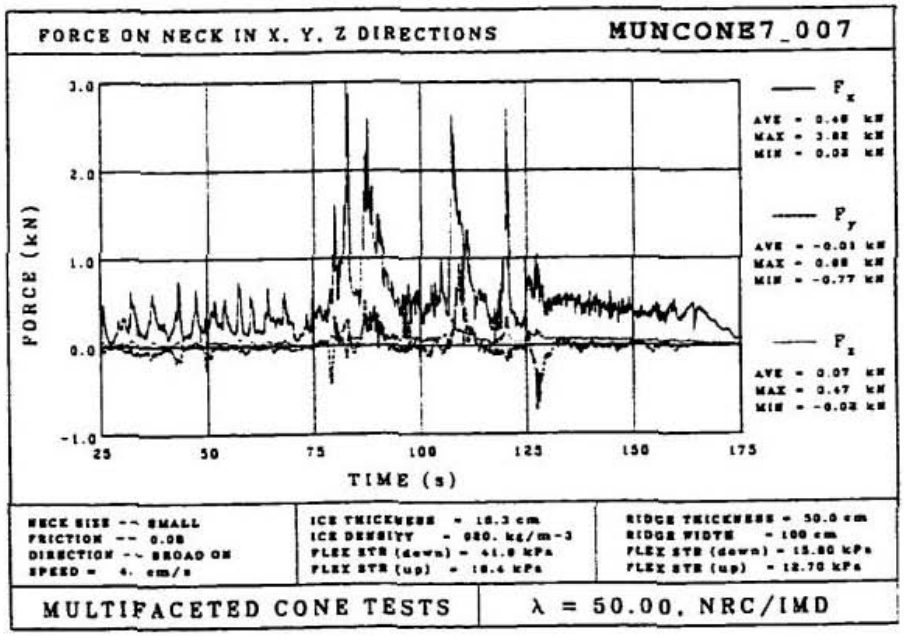

Figure 5.11: Time series trace of forces on the neck in the X, Y and Z directions for test MUNCONE7_007

Neck loads for the entire program were significantly less than those experienced globally as a result of all forces being applied to the neck being a consequence of already failed ice riding up the sloped side of the cone and clearing about the neck. Peak loads for the neck occurred in the X direction during ridge testing and resulted in peak forces of approximately 4 kN in the X direction (MUNCONE7), 2.6 kN in the Y direction (MUNCONE7), and 0.6 kN in the Z direction.

The data from the different scales of the program were subsequently analyzed (Lau et al. 1993; Croasedale et al, 1993), and it was determined that the data scaled as expected, verifying the integrity of the force measurement system.

Table 5.1: Summary of Ridge Test Results

Test	Maximum Global Forces			Maximum Global Moments			Maximum Neck Forces		
	F_x (kN)	F_y[1] (kN)	F_z[2] (kN)	M_x[1] (kN m)	M_y[3] (kN m)	M_z[1] (kN m)	F_{nx} (kN)	F_{ny}[1] (kN)	F_{nz} (kN)
MUNCONE3_003	21.1	1.8	20.8	2.6	26.9	2	2.1	0.2	1.3
MUNCONE3_004	14.6	1.4	14.9	2.3	16.2	2.6	0.7	0.2	0.1
MUNCONE3_006	9.1	2.3	10.9	2.5	8.9	1.2	1.3	0.1	0.2
MUNCONE3_007	12.4	1.9	12.6	3.2	12.7	1.9	1.4	0.5	0.2
MUNCONE4_004	25.5	3.3	23.5	5.4	31.8	2.2	2	1.2	0.3
MUNCONE4_005	14	1.6	12.7	2.2	14.4	2	1.1	0.3	0.3
MUNCONE4_007	14.8	3.1	13.5	3.5	16	3.3	2.8	0.4	0.6
MUNCONE5_003	5.1	0.4	4.5	1	5.8	1	0.2	0.1	0
MUNCONE5_004	7.7	2.1	7.6	2.4	7.1	0.8	1.2	0.5	0.3
MUNCONE6_001	10.9	1	10.4	1.4	11.8	1.2	1	0.2	0.2
MUNCONE6_005	8.6	1.6	8.8	2	8.5	1	1.2	0.4	0.2
MUNCONE7_004	15.2	2.5	14.9	1.4	10.9	1.4	2.8	2.6	0.6
MUNCONE7_005	19.8	1.9	19.7	2.3	14.7	1.2	2.2	1.1	4.3
MUNCONE7_007	9.1	2.9	8	3.4	5.5	1	3.8	1	0.5

Note: 1. Absolute maximum
2. Vertical downward
3. Moment, M_y, about negative Y axis

Chapter 6

6.0 CONCLUSIONS AND FINDINGS

Two sets of experiments were actually used to gauge the performance of this system. The first was a set of tests conducted in the Structures Laboratory of the S.J. Carew Building to study the performance of the system under a variety of loading conditions and two environmental conditions. The second was when the equipment was installed in the IMD for its intended purpose. Examination of the transducer data from the variety of calibration tests conducted permits an evaluation of the system for its intended purpose.

A total of fifteen calibration tests were performed on the global force transducer setup with 14 variations in the force line of action and one test in which one of the connection plates were chilled using ice, resulting in thermal contraction of the plate and loading of the individual load transducers.

Two measures were developed and used to gauge the performance of the transducers. The

first is the MAPE', which gives a good overall indication of the performance of the system along the indicated axis of measurement in the form of a percentage error. The second is the MMAPE, which is a version of the MAPE' desensitized to the capacity of the system along a specific measurement axis. This tool is a difficult one to use when gauging the performance overall, and is useful only for relative performance indices between axes where the same type of parameter (force, moment, etc..) is being measured.

A number of findings for this thesis are presented below:

1. The system generally performed well. The global force error index (MAPE') did not exceed 2% error for any of the tests performed, including the ice test which was intended to simulate the thermal conditions of the ice tank. Force measurements along each axis resulted in larger but still acceptable errors generally less than 5% with the exception of orientations 4, 5 and 6. In these cases, the errors recorded in the measurements of the forces along the Y axis were significantly higher. The direction of the loading in these cases was such that the force was mostly in the X and Z directions, and the minimum force was registered along the Y axis. These small forces measured on a system whose capacity is quite large resulted in larger errors between the measured and applied loads.

2. In addition, the correlation between measured and applied loads along each axis relied on determining the precise line of action of the load in three dimensions. Error in determining the anchor point for the hydraulic actuator used to load the system, or locating the system itself, or possibly the system shifting during the course of the test are all possible sources of error that would account for the discrepancy between the excellent results of the global forces and the larger errors of the resolved forces.

3. Once installed in the IMD for the performance of the final phase of the multifaceted conical structure tests, the equipment once again performed well. Calibrations performed prior to each test sheet of ice and between each run verified the integrity of the transducer setup throughout the program.

4. Power spectrum density analysis of the ice failure data collected during testing demonstrated that the loading frequency was of the order of 0.1 Hz, and the natural frequency of the structure was on the order of 10 Hz, ensuring that resonant action of the test equipment did not corrupt the results.

In the future, more detailed calibrations should be performed on this equipment using methods in which the precise direction and magnitude of the loads being applied with respect to the coordinate system of the force measurement system can be determined. Additionally, using a precise force vector for the applied load, coefficients may be determined for

correcting the output from this force measurement system.

The use of spherical bearings in this manner to protect force transducers from large moments should be further studied.

REFERENCES

Antkowiak, J.H., and Rencis, J.J., (1994), "Geometric Nonlinearities in the Design of Force Transducers", Advances in Engineering Software, Barking, London, England, pp. 11-16.

Cammaert, A.B., and Muggeridge, D.B., (1988), "Ice Interaction with Offshore Structures", Van Nostrand Reinhold, New York, New York.

Castillo, E., Losada, M.A., and Puig-Pey, J., (1997), "Probabilistic Analysis of the Number of Waves and Their Influence Inthe Design Wave Height of Marine Structures", Safety of Structures Under Dynamic Loading, (Tapir, Norwegian Institute of Technology), Trondheim, Norway, pp. 720-729.

Croasedale, K.R., and Muggeridge, D.B., (1993), "A Collaborative Research Program to Investigate Ice Loads on Multifaceted Conical Structures", Proc. 12th Intl Conf. On Port and Ocean Engineering under Arctic Conditions, Vol. 2, Hamburg, pp. 475-486.

Fan, L.C., and Jin, Y.G., (1990), "Ice Survey in Liao Dong Bay and Ice Force Measurement on JZ20-2-1 Platform", SMM '90, International Shipping and Marine Technology Market with Congress. Proceedings, Hamburg, Germany, pp. 133-137.

Irani, M.B., Timco, G.W., and Muggeridge, D.B., (1992), "Ice Loading on a Multifaceted Conical Structure", Technical Report IME-CRE-TR-005, National Research Council of Canada, Institute for Mechanical Engineering, Cold Regions Engineering, Ottawa, Ontario.

Lau, M., Jones, S., Tucker, J., and Muggeridge, D.B., (1993), "Model Ice Forces on a Multifaceted Cone", Proc. 12th Intl Conf. On Port and Ocean Engineering under Arctic Conditions, Vol. 2, Hamburg, pp. 537-546.

Lau, M., Tucker, J., Jones, S., and Muggeridge, D.B., (1993), "Model Ice Forces on an Upward Breaking Multifaceted Cone", NRC Canada Report, TR-1993-07.

Maatanen, M., (1977), "Ice Force Measurements at the Gulf of Bothnia by the Instrumented Kemi-I Lighthouse", Proc. 4th Intl. Conf. On Port and Ocean Engineering under Arctic Conditions, Vol. 2, St. John's, pp. 730-740.

Masroor, S.A., and Zachary, L.W., (1991), "Designing an All-purpose Force Transducer", The 1990 SEM Spring Conference on Experimental Mechanics, pp. 33-35, Albuquerque, NM.

McConnell, K.G., (1995), "Vibration Testing", John Wiley and Sons, New York.

McConnell, K.G., and Varoto, P.S., (1993), "A Model for Force Transducer Bending Moment Sensitivity and Response During Calibration", The 11th International Modal Analysis Conference, Vol. 1, pp. 364-368, Kissimmee, Florida.

Metge, M., and Tucker, J.R., (1990), "Multifaceted Cone Tests - Year Two, 1989-1990", Technical Report, Esso Resources Canada Limited, Calgary, Alberta.

Metge, M., and Weiss, R.T., (1989), "Multifaceted Cone Tests 1988-1989", Technical Report, Esso Resources Canada Limited, Calgary, Alberta.

Murray, J.J., Winsor, F.N., (1997), "Impact Forces on a Jacket Deck in Regular Waves and Irregular Wave Groups", The 1997 Offshore Technology Conference, pp. 45-54, Houston, Texas.

Nevel, D.E., (1972), "The Ultimate Failure of a Floating Ice Sheet", Proc. 2nd IAHR Ice Symposium, Leningrad, U.S.S.R., pp. 23-27.

Ralston, T.D., (1977), "Plastic Limit Analysis of Sheet Ice Loads on Conical Structures", Proc. IUTAM Symposium on Physics and Mechanics of Ice, Copenhagen, Ed. Tryde, P., Springer-Verlag, Berlin, 1980, pp. 289-308.

Saeki, H., Hamanaka, K., and Ozaki, A., (1977), Experimental Study on Ice Force on a Pile", 4th International Conference on Port and Ocean Under Arctic Conditions, St. John's, Newfoundland, Canada, pp. 695-706.

Spencer, D., Hill, B., Kirby, C., and Nevel D., (1991), "Properties of Multi-Year Ridges Built in IMD's Ice Tank", The 11th International Conference on Port and Ocean Engineering under Arctic Conditions, Vol. 2, pp. 635-648, St. John's, Newfoundland.

Wessels, E., and Jochmean, P., (1991), "Model/full scale correlation of ice forces on a jacket platform in Bohai Bay", Proc. 11th Intl. Conf. On Port and Ocean Engineering under Arctic Conditions, St. John's, Canada, pp.198-212.

Wessels, E., and Kato K., (1988), "Ice forces on fixed and floating conical structures", IAHR Ice Symposium. Proceedings, 9th, Sapporo, Japan, Vol.2, pp.666-691.

APPENDIX A

SPECIFICATION SHEETS

Angular contact spherical plain bearings

Sliding contact surfaces: hard chromium/PTFE

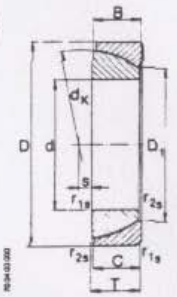

GE..SW - sliding material: PTFE fabric

Designation	Dimensions												
	d		D		B		d_K	D_1	C		T		
	mm												
GE 25 SW	25	-0,012	47	-0,014	15	±0,25	42,5	31,4	14	-0,20	14	-0,20	1
GE 28 SW	28	-0,012	52	-0,016	16	±0,25	47	35,7	15	-0,20	15	-0,20	1
GE 30 SW	30	-0,012	55	-0,016	17	±0,25	50	36,1	16	-0,20	16	-0,20	2
GE 32 SW	32	-0,012	58	-0,016	17	±0,25	53	39,3	16	-0,24	16	-0,24	2,5
GE 35 SW	35	-0,012	62	-0,016	18	±0,25	56	42,4	17	-0,24	17	-0,24	2
GE 40 SW	40	-0,012	68	-0,016	19	±0,25	60	46,8	18	-0,24	18	-0,24	1,5
GE 45 SW	45	-0,012	75	-0,016	20	±0,25	66	52,9	19	-0,24	19	-0,24	1,5
GE 50 SW	50	-0,012	80	-0,016	20	±0,25	74	59,1	19	-0,24	19	-0,24	4
GE 55 SW	55	-0,015	90	-0,018	23	±0,25	80	62	22	-0,30	22	-0,30	4
GE 60 SW	60	-0,015	95	-0,018	23	±0,25	86	68,1	22	-0,30	22	-0,30	5
GE 65 SW	65	-0,015	100	-0,018	23	±0,25	92	75,6	22	-0,30	22	-0,30	5
GE 70 SW	70	-0,015	110	-0,018	25	±0,25	102	82,2	24	-0,30	24	-0,30	7
GE 75 SW	*75*	*-0,015*	*115*	*-0,018*	*25*	*±0,25*	*105*	85,9	*24*	-0,30	*24*	-0,30	7
GE 80 SW	80	-0,015	125	-0,020	29	±0,25	115	90,5	27	-0,30	27	-0,30	10
GE 85 SW	85	-0,020	130	-0,020	29	±0,25	120	96,9	27	-0,40	27	-0,40	10
GE 90 SW	90	-0,020	140	-0,020	32	±0,25	130	103,3	30	-0,40	30	-0,40	11
GE 95 SW	95	-0,020	145	-0,020	32	±0,25	130	107,7	30	-0,40	30	-0,40	8
GE 100 SW	100	-0,020	150	-0,020	32	±0,25	140	114,3	30	-0,40	30	-0,40	12
GE 105 SW	105	-0,020	160	-0,025	35	±0,25	150	119,4	33	-0,40	33	-0,40	14
GE 110 SW	110	-0,020	170	-0,025	38	±0,25	160	125,8	36	-0,40	36	-0,40	15
GE 120 SW	120	-0,020	180	-0,025	38	±0,25	170	135,4	36	-0,40	36	-0,40	17
GE 130 SW	130	-0,025	200	-0,030	45	±0,35	190	148	42	-0,50	42	-0,50	20
GE 140 SW	140	-0,025	210	-0,030	45	±0,35	200	160,6	42	-0,50	42	-0,50	20
GE 150 SW	150	-0,025	225	-0,030	48	±0,35	213	170,9	45	-0,50	45	-0,50	21
GE 160 SW	160	-0,025	240	-0,030	51	±0,35	225	181,4	48	-0,50	48	-0,50	21
GE 170 SW	*170*	*-0,025*	*260*	*-0,035*	*57*	*±0,35*	*250*	194,3	54	-0,50	54	-0,50	27
GE 180 SW	180	-0,025	280	-0,035	64	±0,35	260	205,5	61	-0,50	61	-0,50	21
GE 190 SW	190	-0,030	290	-0,035	64	±0,35	275	211,8	61	-0,60	61	-0,60	29
GE 200 SW	200	-0,030	310	-0,035	70	±0,35	290	229,2	66	-0,60	66	-0,60	26
GE 220 SW	220	-0,030	340	-0,040	76	±0,35	320	251,6	72	-0,60	72	-0,60	30
GE 240 SW	240	-0,030	360	-0,040	76	±0,35	340	273,8	72	-0,60	72	-0,60	32
GE 260 SW	260	-0,035	400	-0,040	87	±0,35	375	298,8	83	-0,70	83	-0,70	33,5
GE 280 SW	280	-0,035	420	-0,045	87	±0,35	*400*	*312,5*	*83*	*-0,70*	*83*	*-0,70*	45
GE 300 SW	300	-0,035	460	-0,045	100	±0,35	430	341,2	96	-0,70	96	-0,70	38

Lightly printed designations indicate items belonging to the range of

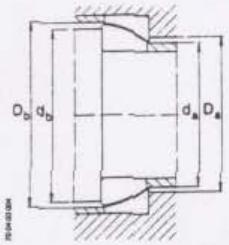

d	Basic load ratings (radial) dyn. C_r kN	stat. C_{0r} kN	Chamfer dimensions $r_{s\,min}$ mm	$r_{1\,min}$ mm	Mounting dimensions $d_{a\,min}$ mm	$d_{b\,max}$	$D_{a\,min}$	$D_{b\,min}$	Mass kg
25	71,0	140	0,6	0,2	30,1	39,5	34	43	0,14
28	90,0	180	1,0	0,3	34,4	42	40	48	0,18
30	95,0	190	1,0	0,3	34,6	45	40,5	51	0,22
32	102	204	1,0	0,3	37,9	47,5	44	54	0,24
35	116	232	1,0	0,3	41,1	50	47	57	0,28
40	134	270	1,0	0,3	45,5	54	52	61	0,34
45	160	320	1,0	0,3	51,7	60	58	67	0,43
50	176	355	1,0	0,3	57,9	67	65	75	0,47
55	220	440	1,5	0,6	60,7	71	70	81	0,70
60	240	480	1,5	0,6	66,9	77	76	87	0,75
65	260	520	1,5	0,6	74,4	83	84	93	0,80
70	315	630	1,5	0,6	80,9	92	90	104	1,0
75	325	655	1,5	0,6	84,7	95	94	107	1,1
80	375	750	1,5	0,6	88	104	99	117	1,6
85	400	800	1,5	0,6	94,4	109	105	122	1,7
90	480	965	2,0	0,6	100,8	118	112	132	2,2
95	490	980	2,0	0,6	105,4	119	117	132	2,3
100	520	1040	2,0	0,6	112	128	123	142	2,4
105	610	1220	2,5	0,6	116,8	137	129	152	3,0
110	710	1430	2,5	0,6	123,2	146	135	162	3,7
120	765	1530	2,5	0,6	132,9	155	145	172	4,0
130	965	1930	2,5	0,6	143,9	174	158	192	6,0
140	1020	2040	2,5	0,6	156,9	184	171	202	6,4
150	1180	2360	3,0	1,0	167,1	194	184	216	7,9
160	1340	2700	3,0	1,0	177,7	206	195	228	9,6
170	1660	3350	3,0	1,0	190,4	228	208	253	13,0
180	2000	4000	3,0	1,0	201,7	240	220	263	17,5
190	2080	4150	3,0	1,0	207,9	252	226	278	18,0
200	2360	4750	3,0	1,0	224,1	268	244	293	23,0
220	2850	5700	4,0	1,0	246,5	296	267	324	30,0
240	3050	6100	4,0	1,0	268,9	315	290	344	32,5
260	3900	7800	5,0	1,1	293,8	347	318	379	48,0
280	4150	8300	5,0	1,1	307,3	367	332	404	51
300	5200	10400	5,0	1,1	336,2	399	362	435	73







SRMC8 SERIES

MULTI-COMPONENT TRANSDUCERS

DESCRIPTION

The SRMC8 transducers have the highest capacity of AMTI's standard line of multi-component force and moment sensors. These precision sensors feature high stiffness, high sensitivity, low crosstalk, excellent repeatability and long-term stability. They exhibit the inherent ruggedness of bonded strain gage transducers and they incorporate special seals to prevent water and oil contamination.

The SRMC8 transducer is available with one to six outputs corresponding to Fx, Fy, Fz, Mx, My, and Mz. Standard vertical load capacities are 10,000 and 20,000 pounds. Horizontal load capacities are half of the vertical rating. Models with custom capacities and layouts are available for special applications.

The instrument has eight-inch square top and bottom plates manufactured from tool steel for heavy duty applications, and nickel plating protects the transducer from corrosion. Elastomeric O-ring seals protect the strain gages and wiring, while internal potting of the strain gages further insures long life and consistent, reliable performance.

AMPLIFICATION

The SRMC8 transducer incorporates strain gages and a precision element to isolate and measure applied forces and moments. As with all conventional strain gage transducers, bridge excitation and signal amplification are required. AMTI's MCA series amplifiers are high-gain devices which provide excitation and amplification for multiple channels in one convenient package. These amplifiers process the signals from a transducer and provide outputs suitable for an A/D converter and digital computer or other recording instrument.

APPLICATIONS

This instrument is particularly suitable for applications requiring simultaneous measurement of several forces and moments, or measurement of forces that change direction and position over time. Applications for this transducer include research and development in machining, robotics, and dynamics. These sensors are also well suited for monitoring production processes.

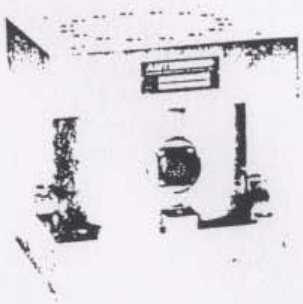

SPECIFICATIONS

The accompanying specifications are for estimating purposes. Actual precision calibrations are furnished with each instrument. The manufacturer reserves the right to alter the specifications without notice.

SRMC8 SERIES SPECIFICATIONS (English Units)

Model: SRMC8-X-	10000	20000	
CAPACITY			
Fz	10000	20000	lb
Fx,Fy	5000	10000	lb
Mz	20000	40000	in-lb
Mx,My	40000	80000	in-lb
TYPICAL SENSITIVITY			
Fz	0.14	0.07	$\frac{\mu V}{V\text{-}lb}$ **
Fx,Fy	0.66	0.33	
Mz	0.14	0.07	$\frac{\mu V}{V\text{-}in\text{-}lb}$ **
Mx,My	0.14	0.07	
STIFFNESS			
Fz	2.5	5.0	$x10^6$ lb/in
Fx,Fy	0.6	1.2	
NON-LINEARITY			
Fx,Fy,Fz	0.2	0.2	±%FSO***
HYSTERESIS			
Fx,Fy,Fz	0.2	0.2	%FSO***
RESONANT FREQUENCY			
Fz	1200	1700	Hertz
Fx,Fy	800	1100	Hertz

μV = microvolts, *%FSO = %Full Scale Output

* U.S. Patent #4493220

Bulletin SRMC8-987

AMTI
ADVANCED MECHANICAL TECHNOLOGY, INC.

SRMC8 SERIES SPECIFICATIONS (Metric Units)

Model: SRM8-X-	10000	20000	
CAPACITY			
Fz	44500	89000	N
Fx,Fy	22250	44500	N
Mz	2260	4520	N-m
Mx,My	4520	9040	N-m
TYPICAL SENSITIVITY			
Fz	0.03	0.02	$\frac{\mu V}{V\text{-}N}$
Fx,Fy	0.15	0.07	
Mz	1.24	0.62	$\frac{\mu V}{V\text{-}N\text{-}m}$
Mx,My	1.24	0.62	
STIFFNESS			
Fz	43.8	87.6	$\times 10^7$ N/m
Fx,Fy	10.5	21.0	
NON-LINEARITY			
Fx,Fy,Fz	0.20	0.20	±%FSO
HYSTERESIS			
Fx,Fy,Fz	0.20	0.20	%FSO
RESONANT FREQUENCY			
Fz	1200	1700	Hertz
Fx,Fy	800	1100	Hertz

GENERAL SPECIFICATIONS

Excitation: 10V
Temperature Range: 0 to 125°F (-17 to 52°C)
Sensitivity change with temperature:
0.02%/°F (0.01%/°C)
Crosstalk: Less than 2% on all channels
Weight: 80 lb (36 Kg)

WIRING

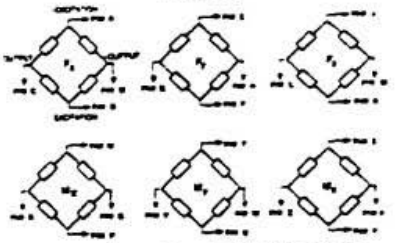

Connector Type: Burndy BTO2E16-26P

SRMC8 — X — XXXX

Series
No. of Channels
Capacity

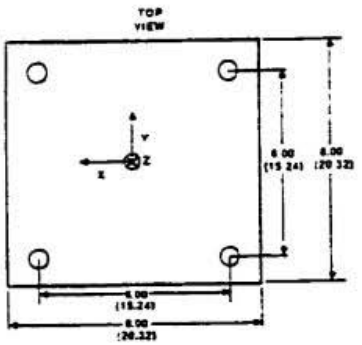

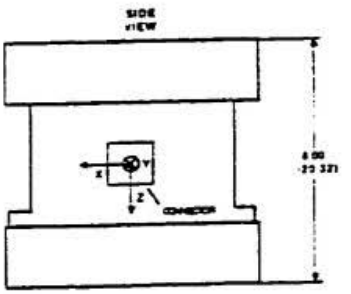

- Four 5/8-11 threaded mounting holes on 6 inch (15.24) centers on top and bottom; will accept 1/2" bolts for through mounting.
- Metric threaded hold-down inserts available.
- All dimensions in inches (cm).

AMTI
ADVANCED MECHANICAL TECHNOLOGY, INC.

APPENDIX B

CALIBRATION TEST RESULTS

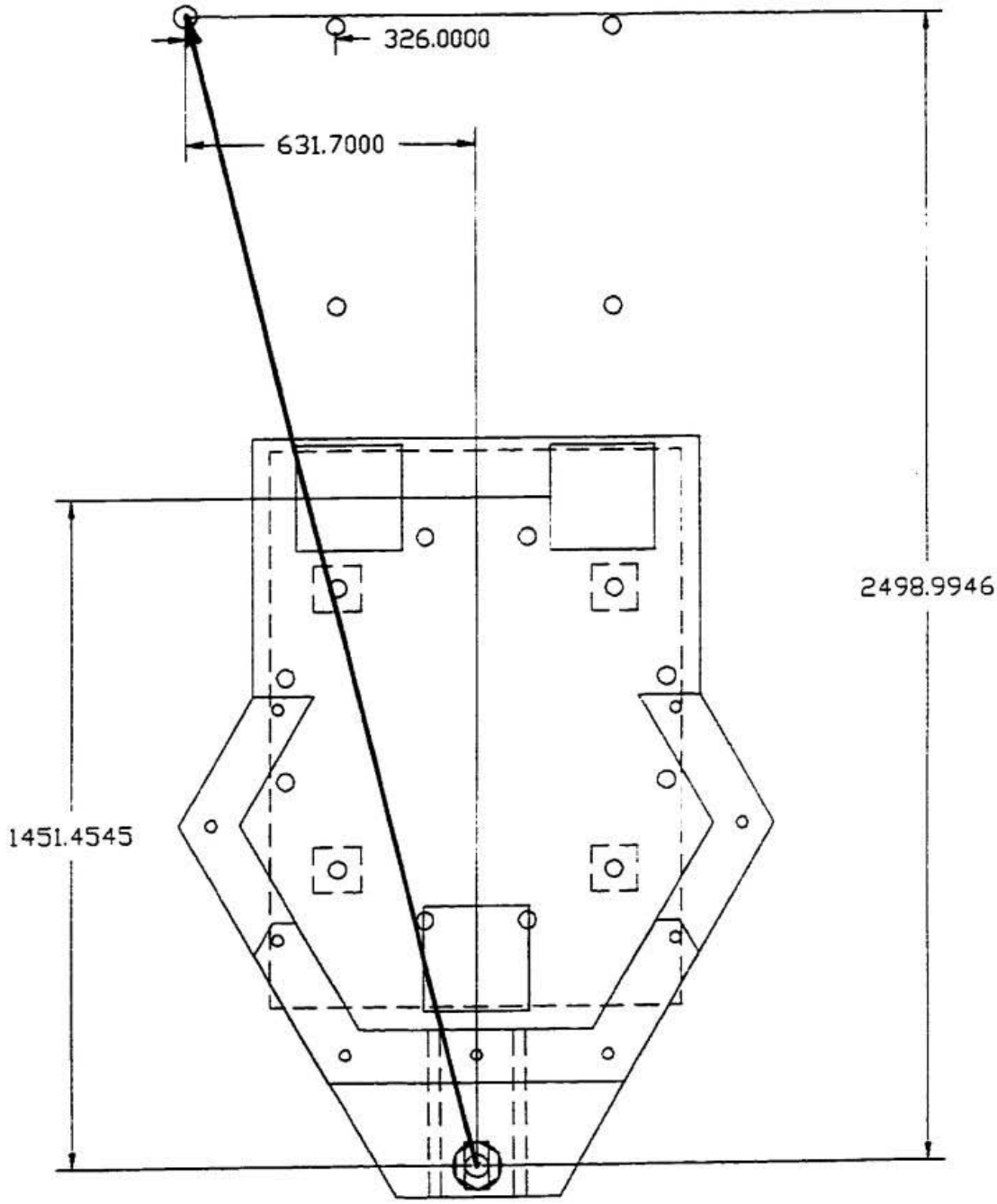

Figure B-1: Direction of Load Application - Orientation 1

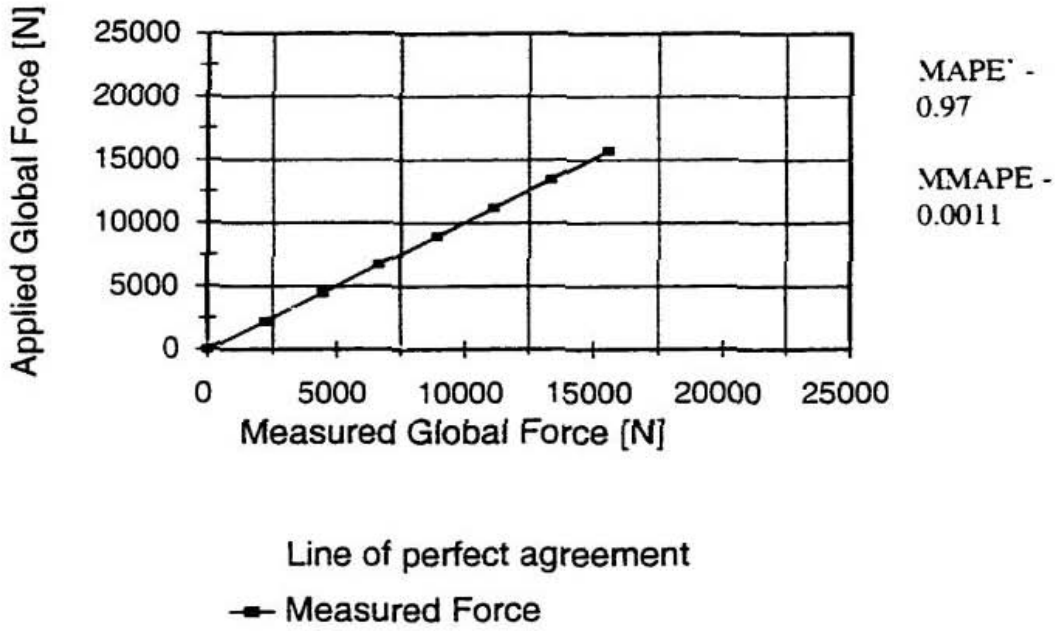

Figure B-2: Global Force Comparison - Orientation 1

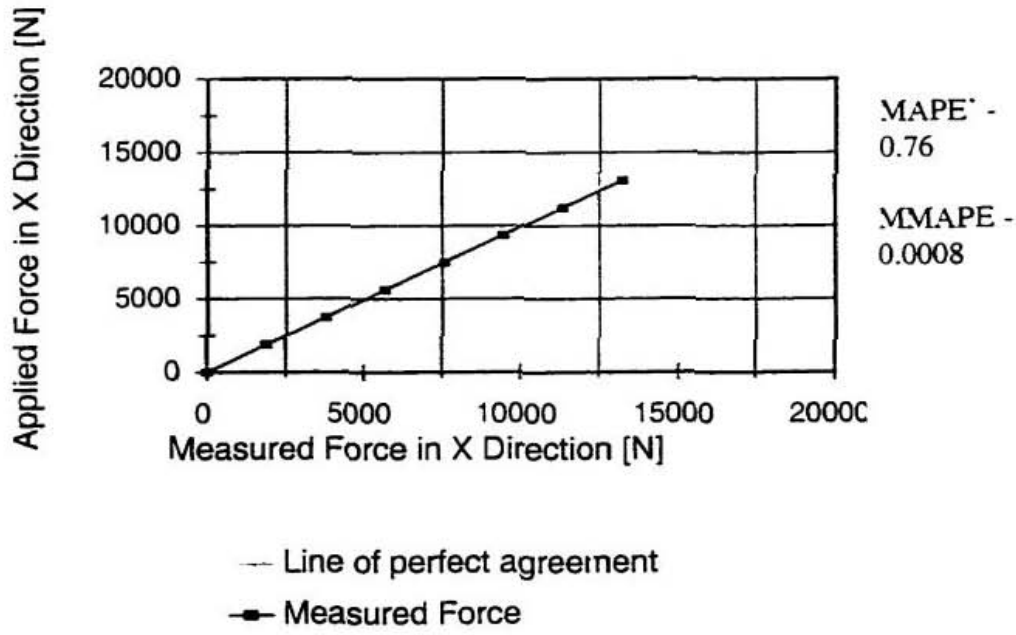

Figure B-3: Comparison of Forces in X Direction - Orientation 1

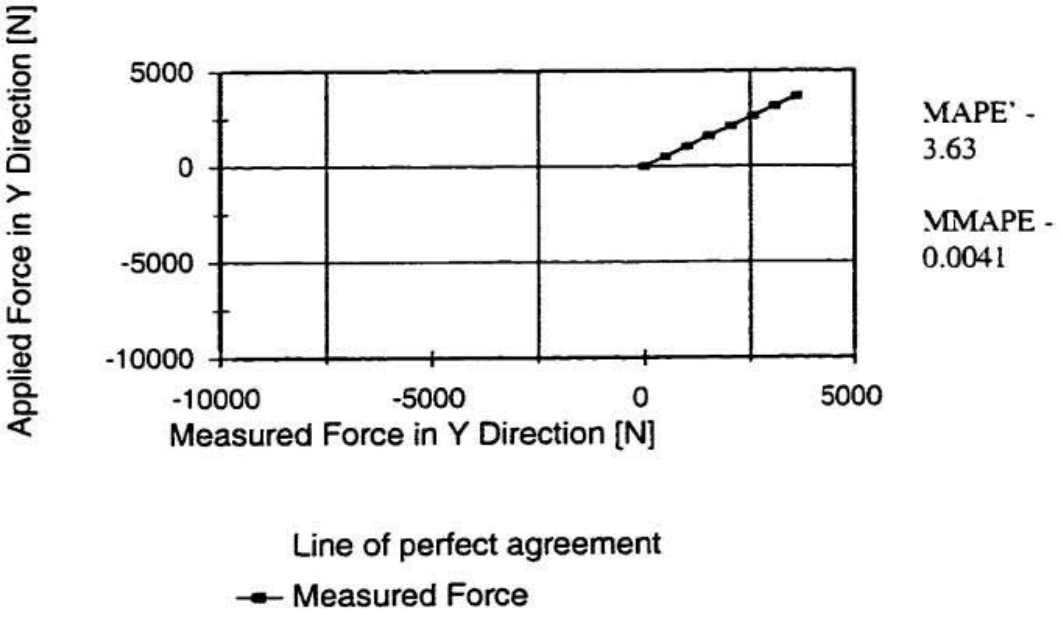

Figure B-4: Comparison of Forces in Y Direction - Orientation 1

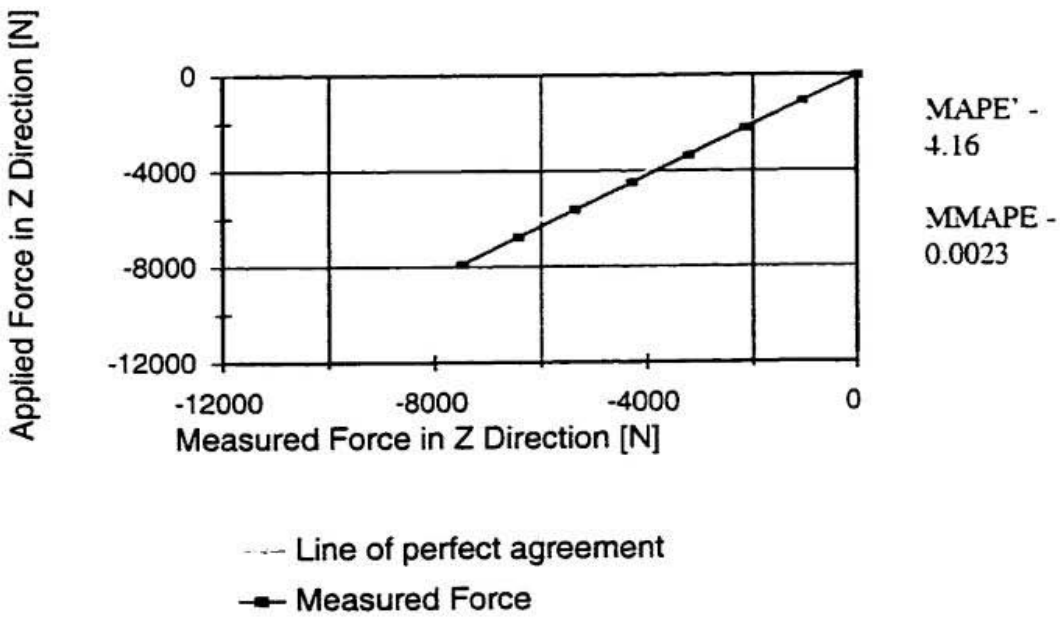

Figure B-5: Comparison of Forces in Z Direction - Orientation 1

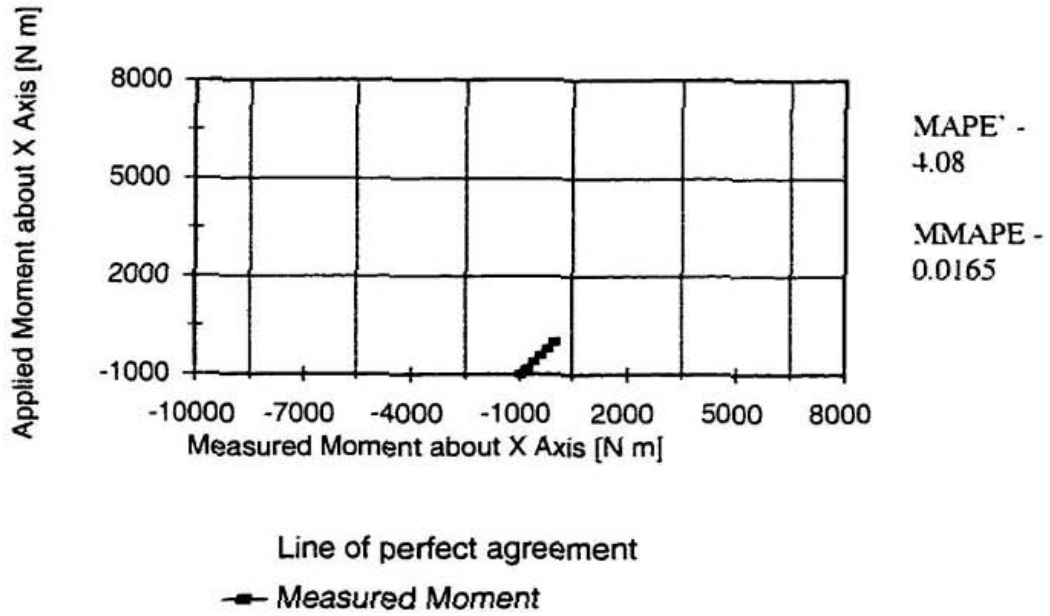

Figure B-6: Comparison of Moments About X Axis - Orientation 1

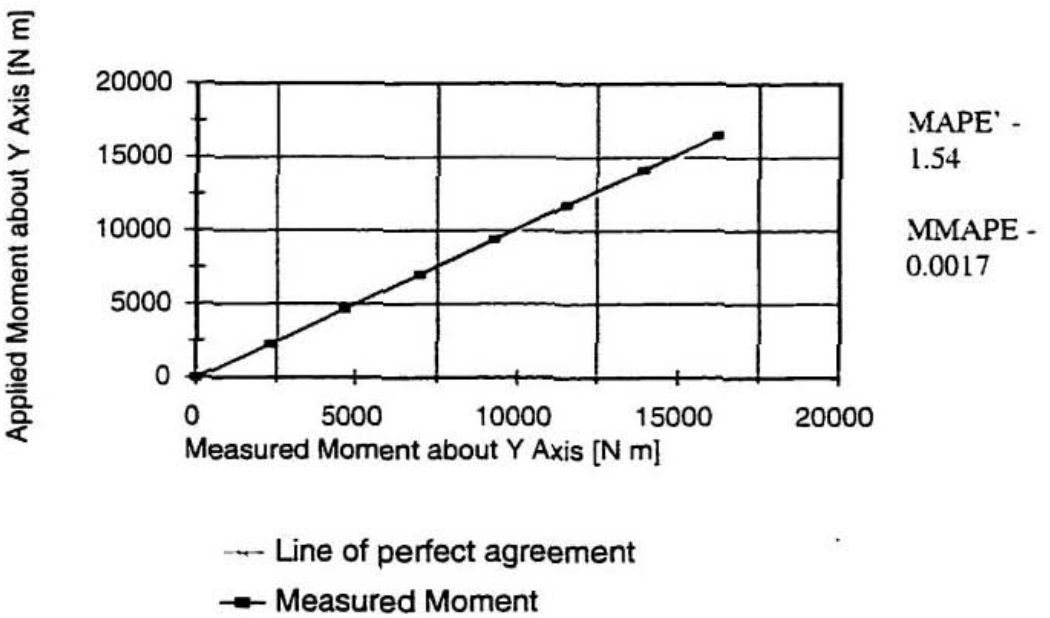

Figure B-7: Comparison of Moments about Y Axis - Orientation 1

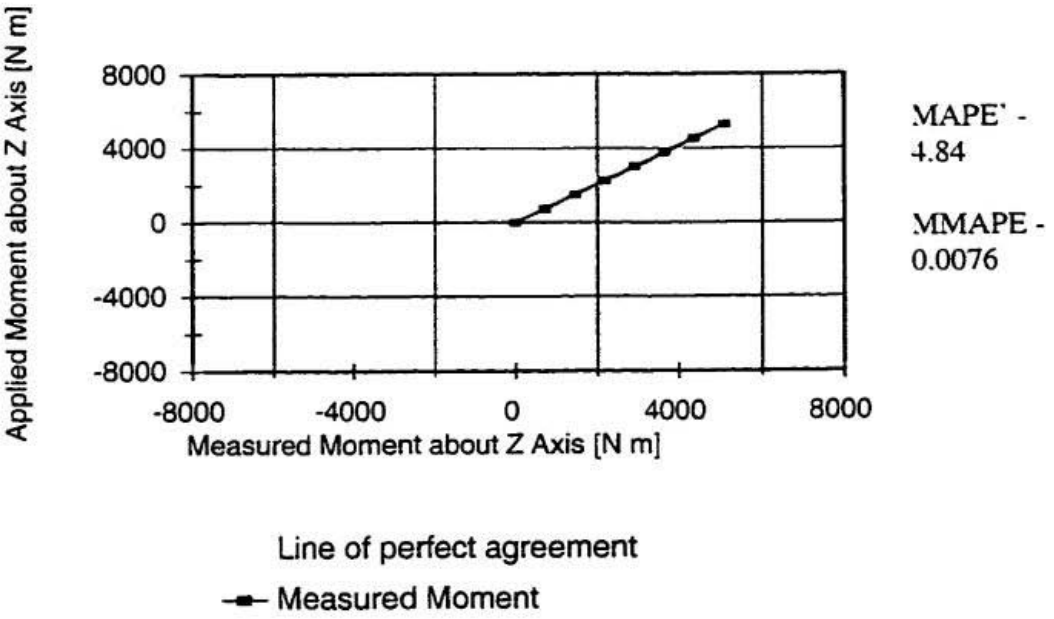

Figure B-8: Comparison of Moments about Z Axis - Orientation 1

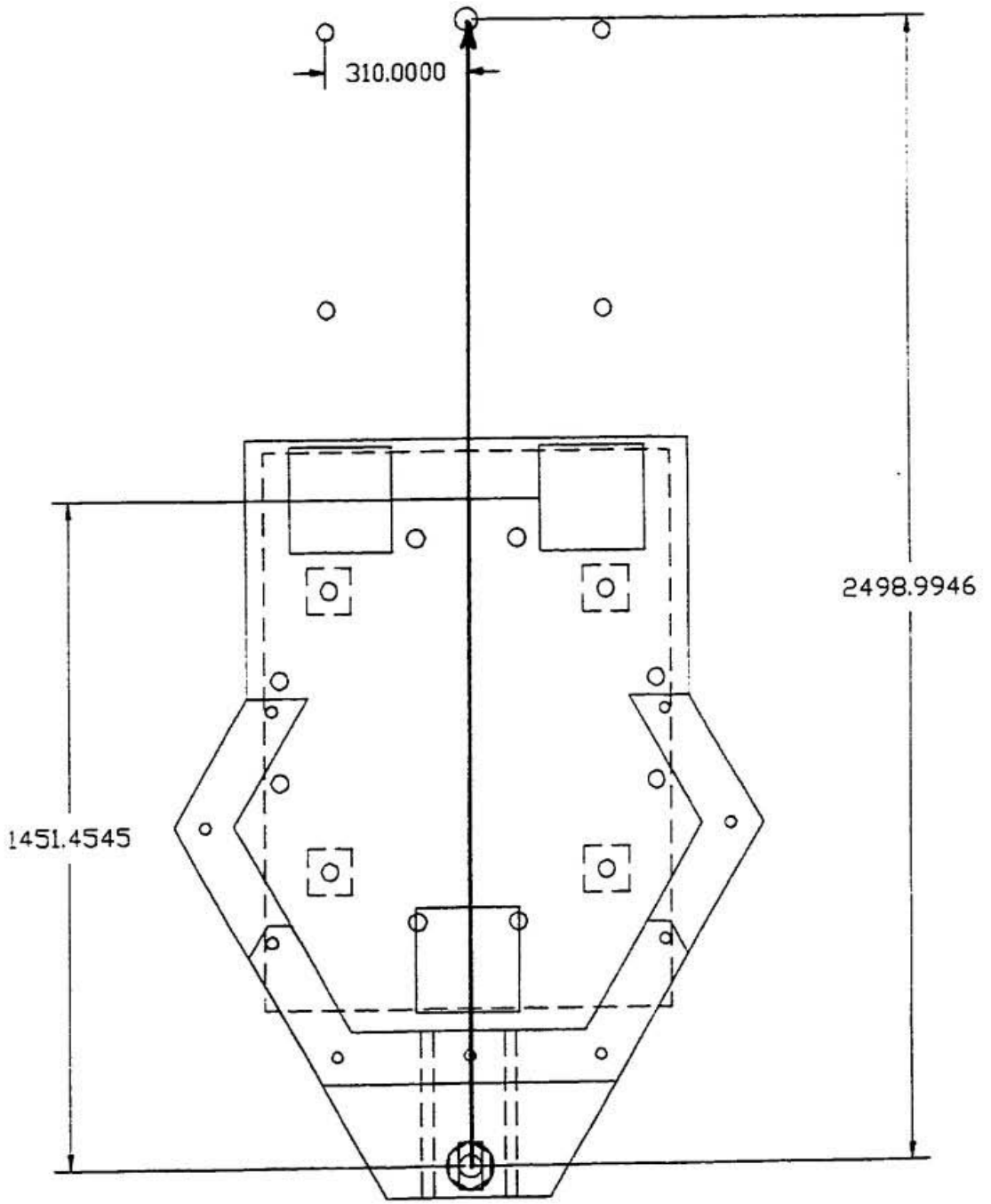

Figure B-9: Direction of Load Application - Orientation 2

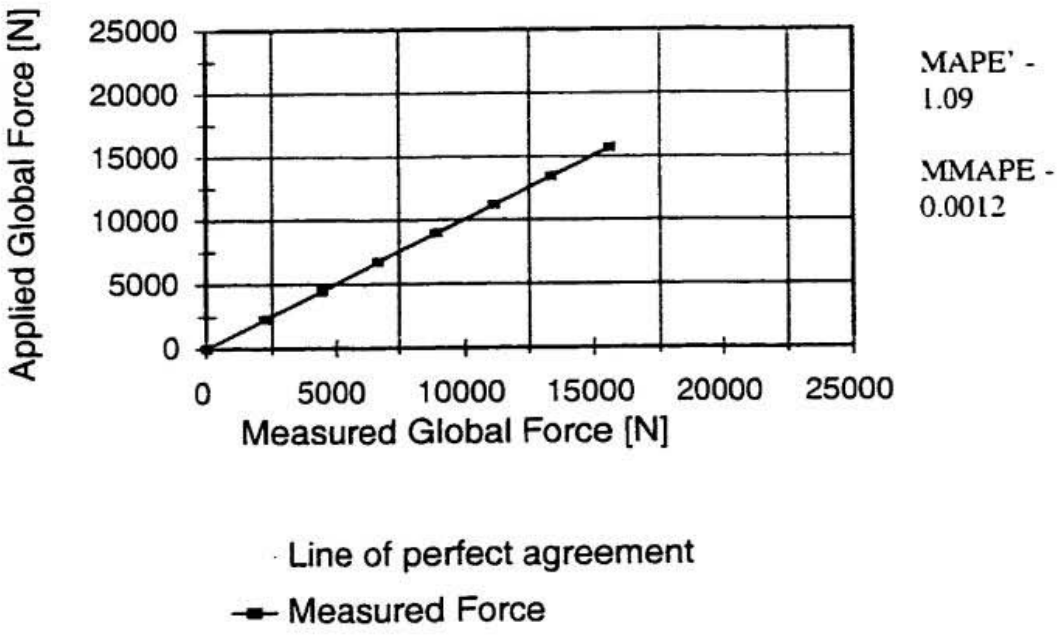

Figure B-10: Global Force Comparison - Orientation 2

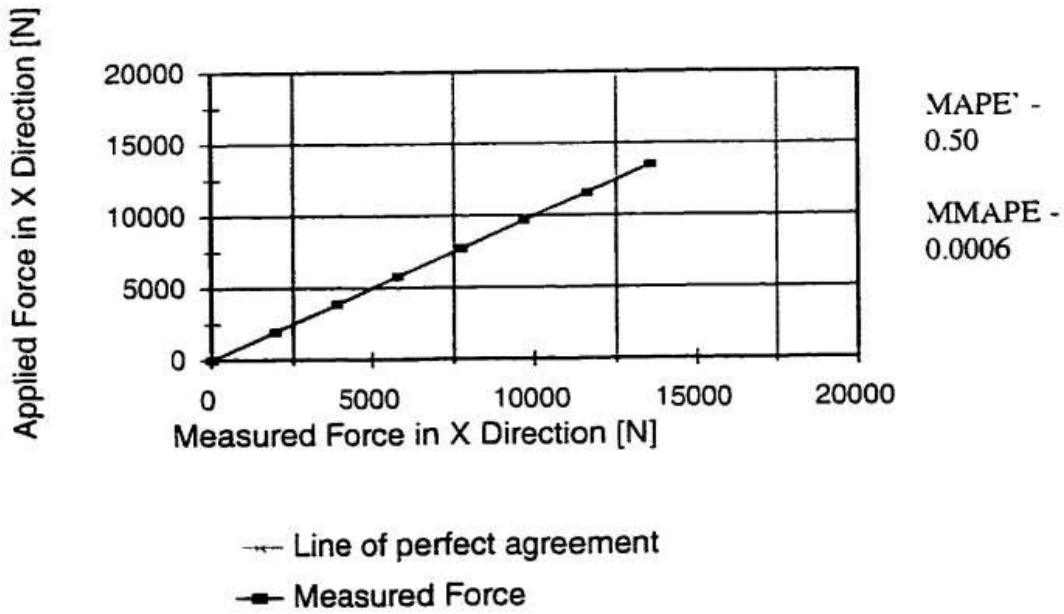

Figure B-12: Comparison of Forces in X Direction - Orientation 2

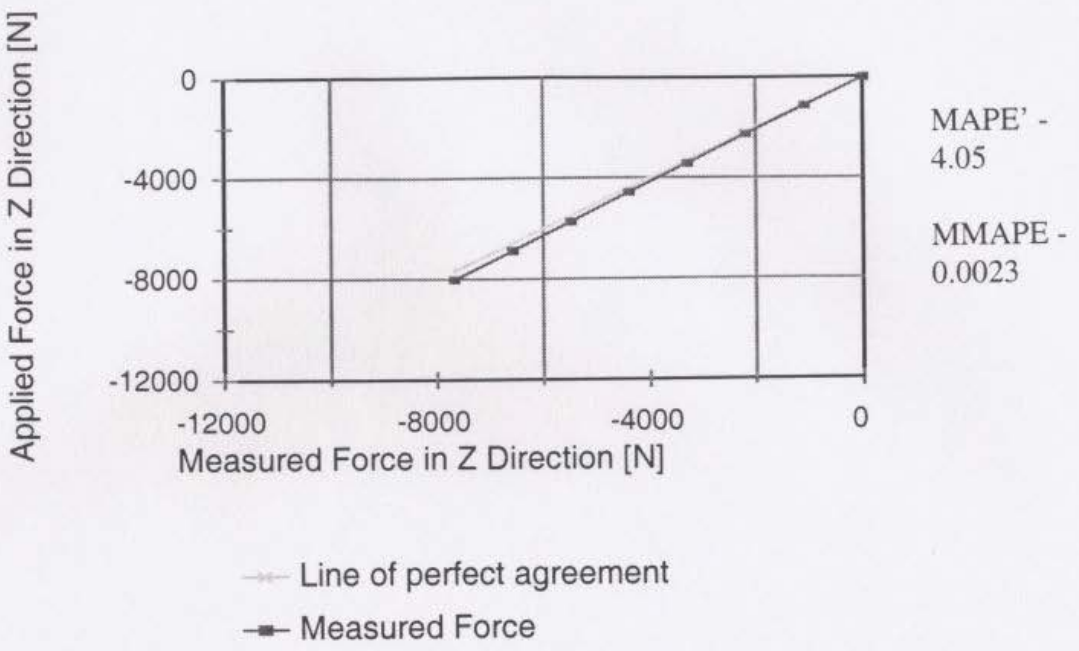

Figure B-13: Comparison of Forces in Z Direction - Orientation 2

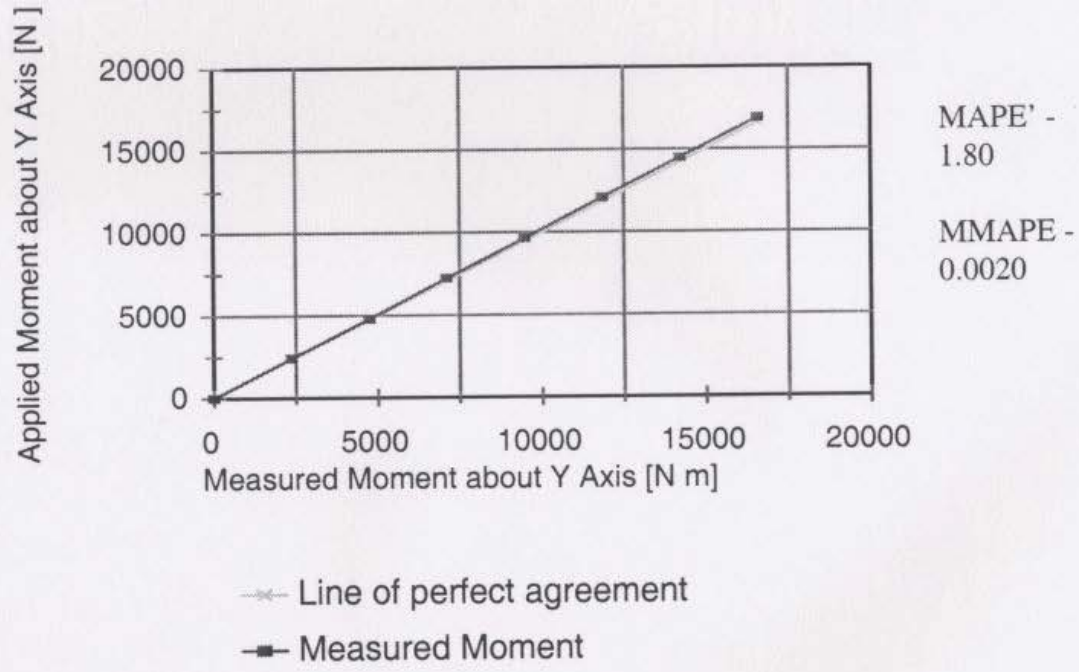

Figure B-14: Comparison of Moments about Y Axis - Orientation 2

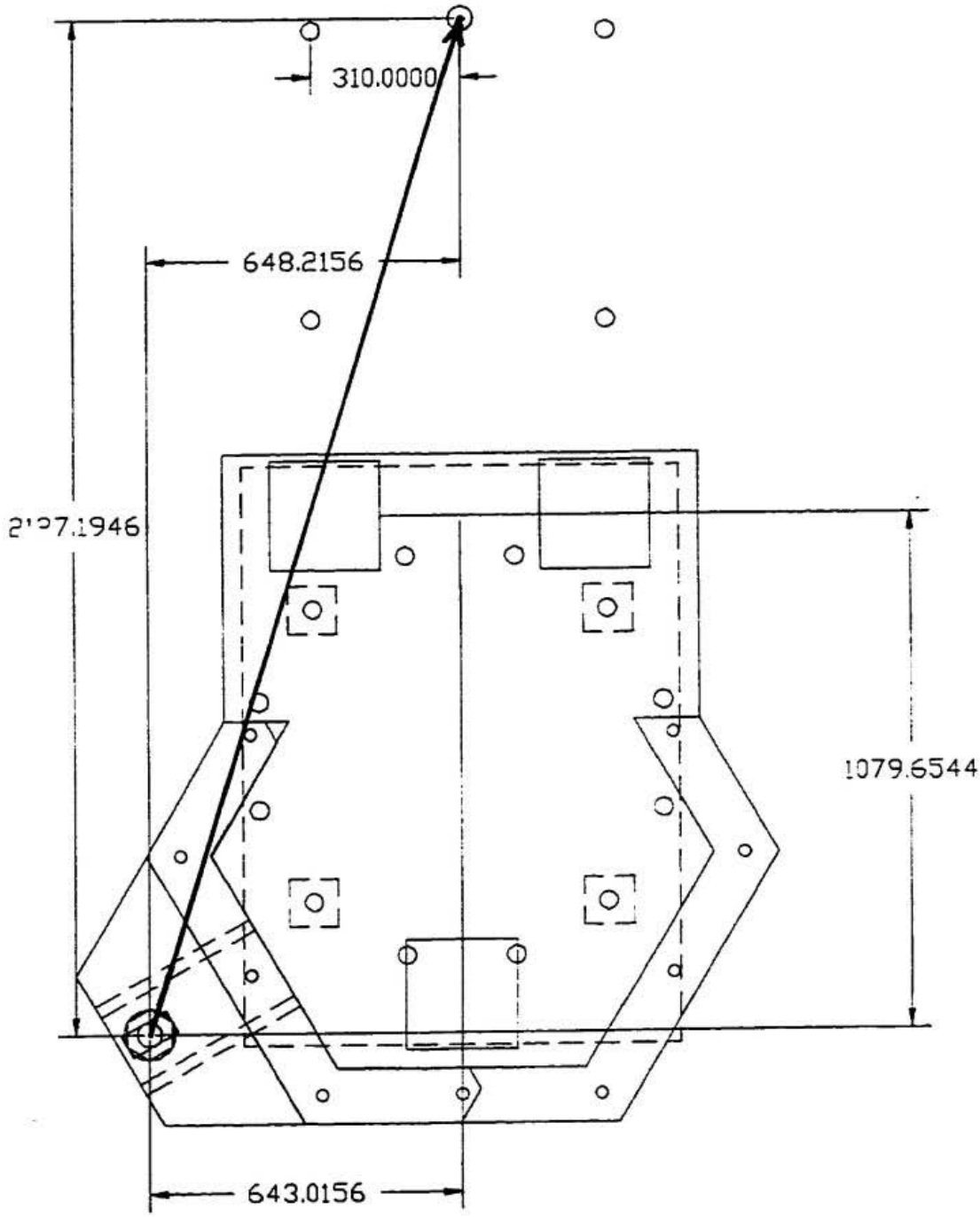

Figure B-14: Direction of Load Application - Orientation 3

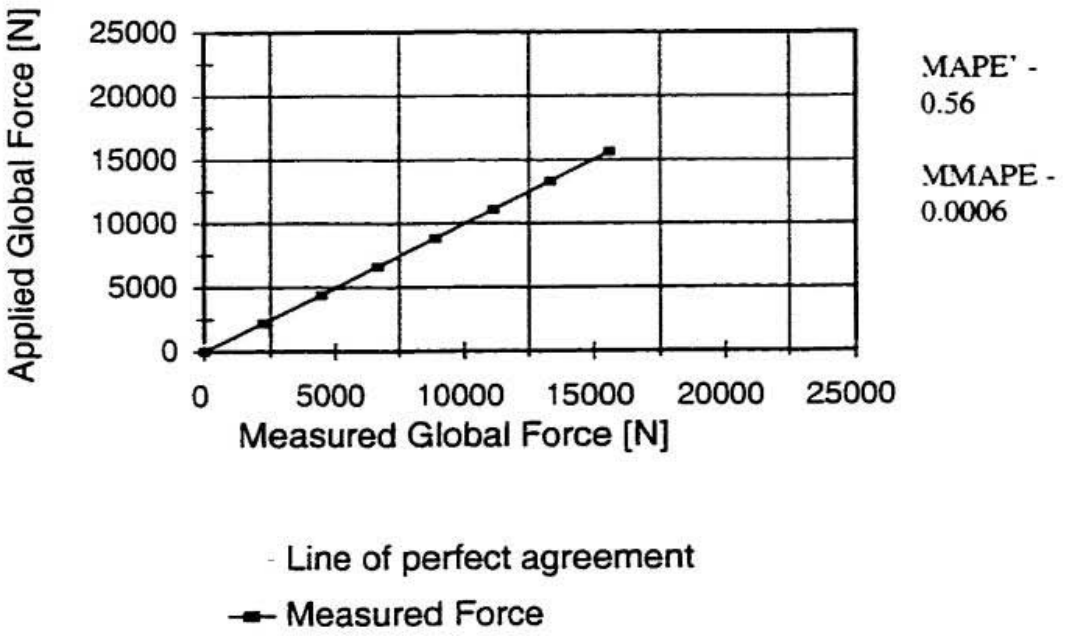

Figure B-15: Global Force Comparison - Orientation 3

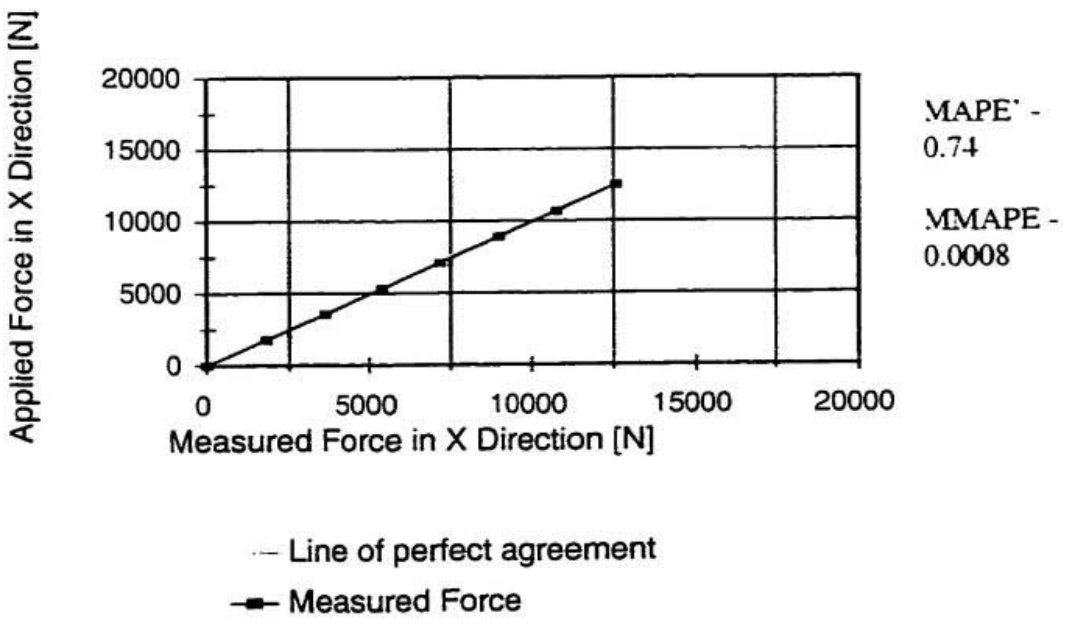

Figure B-16: Comparison of Forces in X Direction - Orientation 3

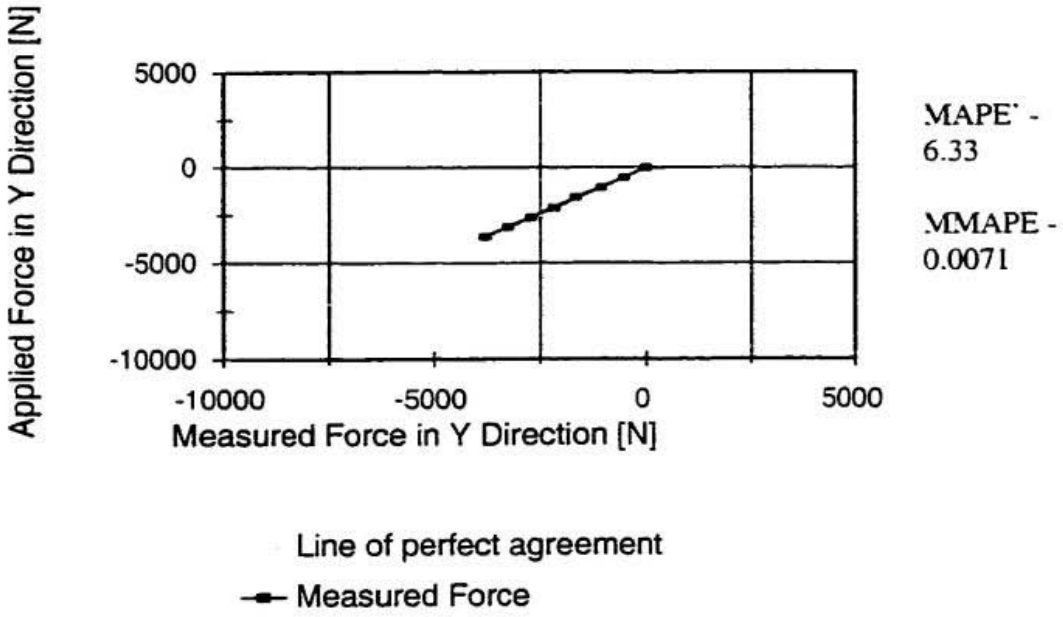

Figure B-17: Comparison of Forces in Y Direction - Orientation 3

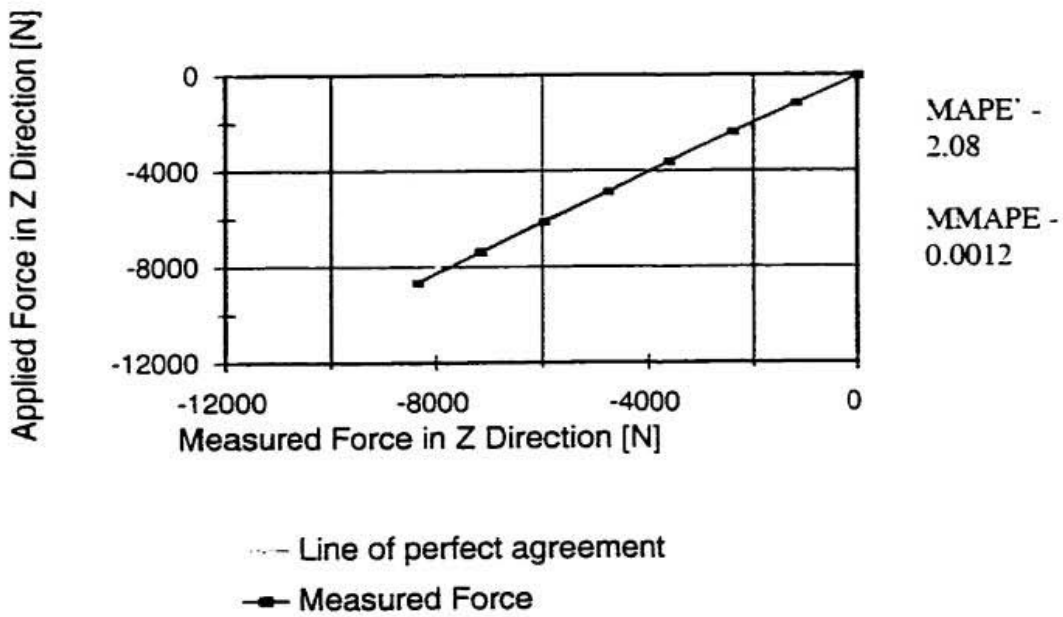

Figure B-18: Comparison of Forces in Z Direction - Orientation 3

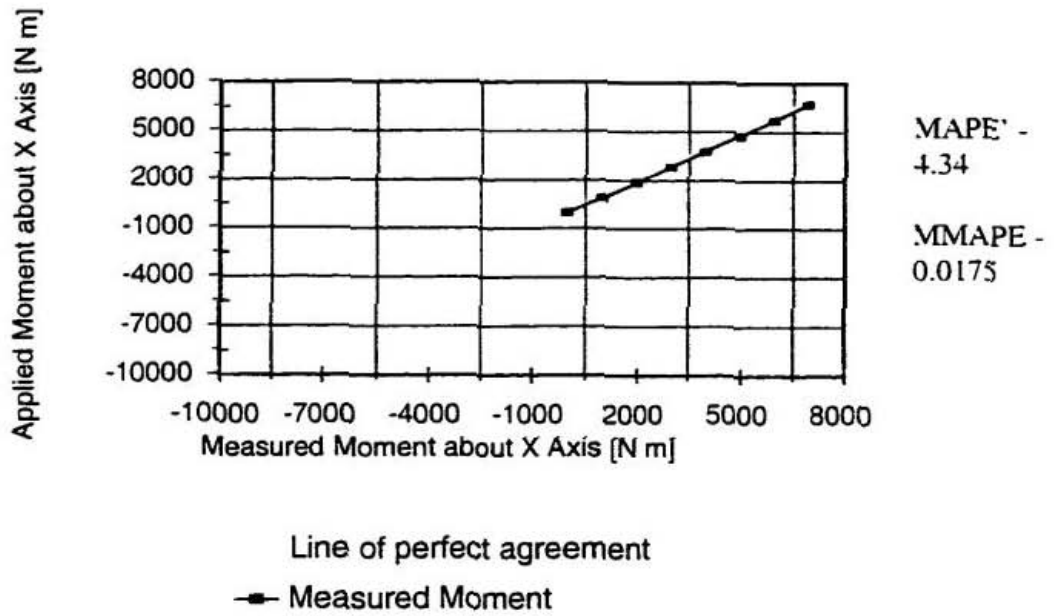

Figure B-19: Comparison of Moments About X Axis - Orientation 3

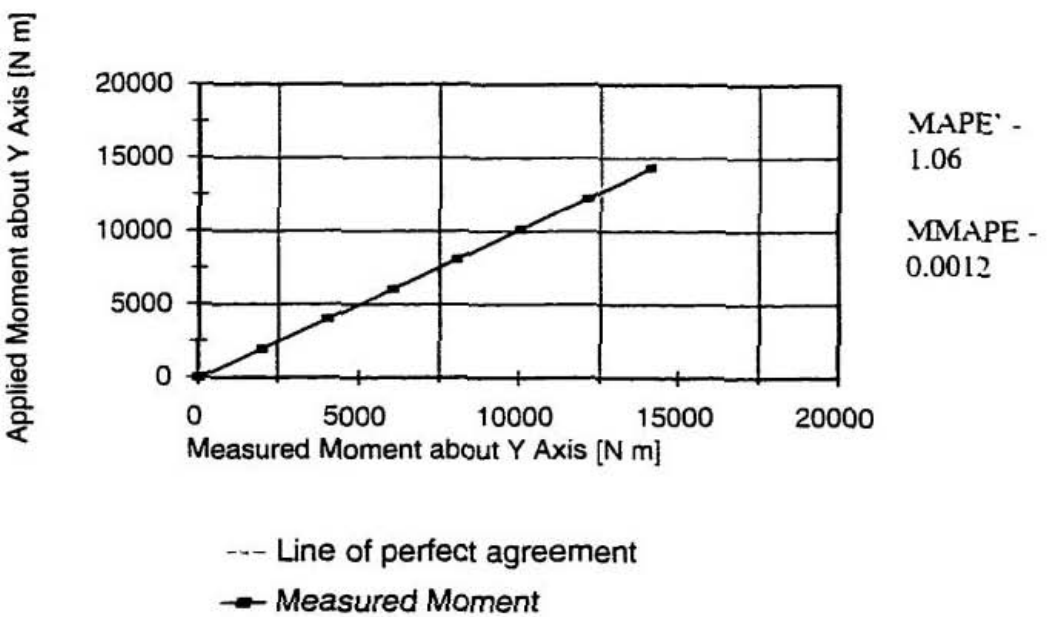

Figure B-20: Comparison of Moments about Y Axis - Orientation 3

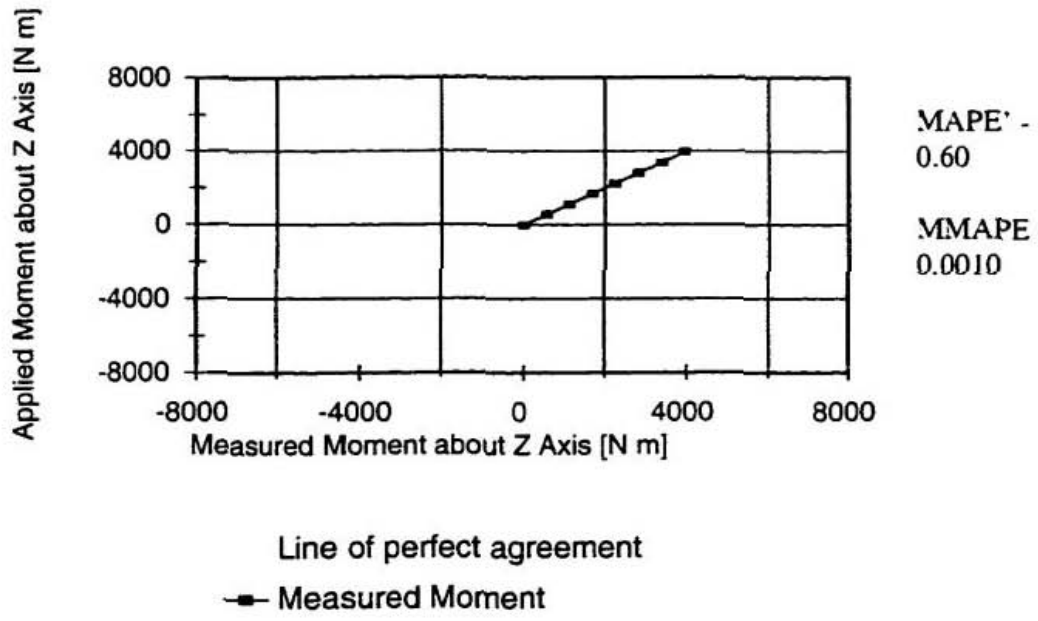

Figure B-21: Comparison of Moments About Z Axis - Orientation 3

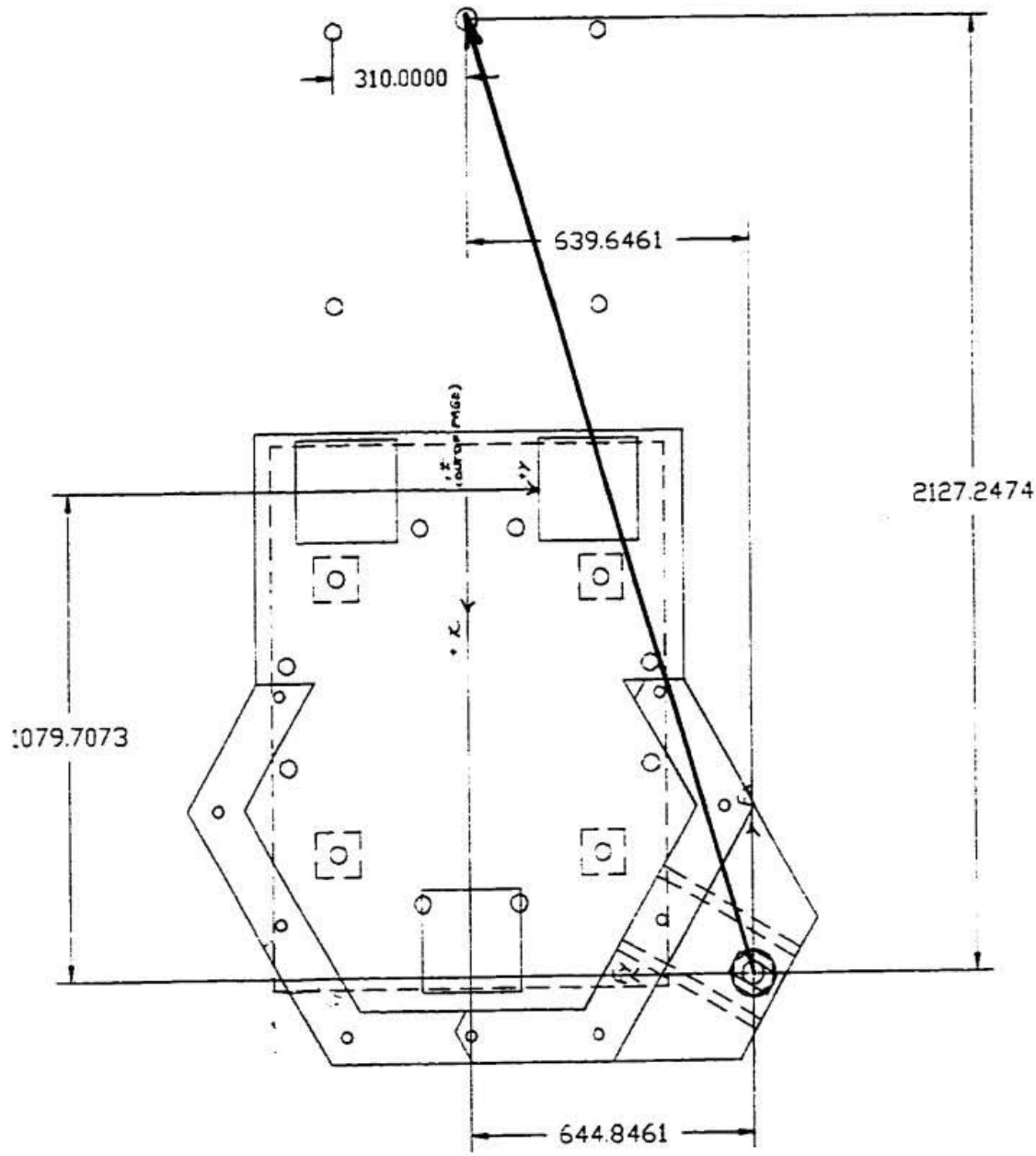

Figure B-22: Direction of Load Application - Orientation 4

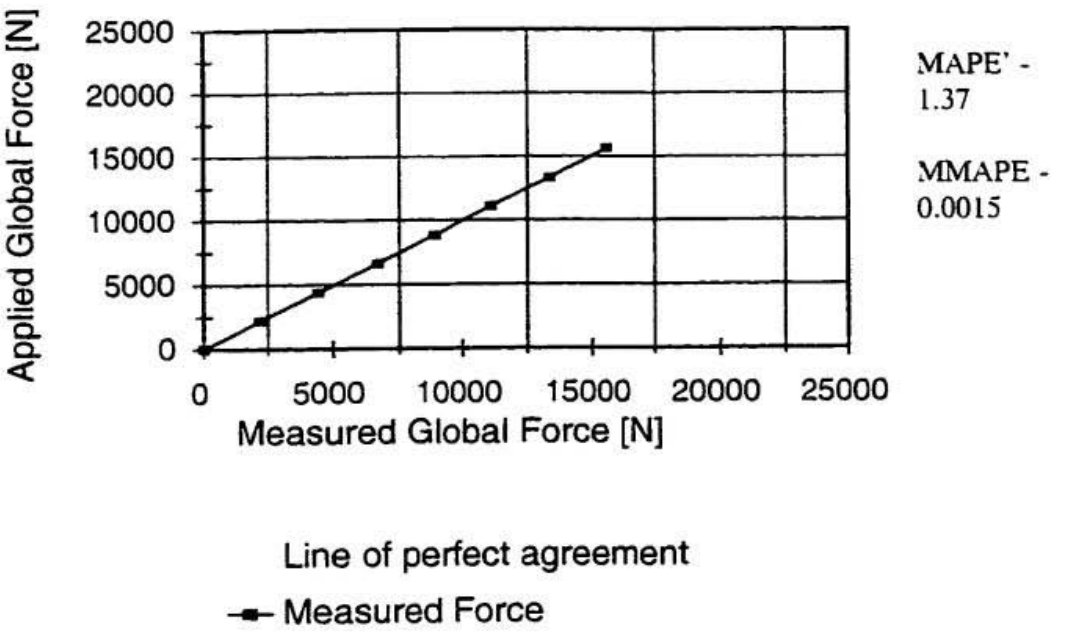

Figure B-23: Global Force Comparison - Orientation 4

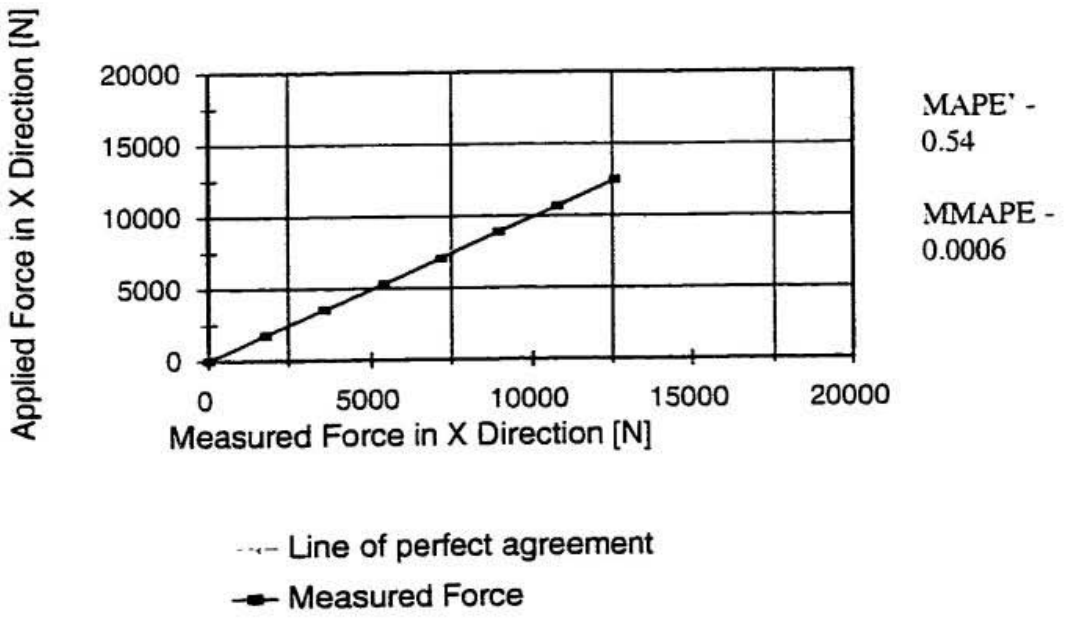

Figure B-24: Comparison of Forces in X Direction - Orientation 4

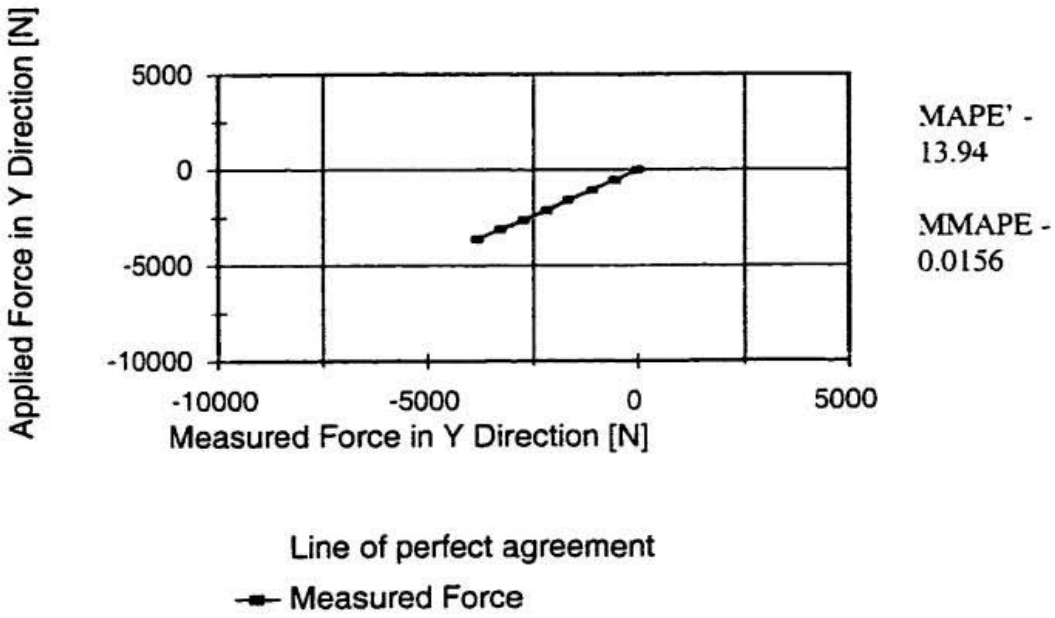

Figure B-25: Comparison of Forces in Y Direction - Orientation 4

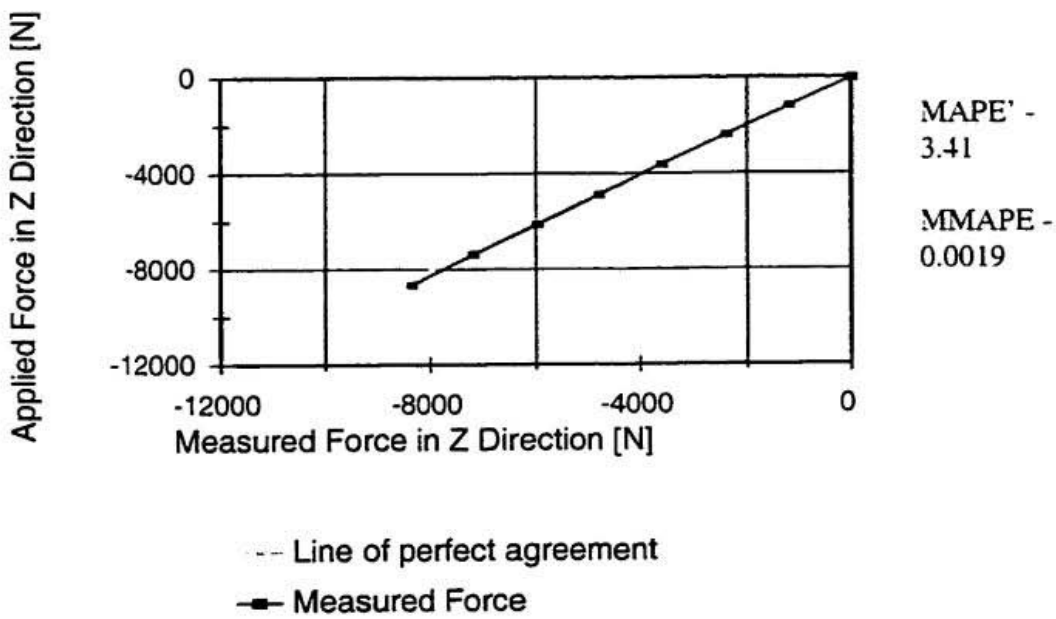

Figure B-26: Comparison of Forces in Z Direction - Orientation 4

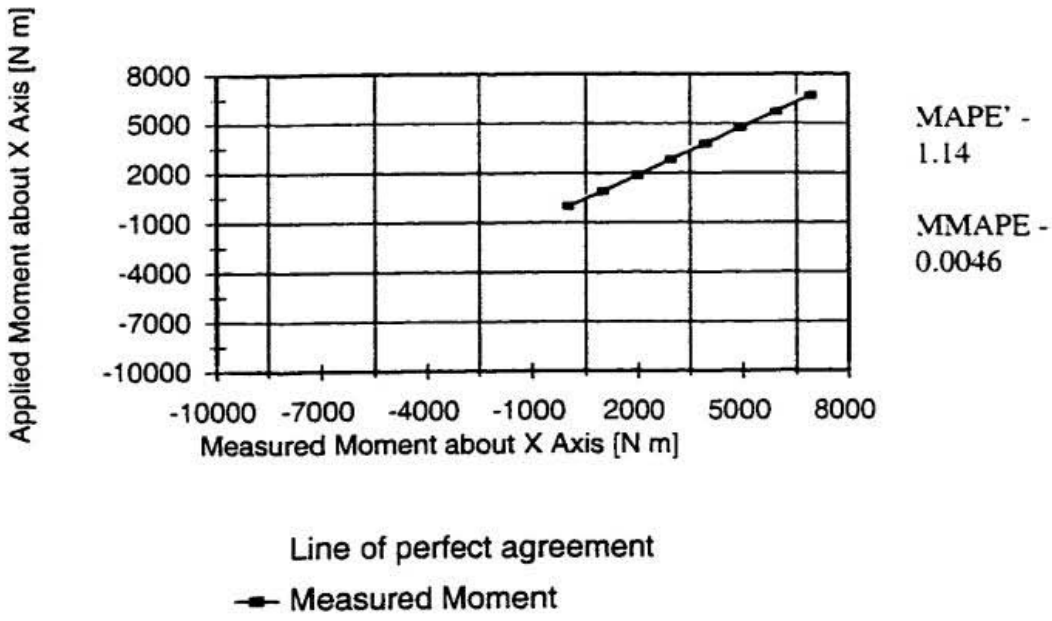

Figure B-27: Comparison of Moments About X Axis - Orientation 4

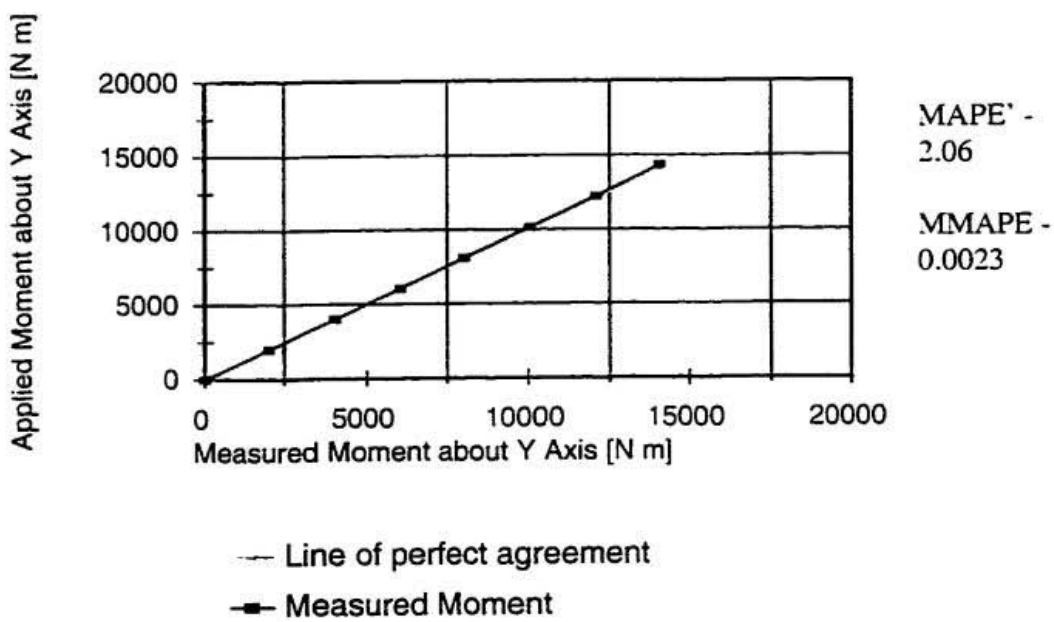

Figure B-28: Comparison of Moments about Y Axis - Orientation 4

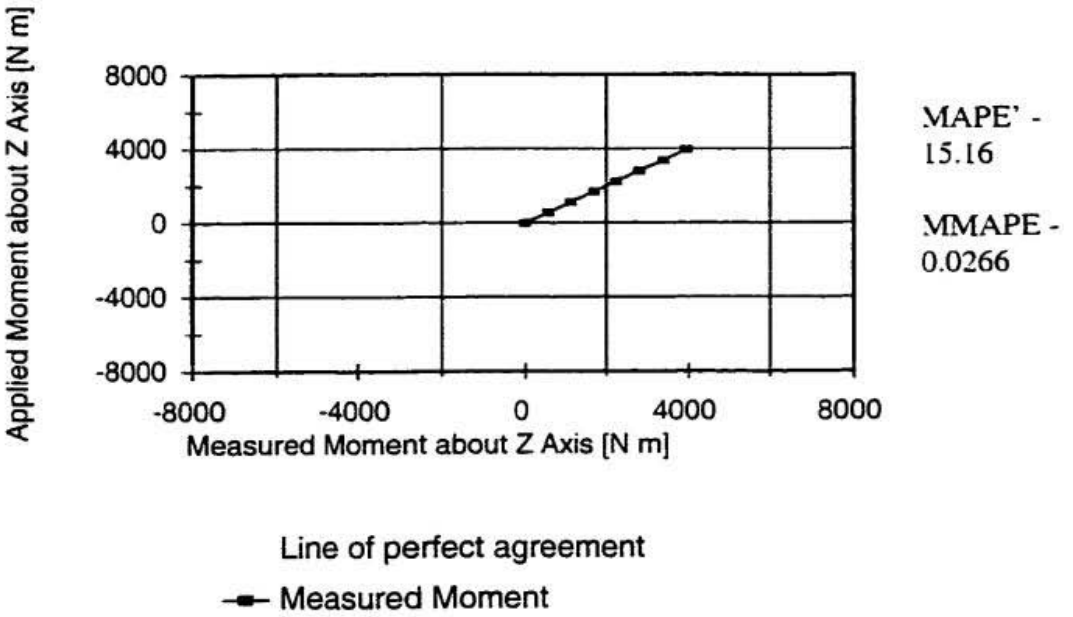

Figure B-29: Comparison of Moments About Z Axis - Orientation 4

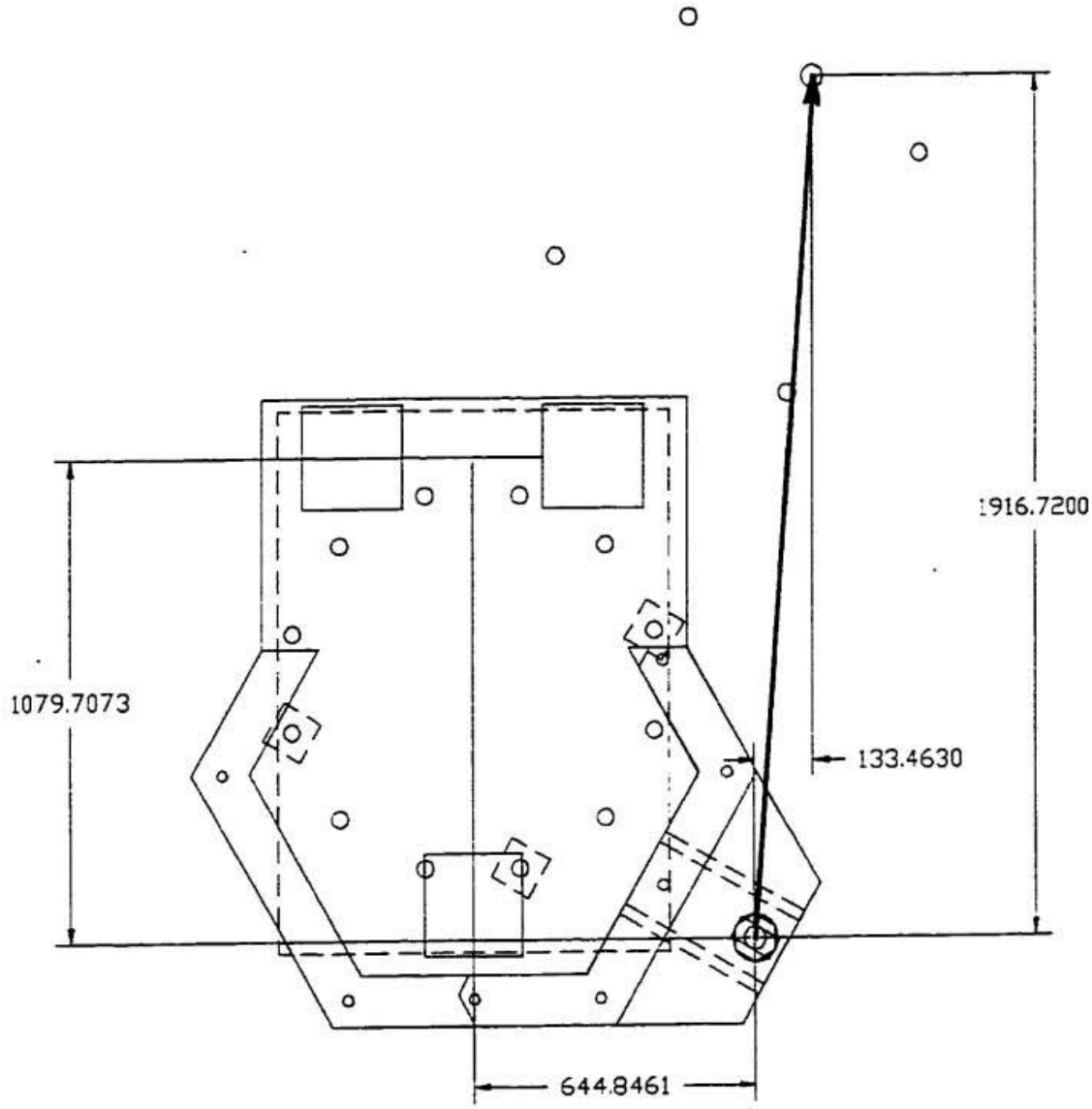

Figure B-30: Direction of Load Application - Orientation 5

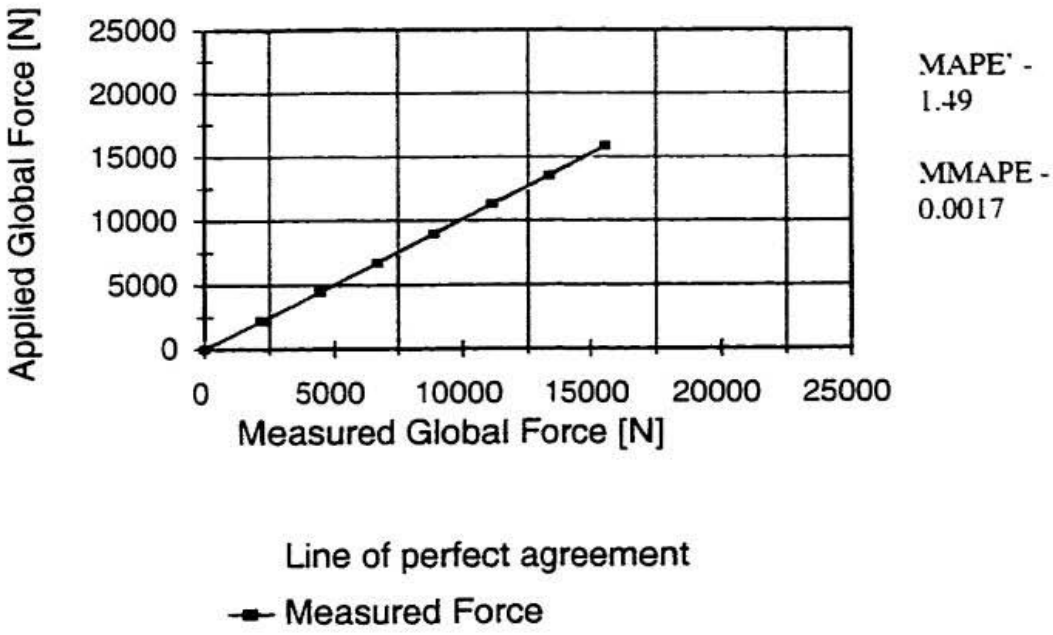

Figure B-31: Global Force Comparison - Orientation 5

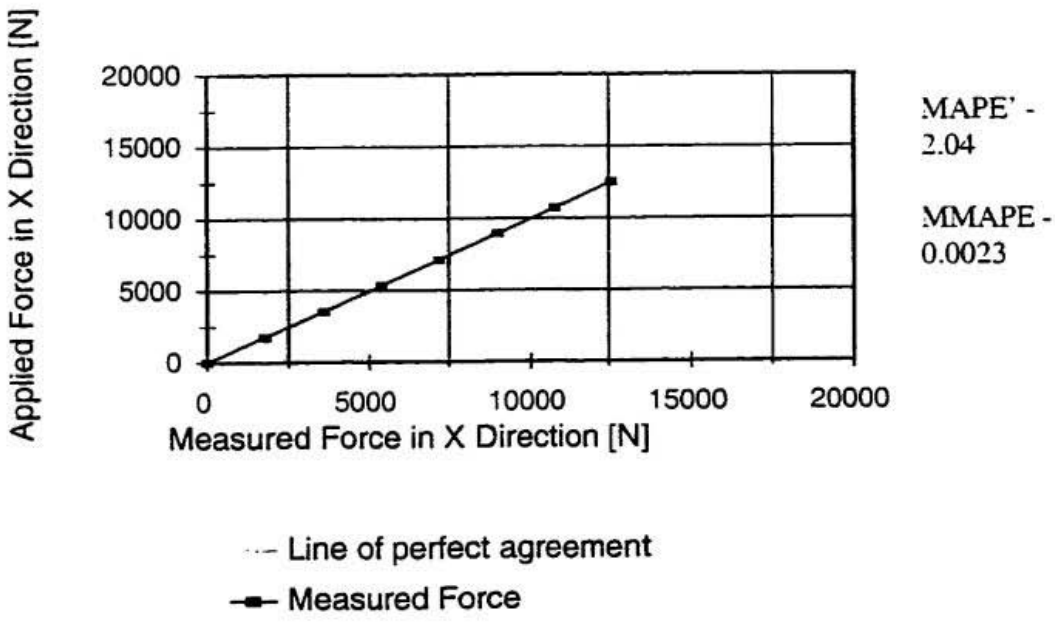

Figure B-32: Comparison of Forces in X Direction - Orientation 5

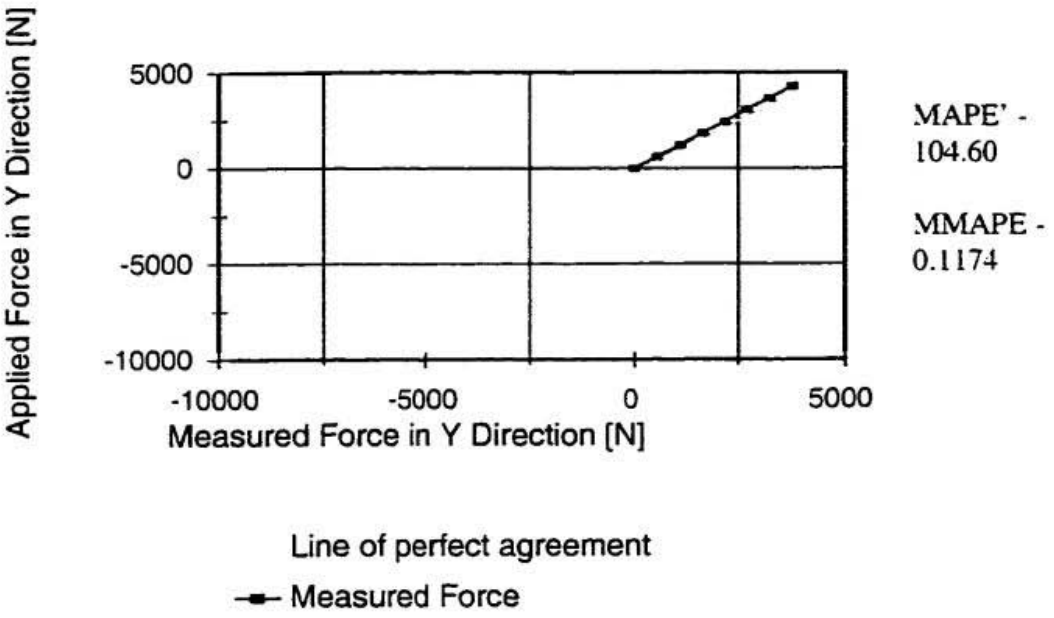

Figure B-33: Comparison of Forces in Y Direction - Orientation 5

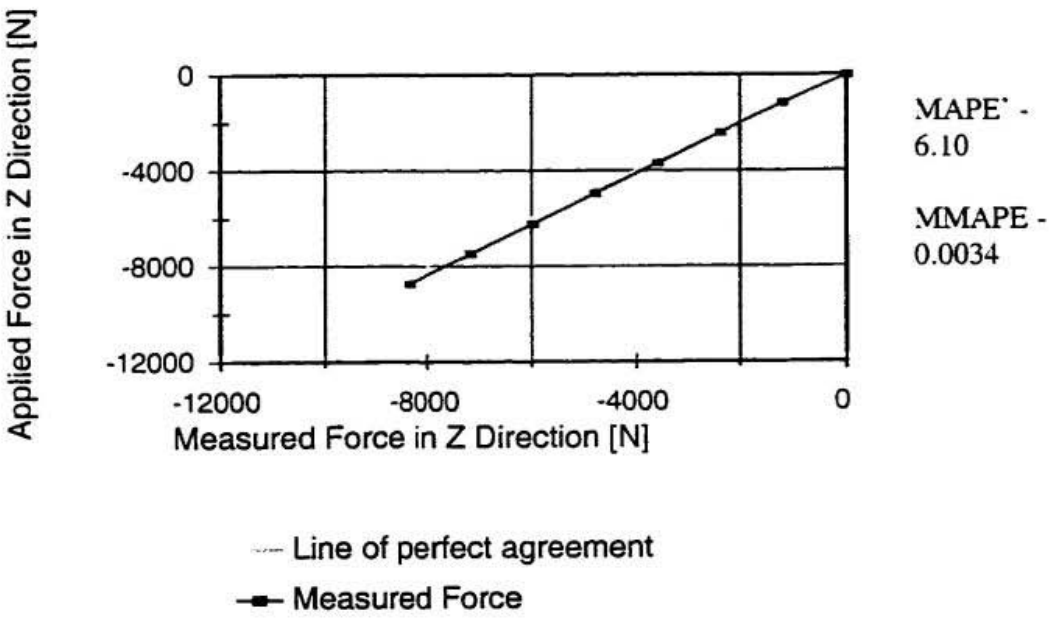

Figure B-34: Comparison of Forces in Z Direction - Orientation 5

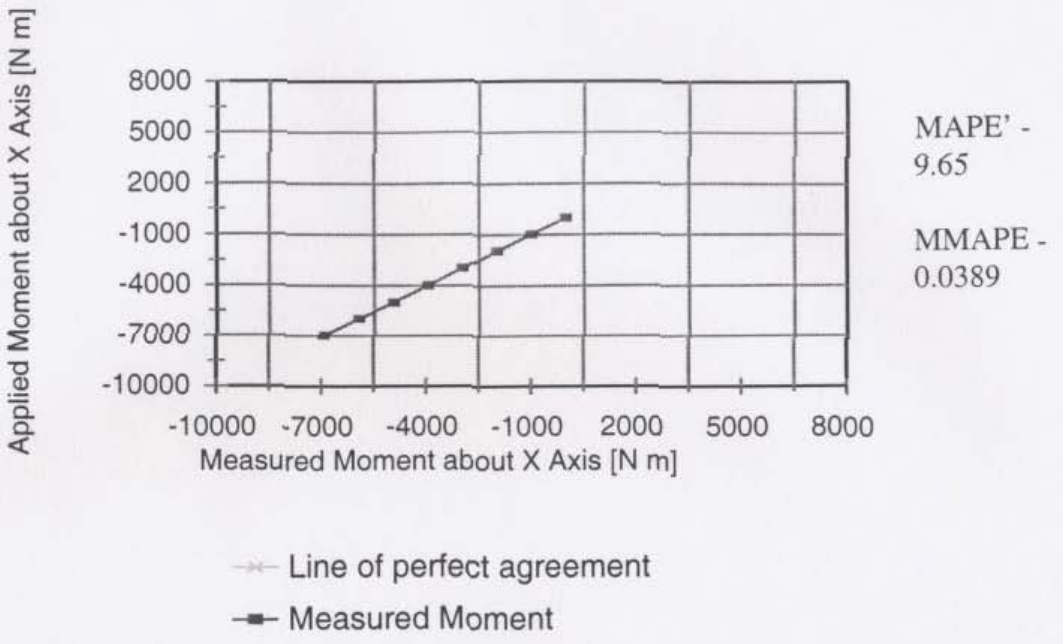

Figure B-35: Comparison of Moments About X Axis - Orientation 5

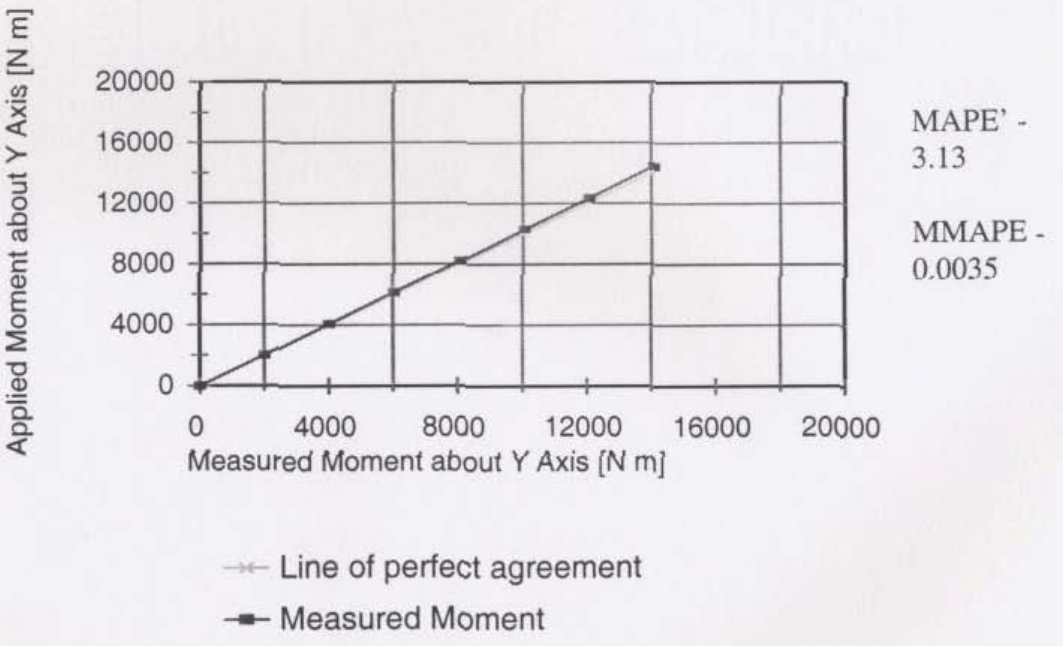

Figure B-36: Comparison of Moments about Y Axis - Orientation 5

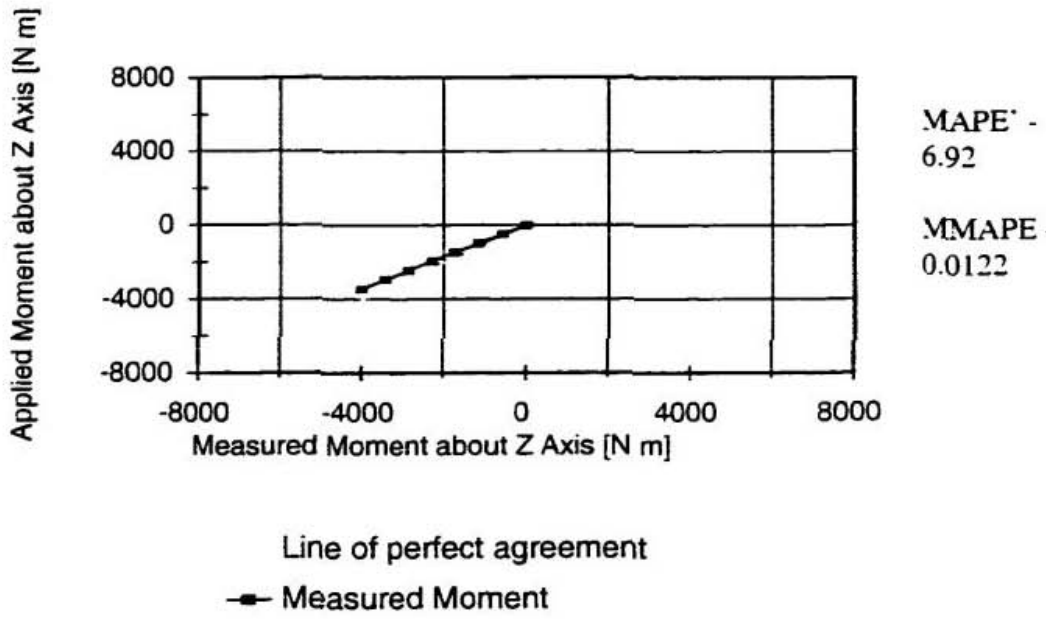

Figure B-37: Comparison of Moments About Z Axis - Orientation 5

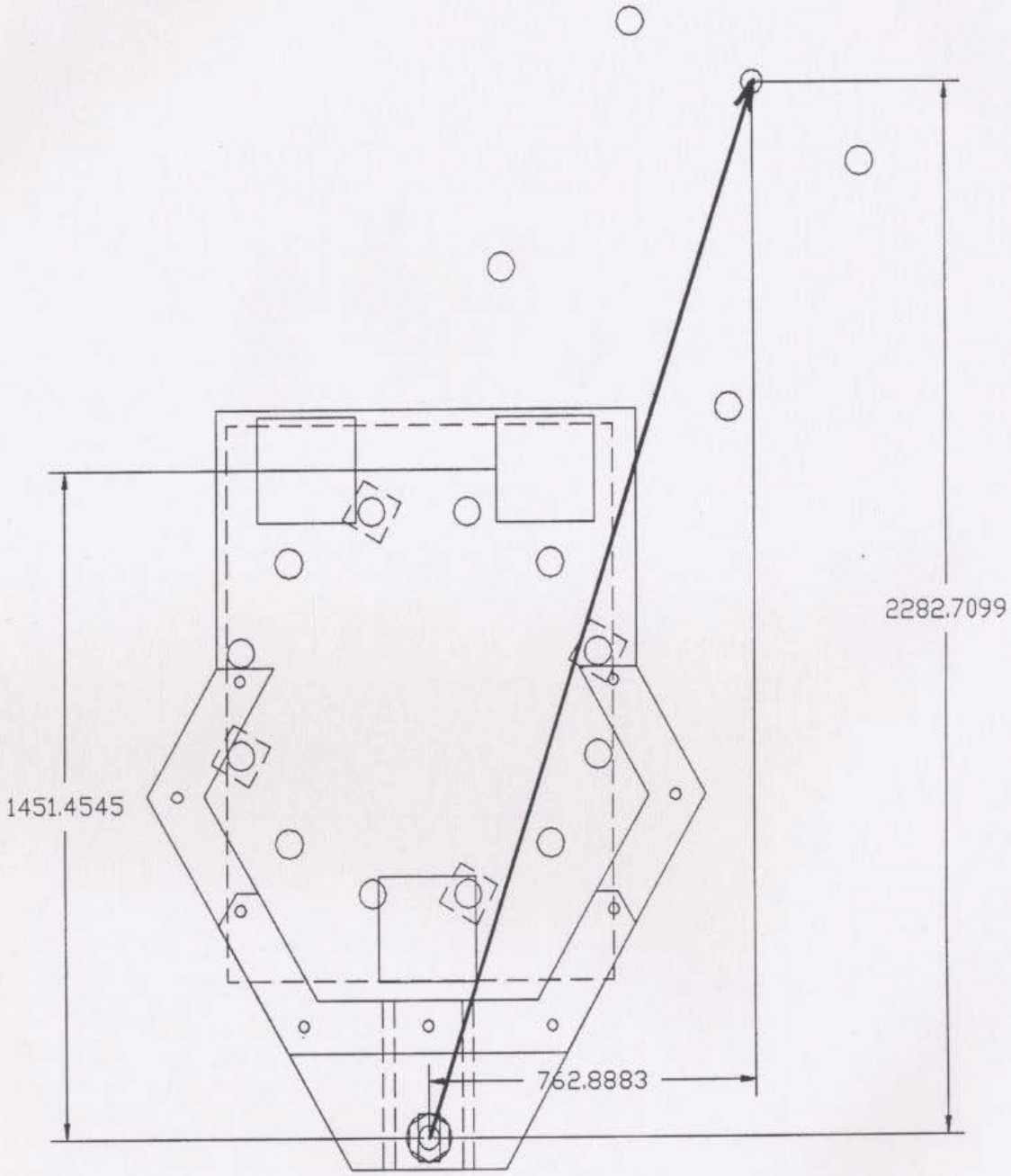

Figure B-38: Direction of Load Application - Orientation 6

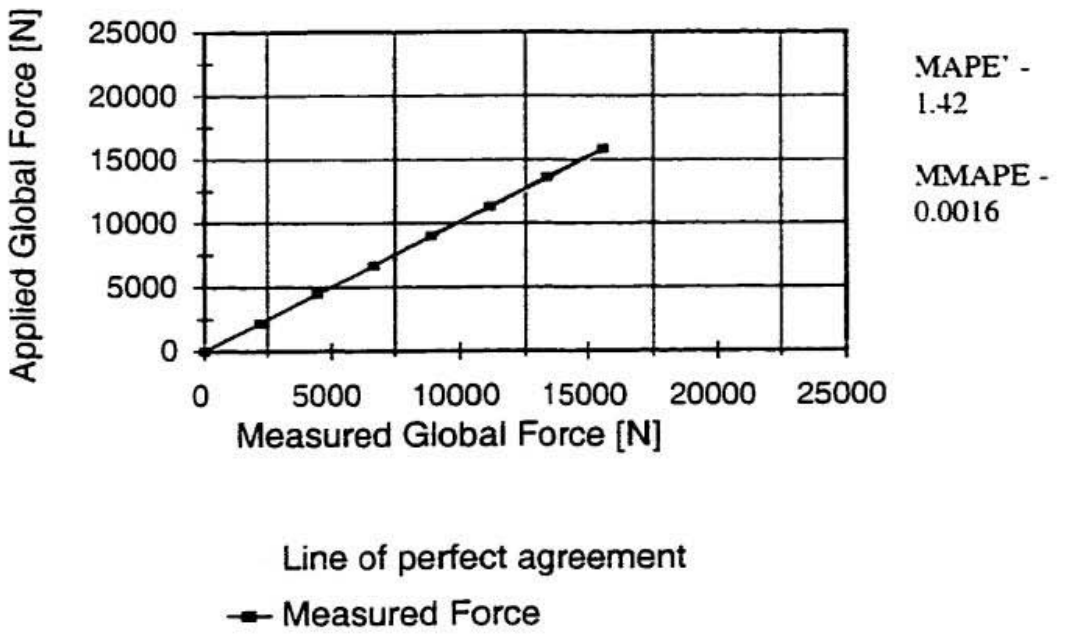

Figure B-39: Global Force Comparison - Orientation 6

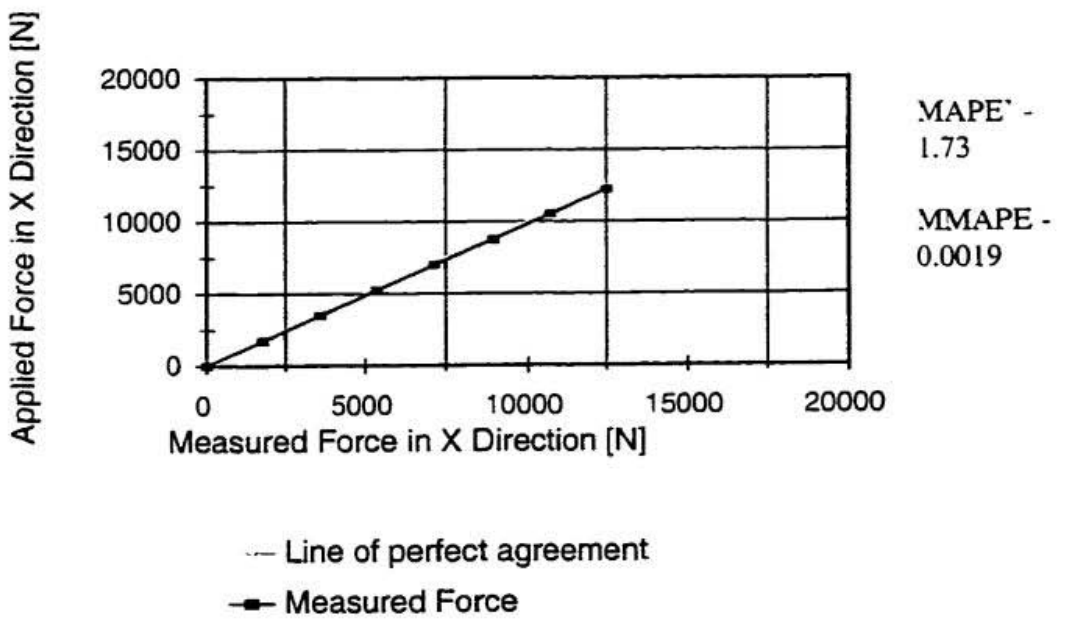

Figure B-40: Comparison of Forces in X Direction - Orientation 6

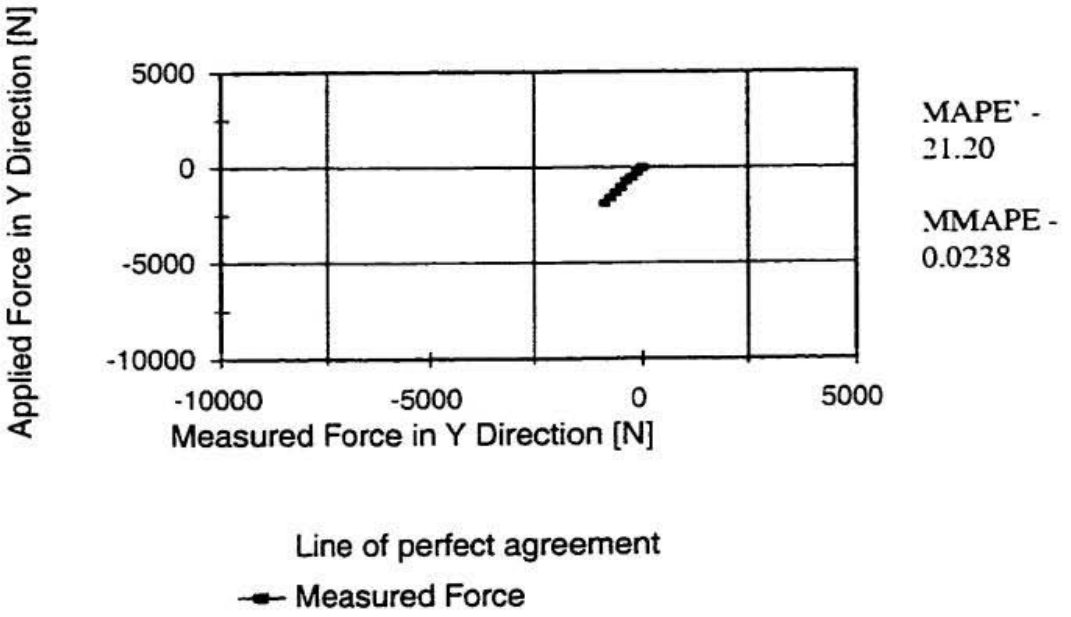

Figure B-41: Comparison of Forces in Y Direction - Orientation 6

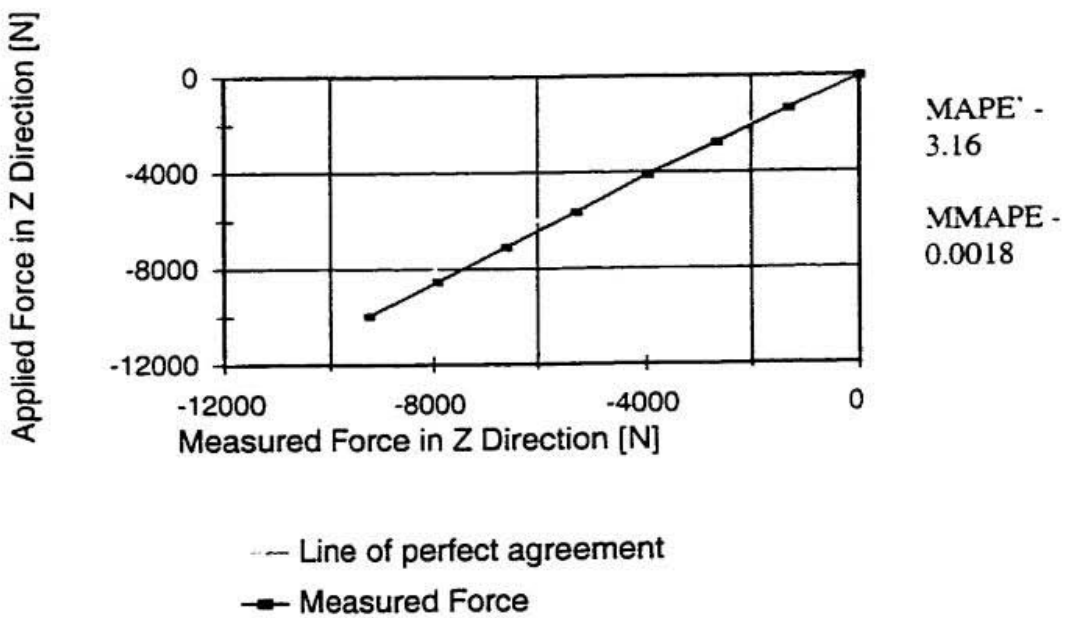

Figure B-42: Comparison of Forces in Z Direction - Orientation 6

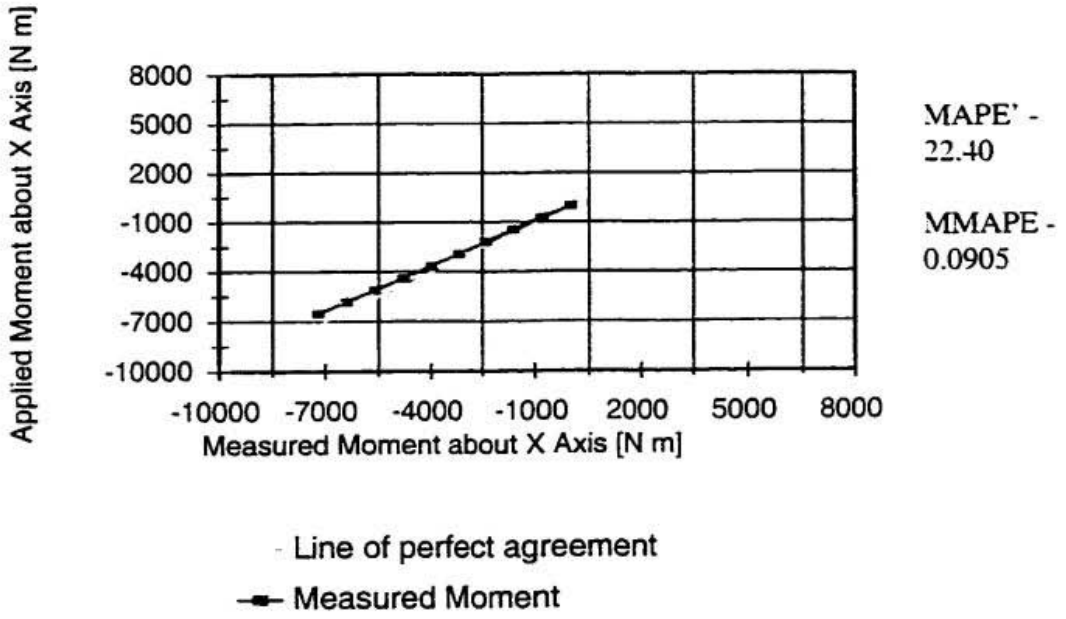

Figure B-43: Comparison of Moments About X Axis - Orientation 6

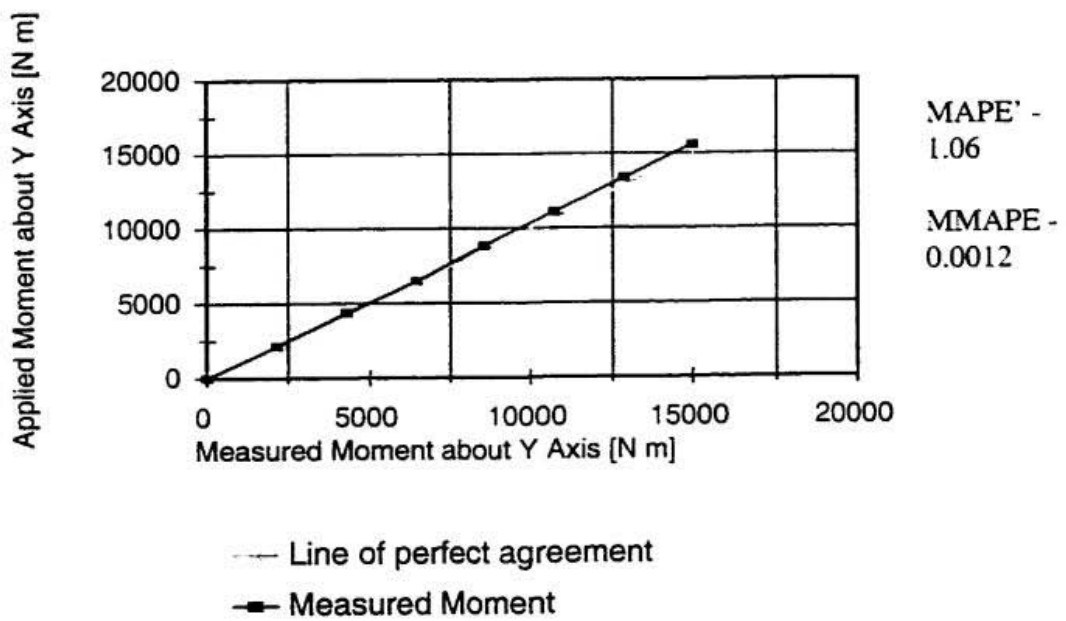

Figure B-44: Comparison of Moments about Y Axis - Orientation 6

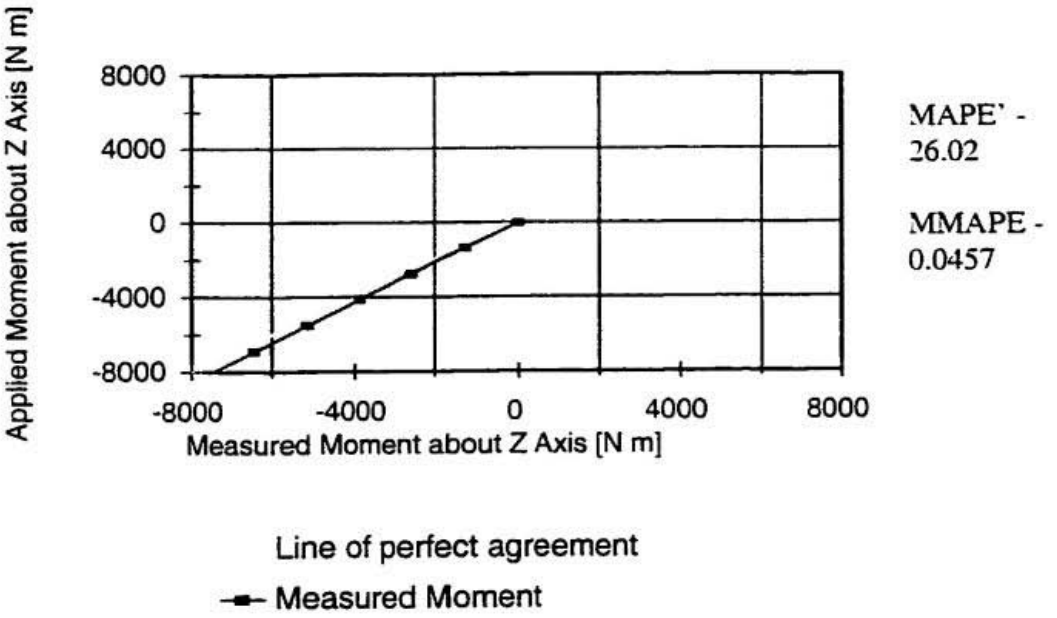

Figure B-45: Comparison of Moments About Z Axis - Orientation 6

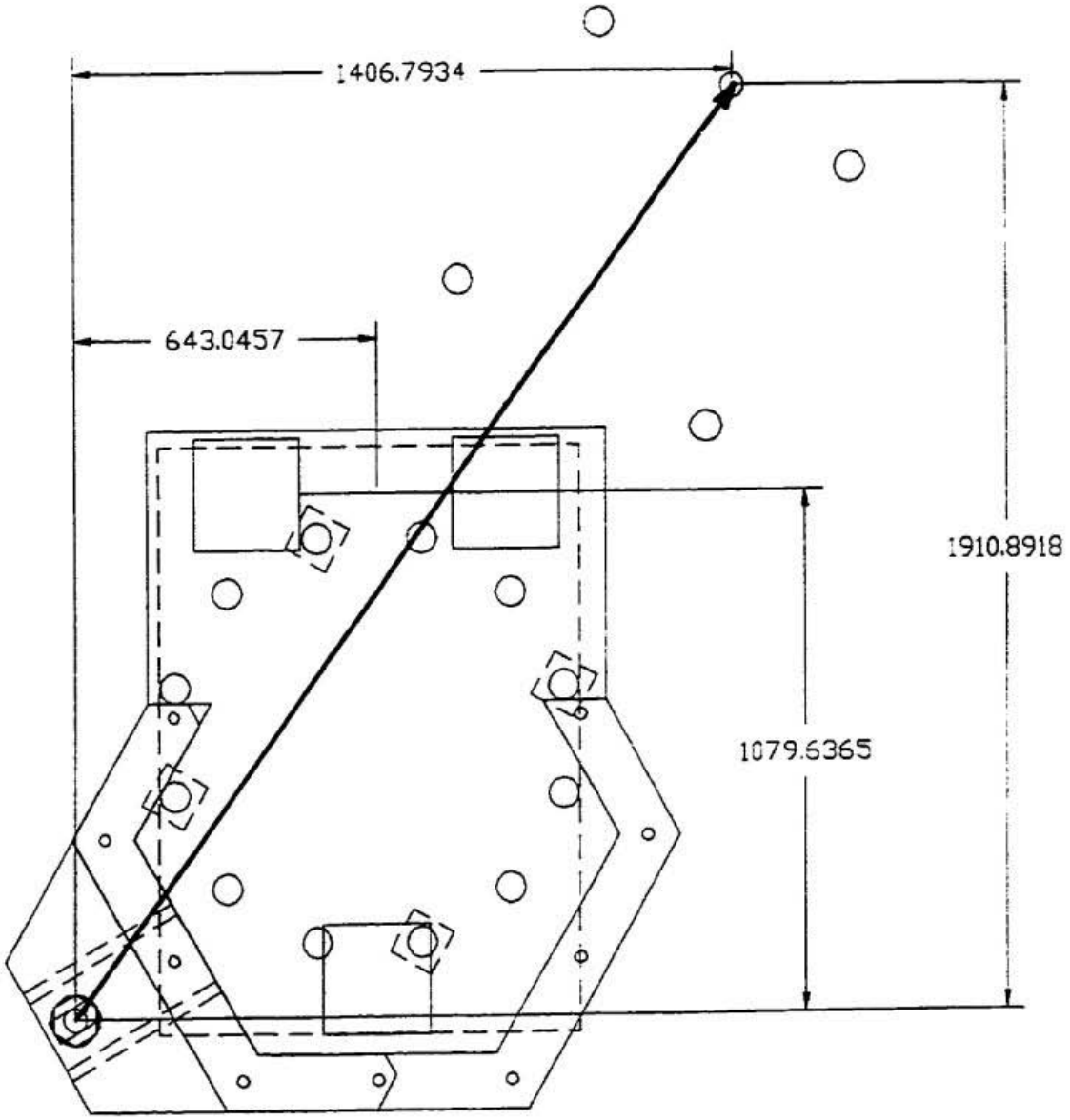

Figure B-46: Direction of Load Application - Orientation 7

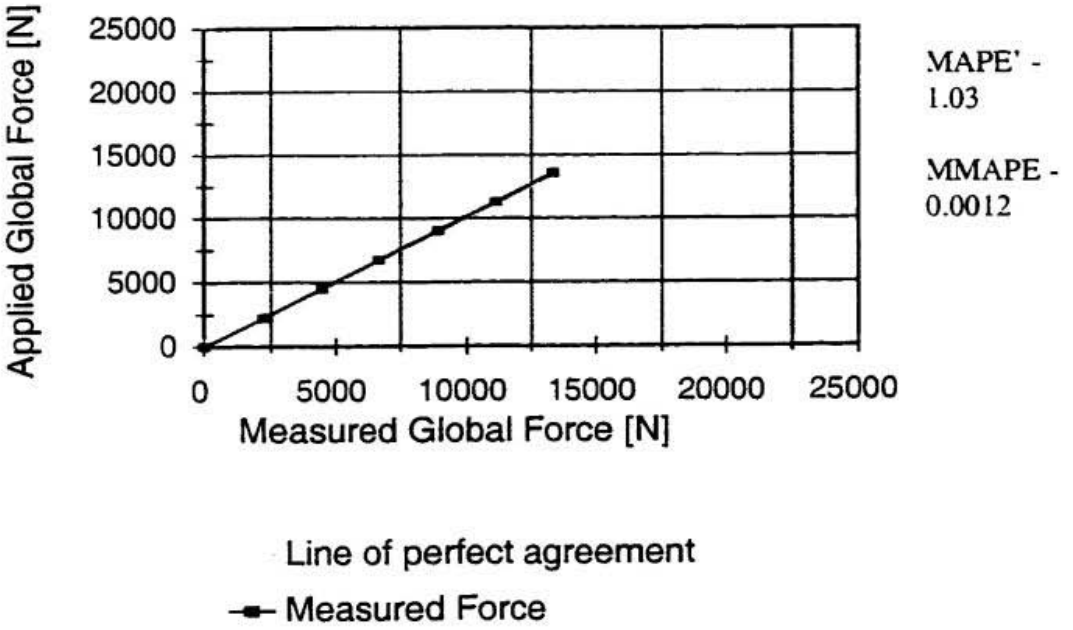

Figure B-47: Global Force Comparison - Orientation 7

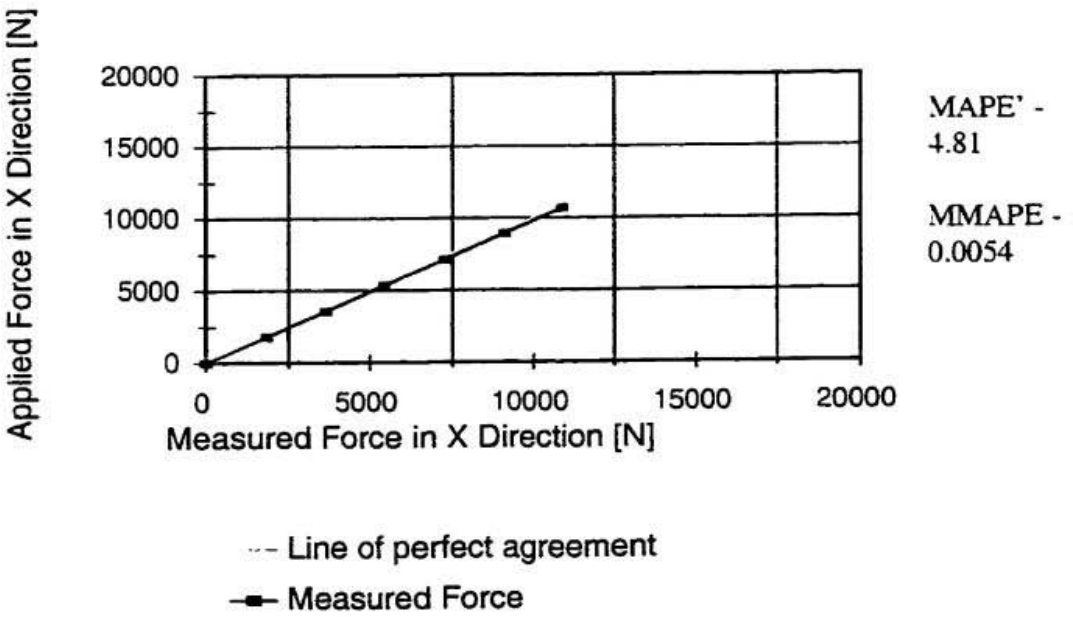

Figure B-48: Comparison of Forces in X Direction - Orientation 7

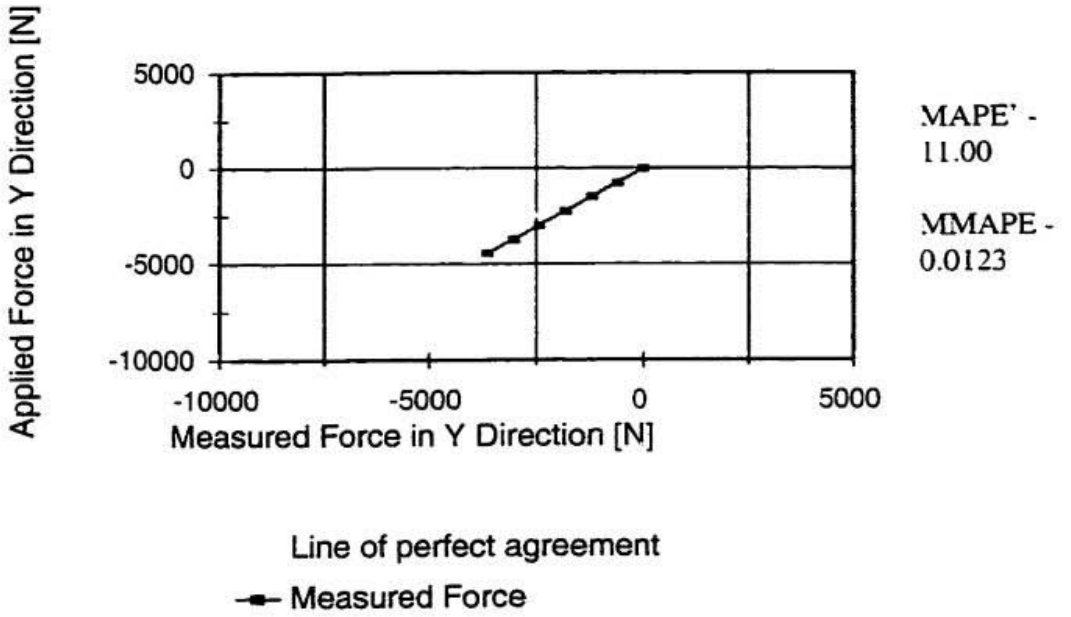

Figure B-49: Comparison of Forces in Y Direction - Orientation 7

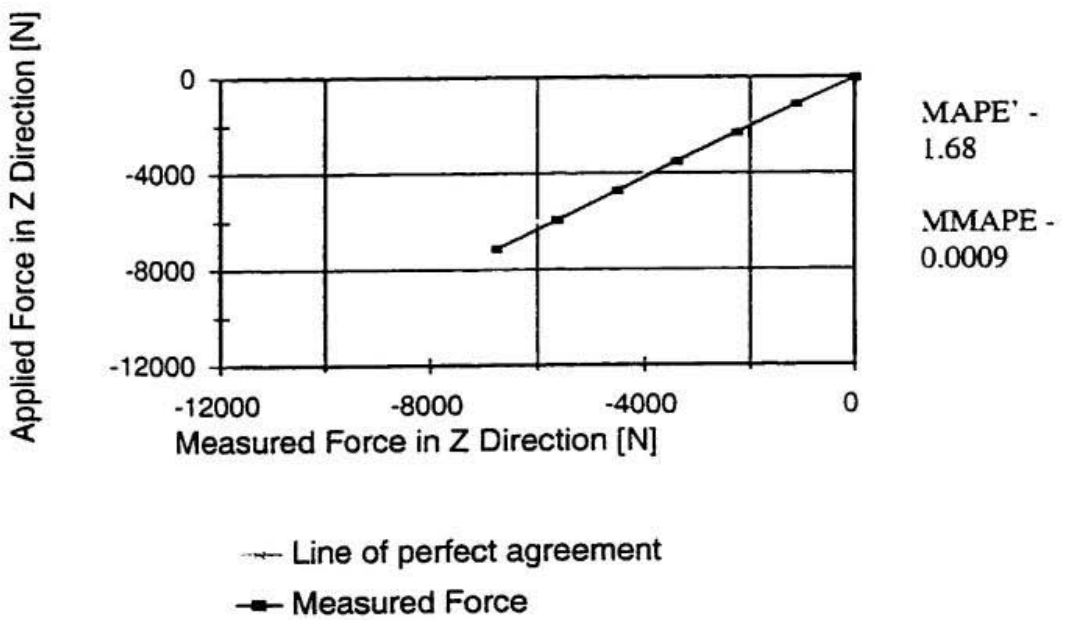

Figure B-50: Comparison of Forces in Z Direction - Orientation 7

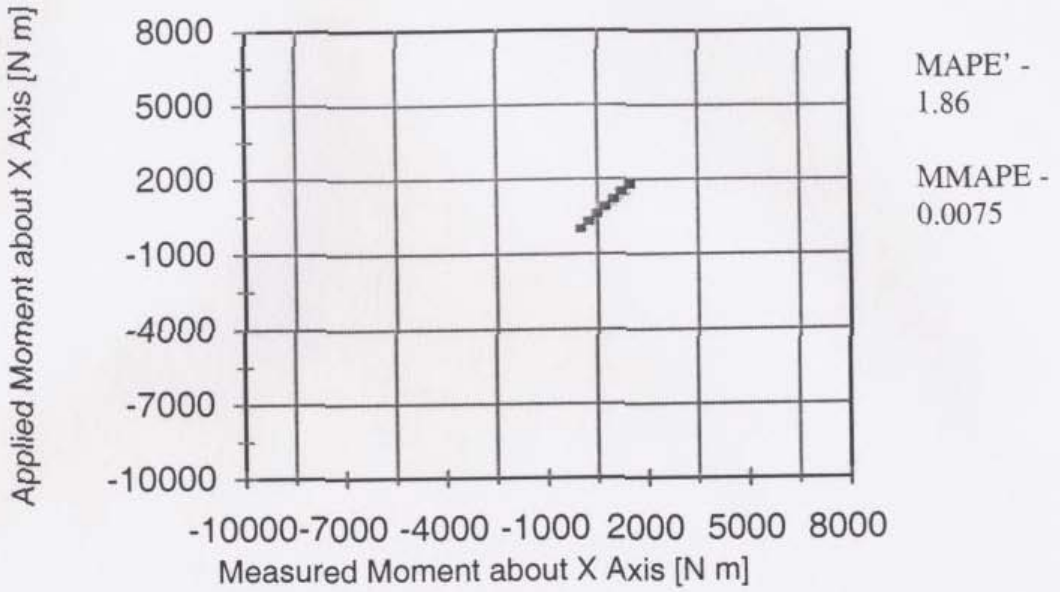

Figure B-51: Comparison of Moments About X Axis - Orientation 7

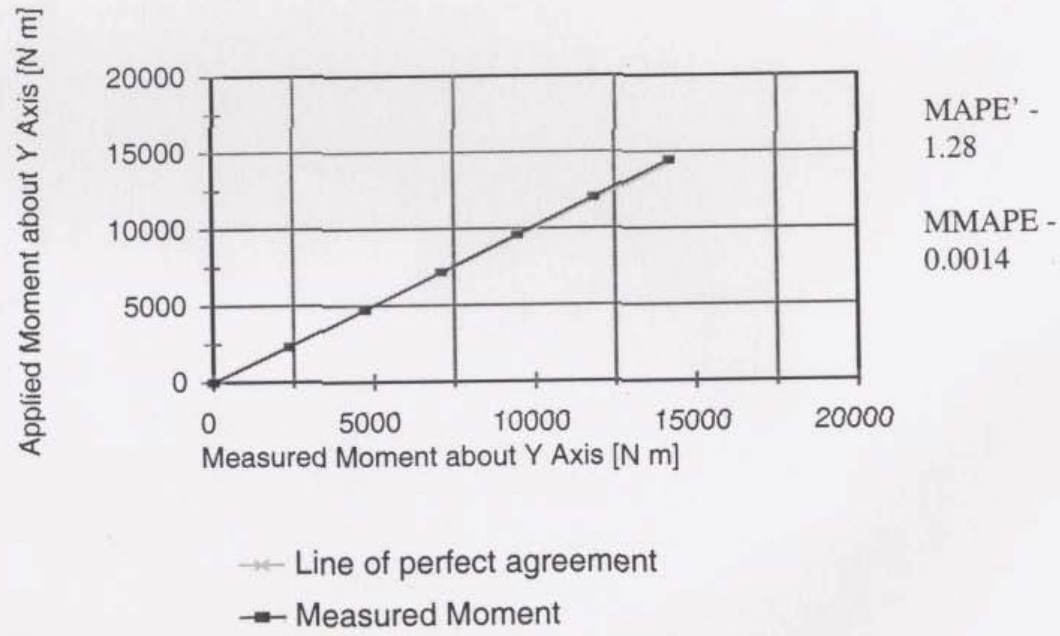

Figure B-52: Comparison of Moments about Y Axis - Orientation 7

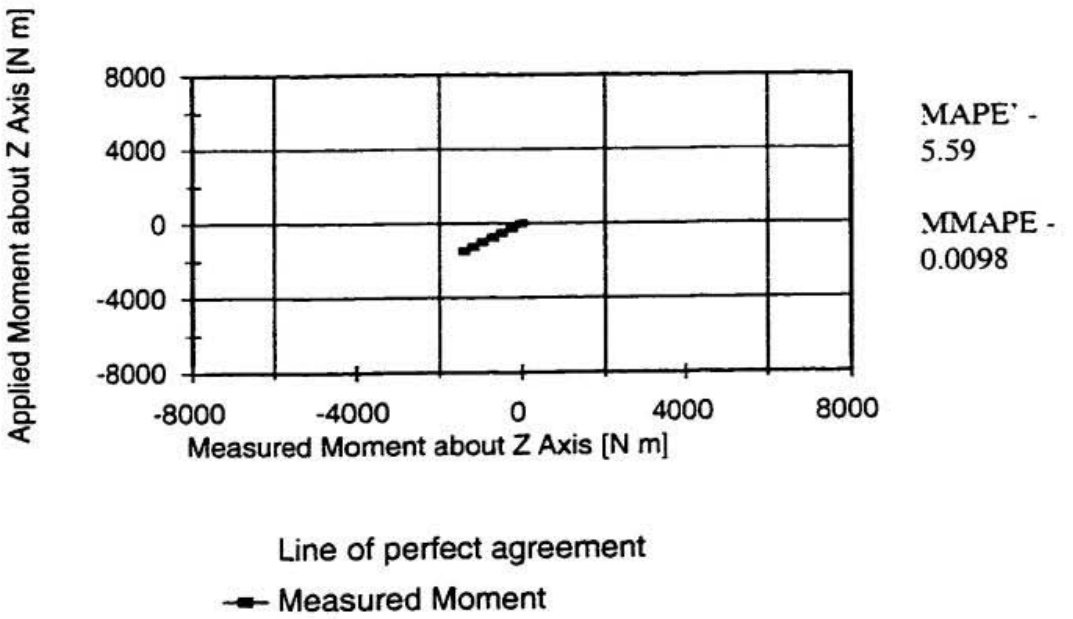

Figure B-53: Comparison of Moments About Z Axis - Orientation 7

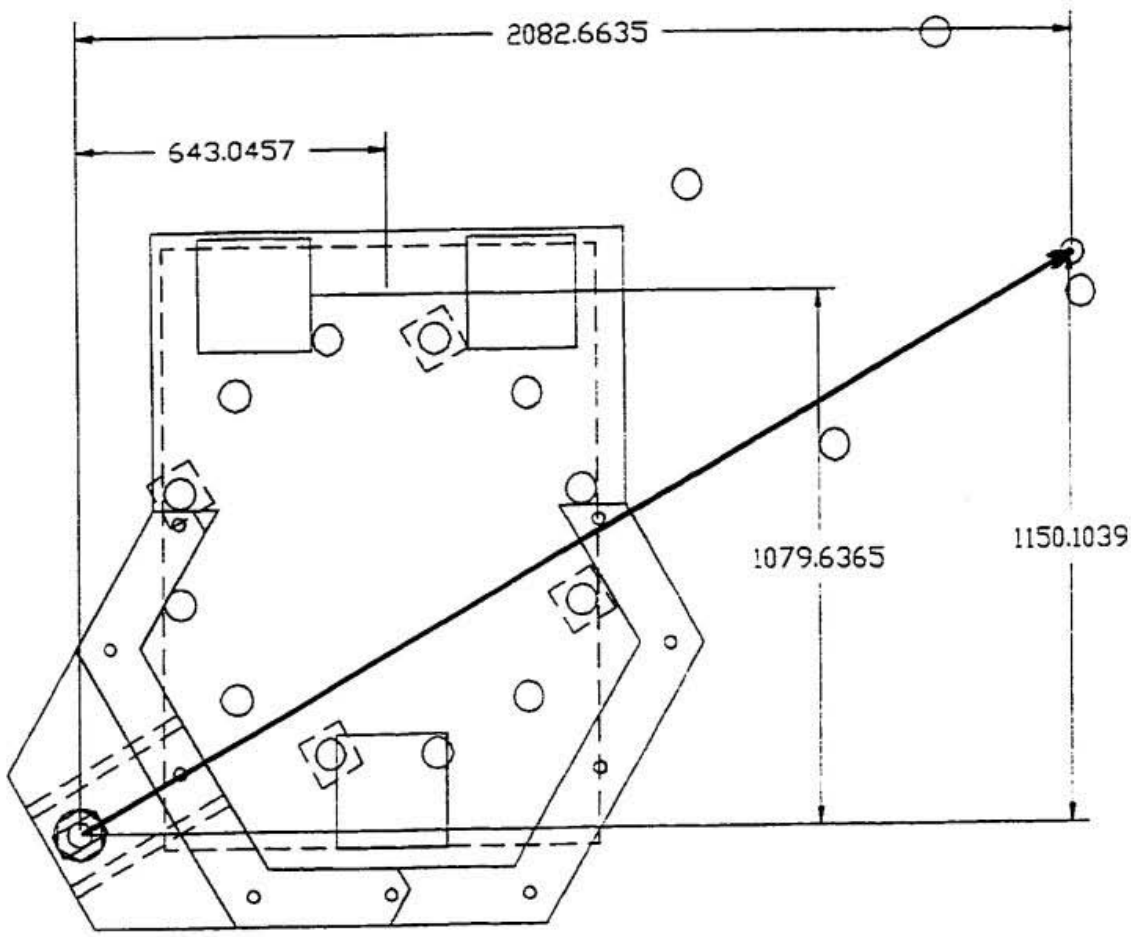

Figure B-54: Direction of Load Application - Orientation 8

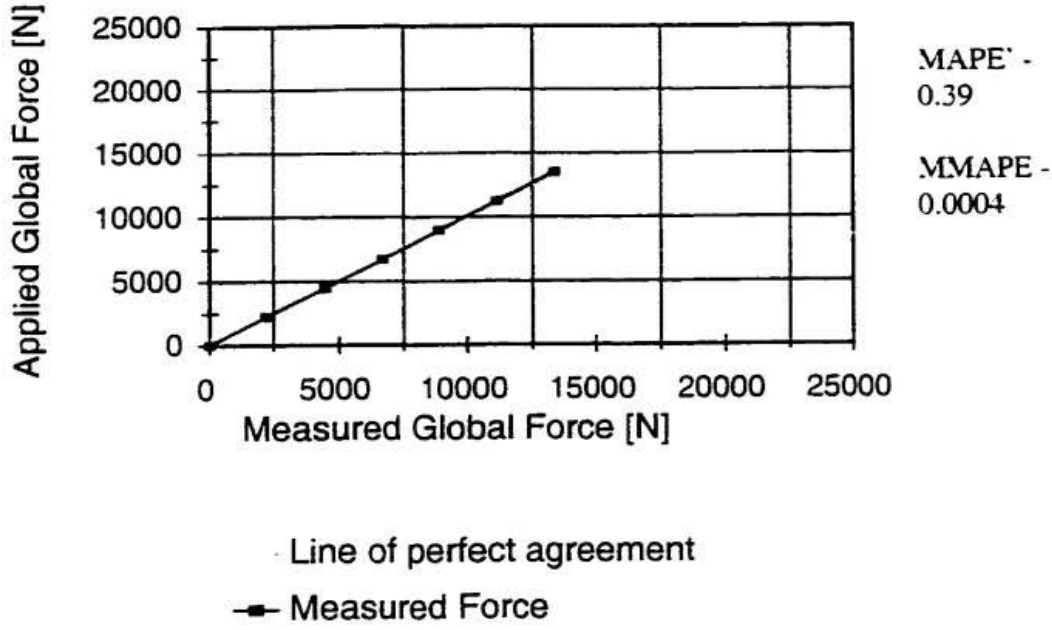

Figure B-55: Global Force Comparison - Orientation 8

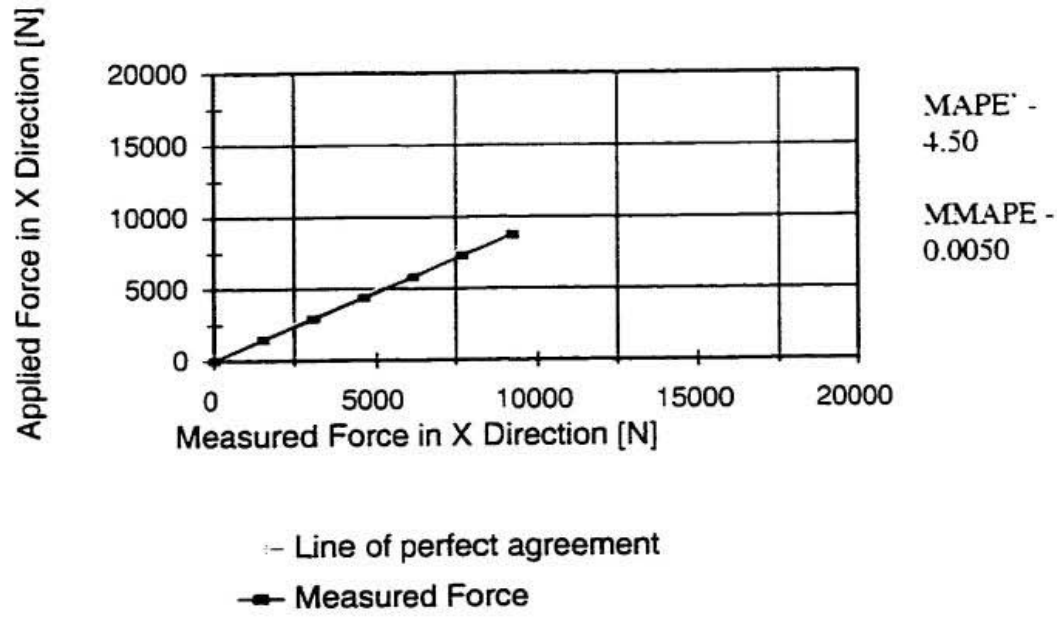

Figure B-56: Comparison of Forces in X Direction - Orientation 8

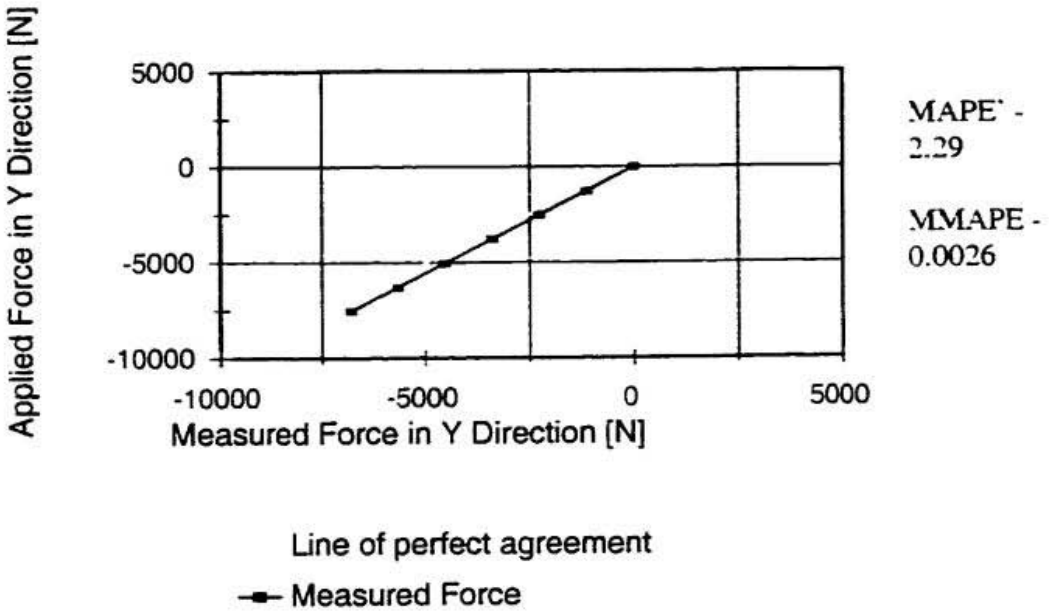

Figure B-57: Comparison of Forces in Y Direction - Orientation 8

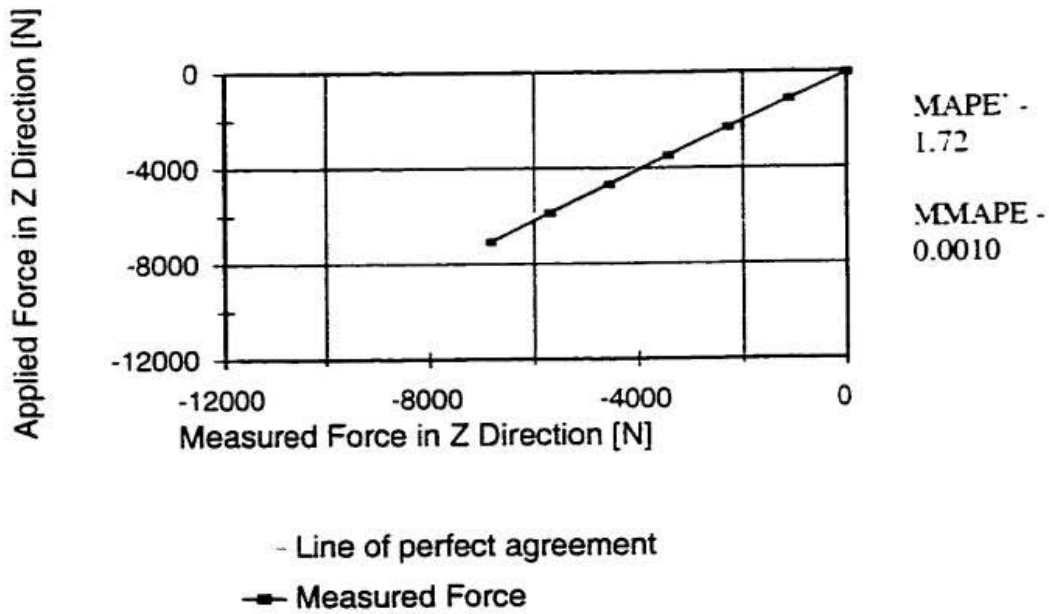

Figure B-58: Comparison of Forces in Z Direction - Orientation 8

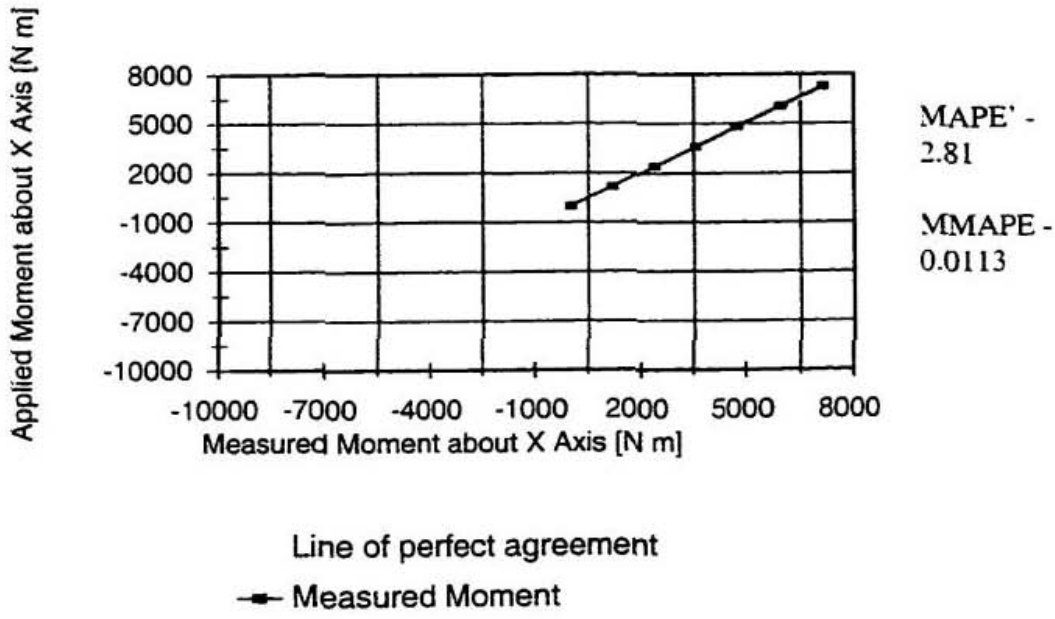

Figure B-59: Comparison of Moments About X Axis - Orientation 8

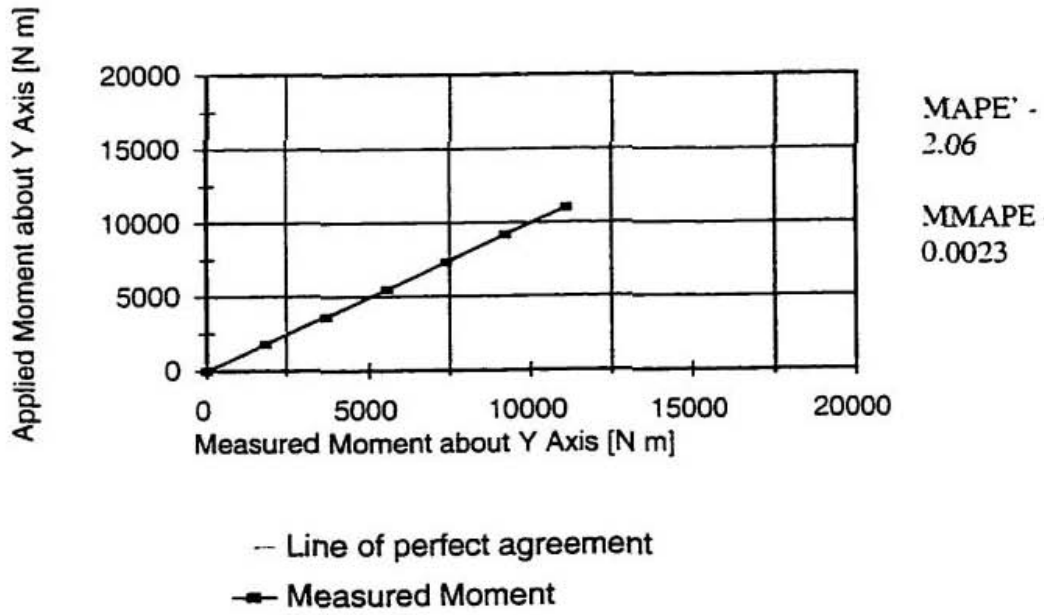

Figure B-60: Comparison of Moments about Y Axis - Orientation 8

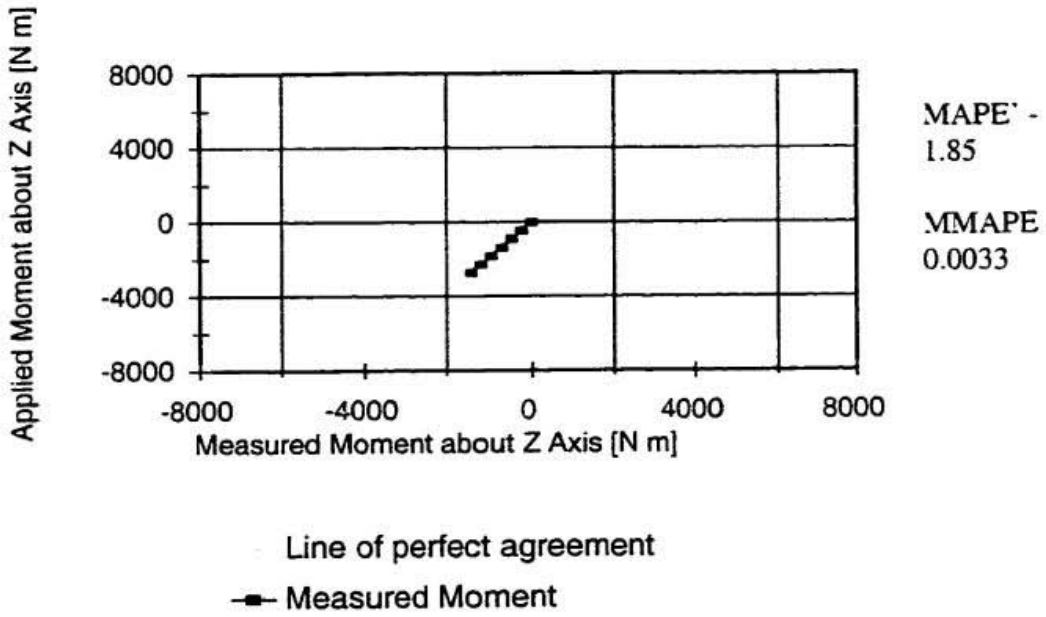

Figure B-61: Comparison of Moments About Z Axis - Orientation 8

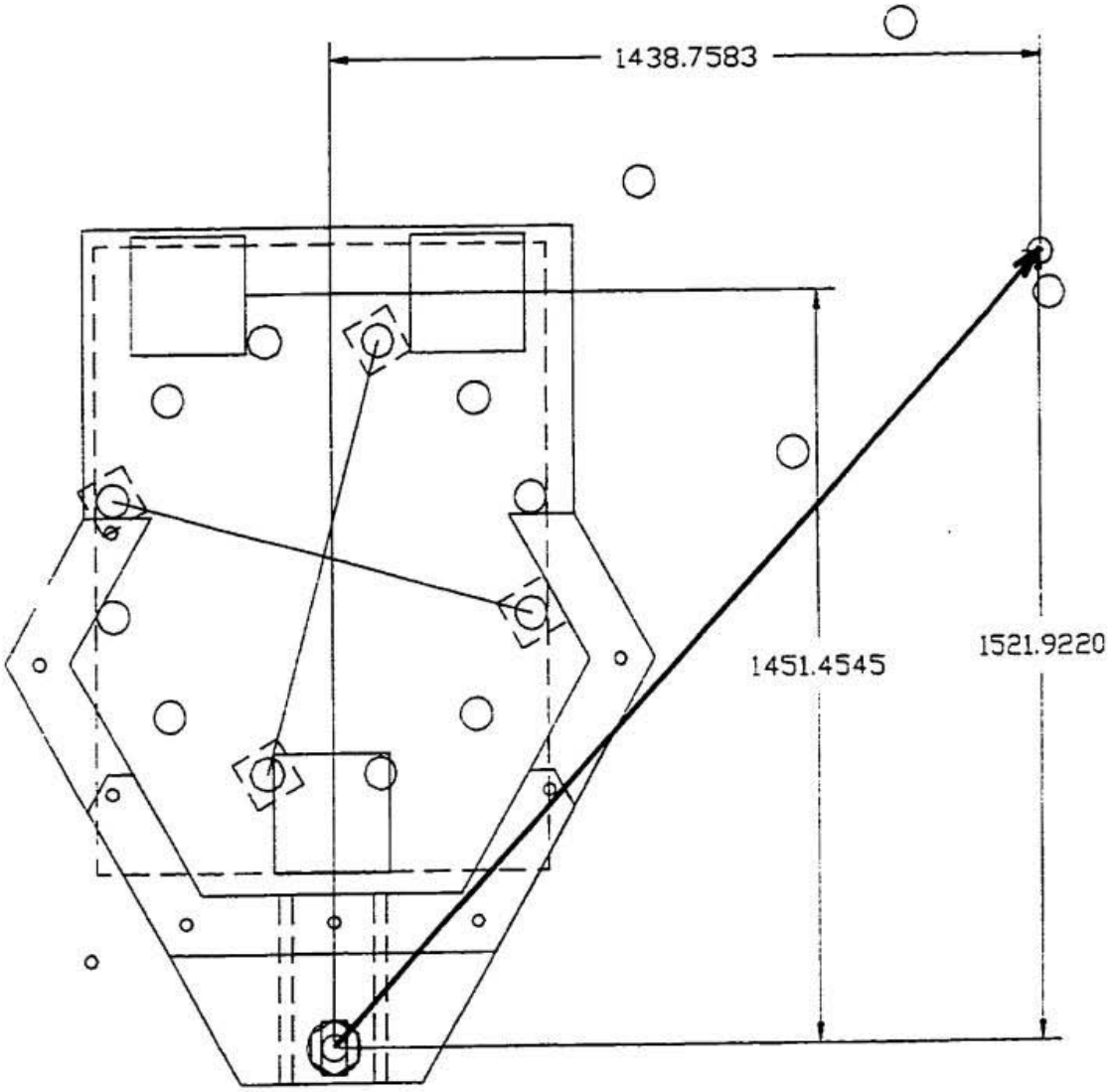

Figure B-62: Direction of Load Application - Orientation 9

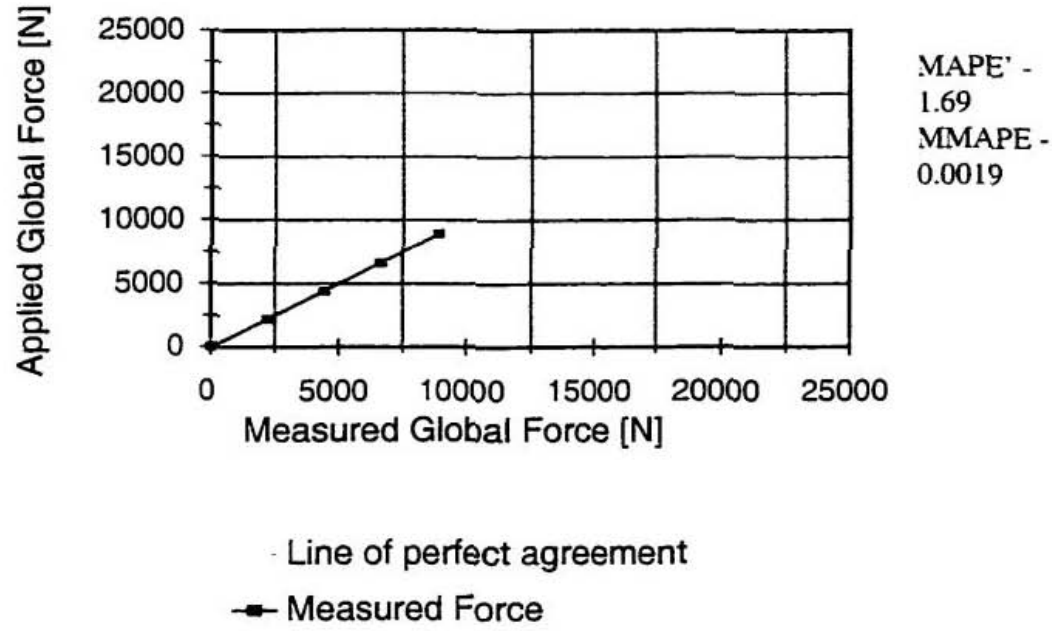

Figure B-63: Global Force Comparison - Orientation 9

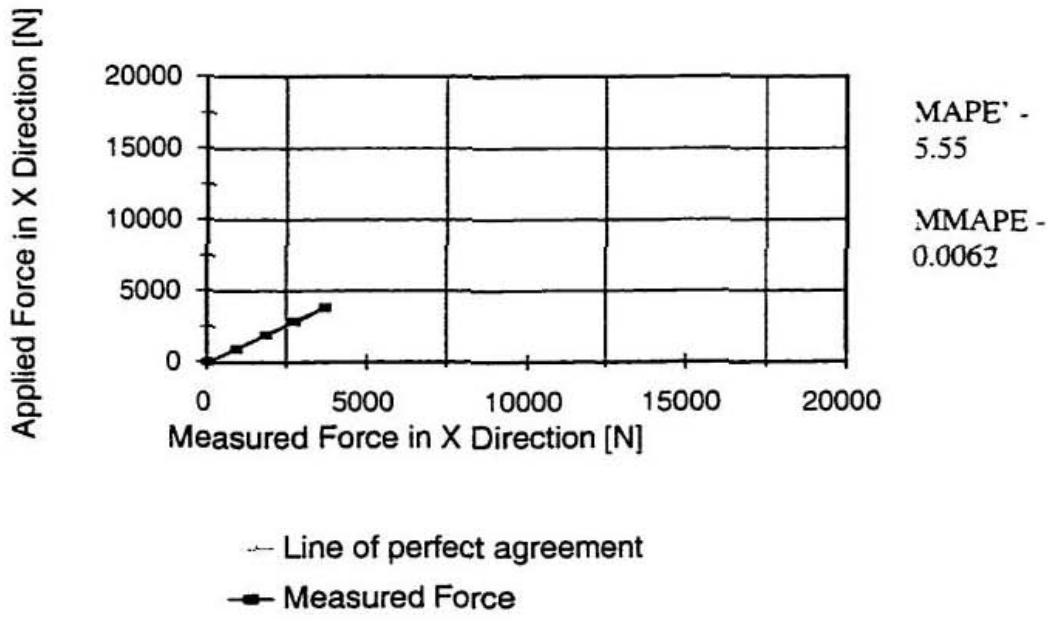

Figure B-64: Comparison of Forces in X Direction - Orientation 9

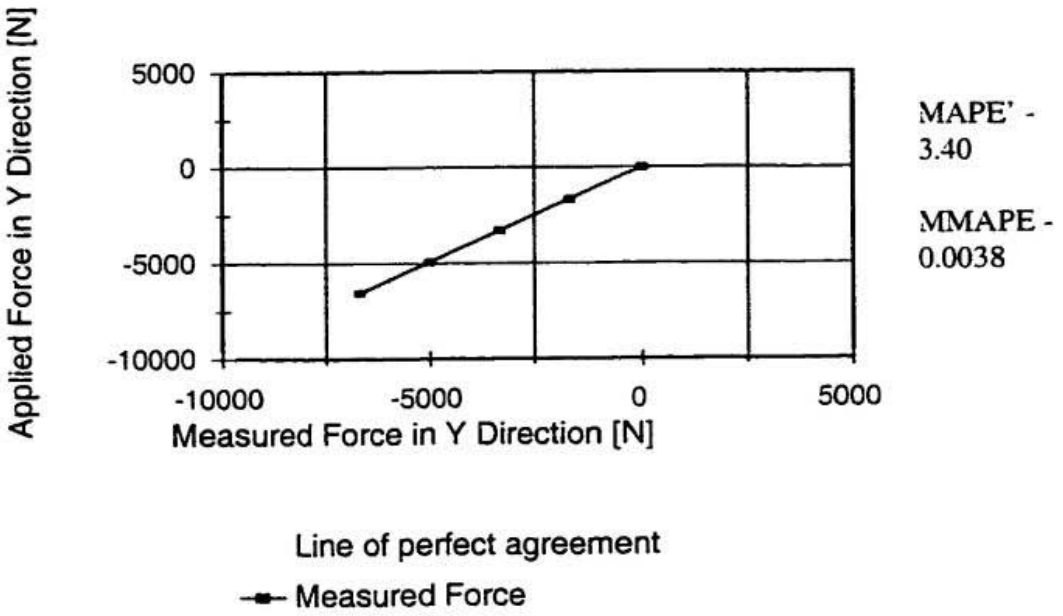

Figure B-65: Comparison of Forces in Y Direction - Orientation 9

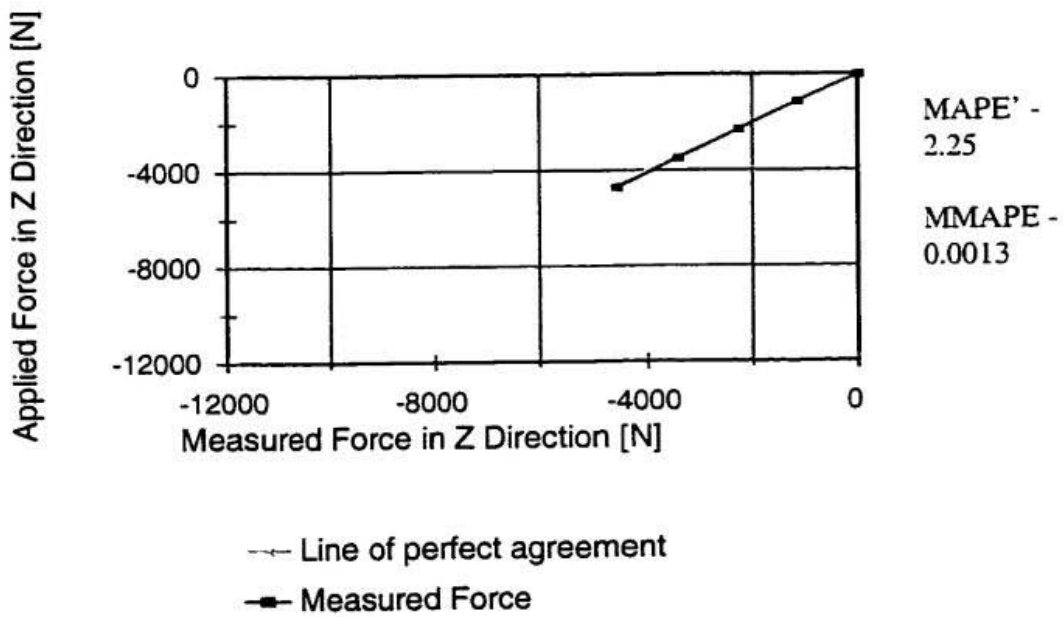

Figure B-66: Comparison of Forces in Z Direction - Orientation 9

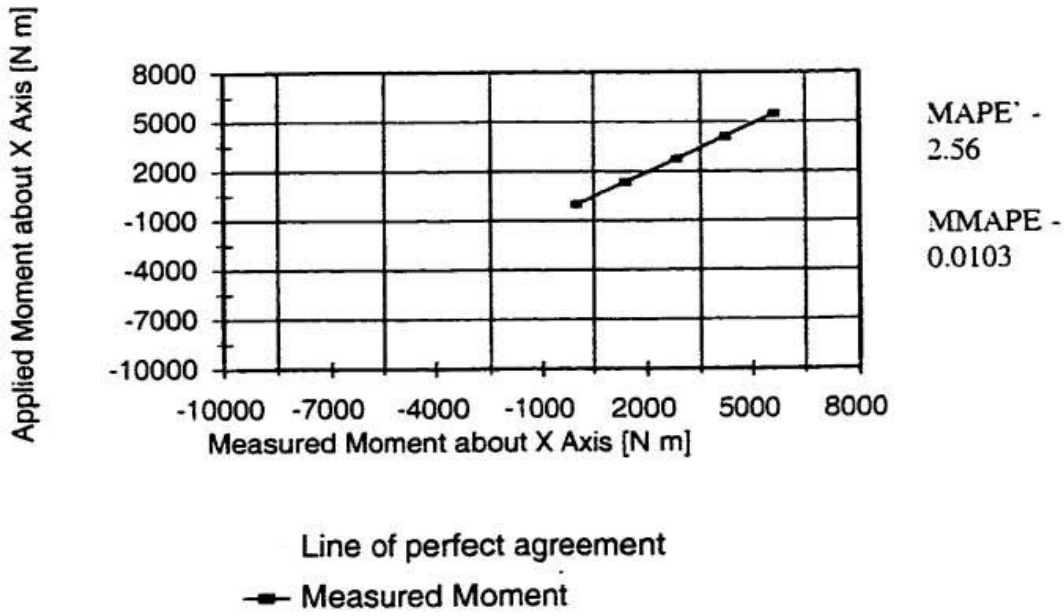

Figure B-67: Comparison of Moments About X Axis - Orientation 9

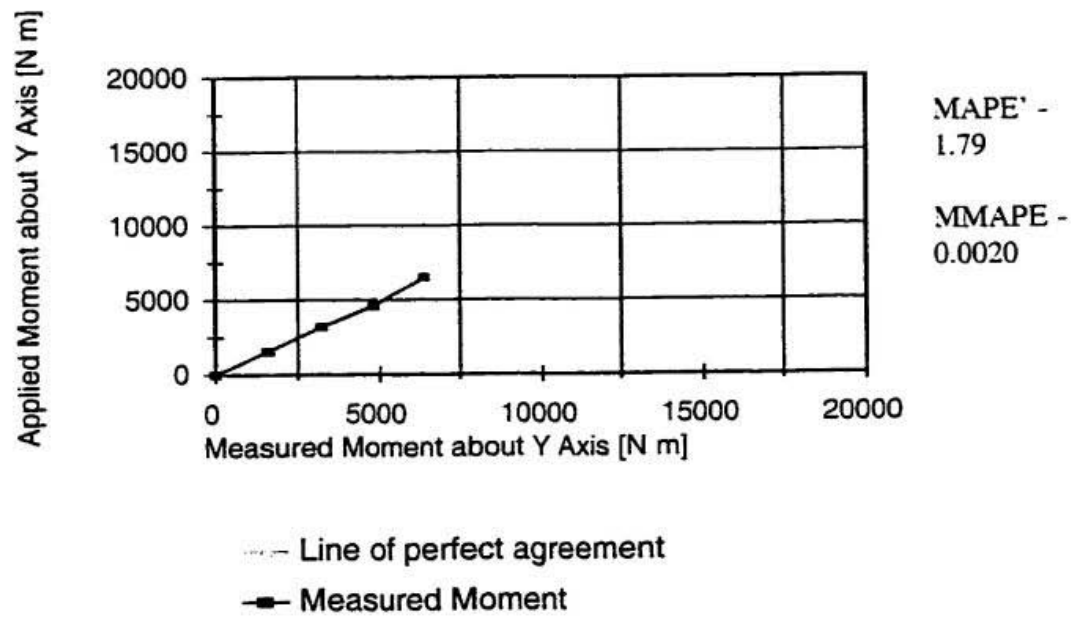

Figure B-68: Comparison of Moments about Y Axis - Orientation 9

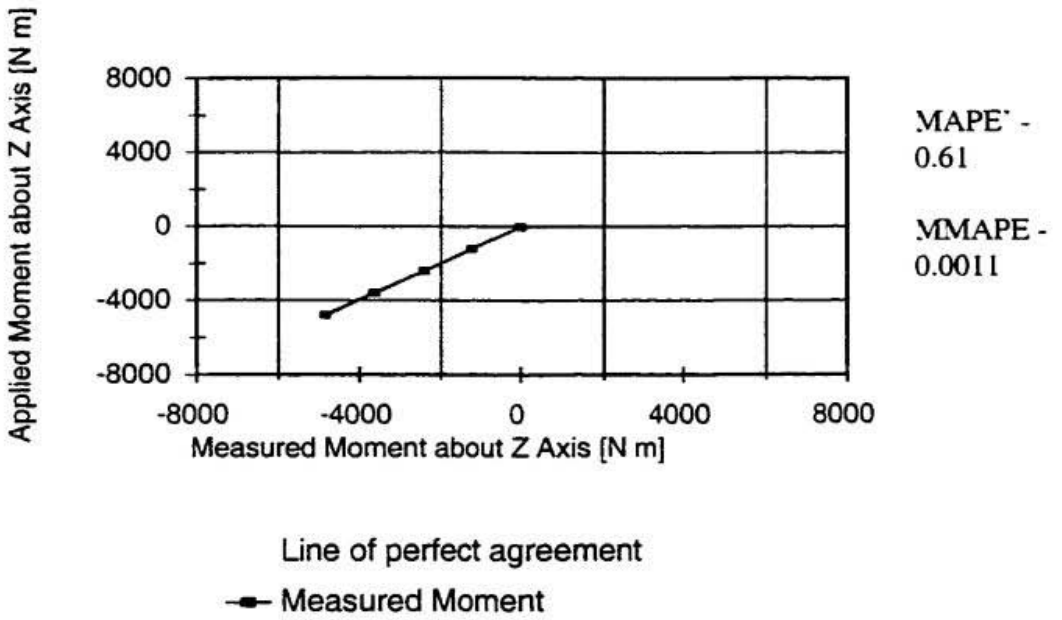

Figure B-69: Comparison of Moments About Z Axis - Orientation 9

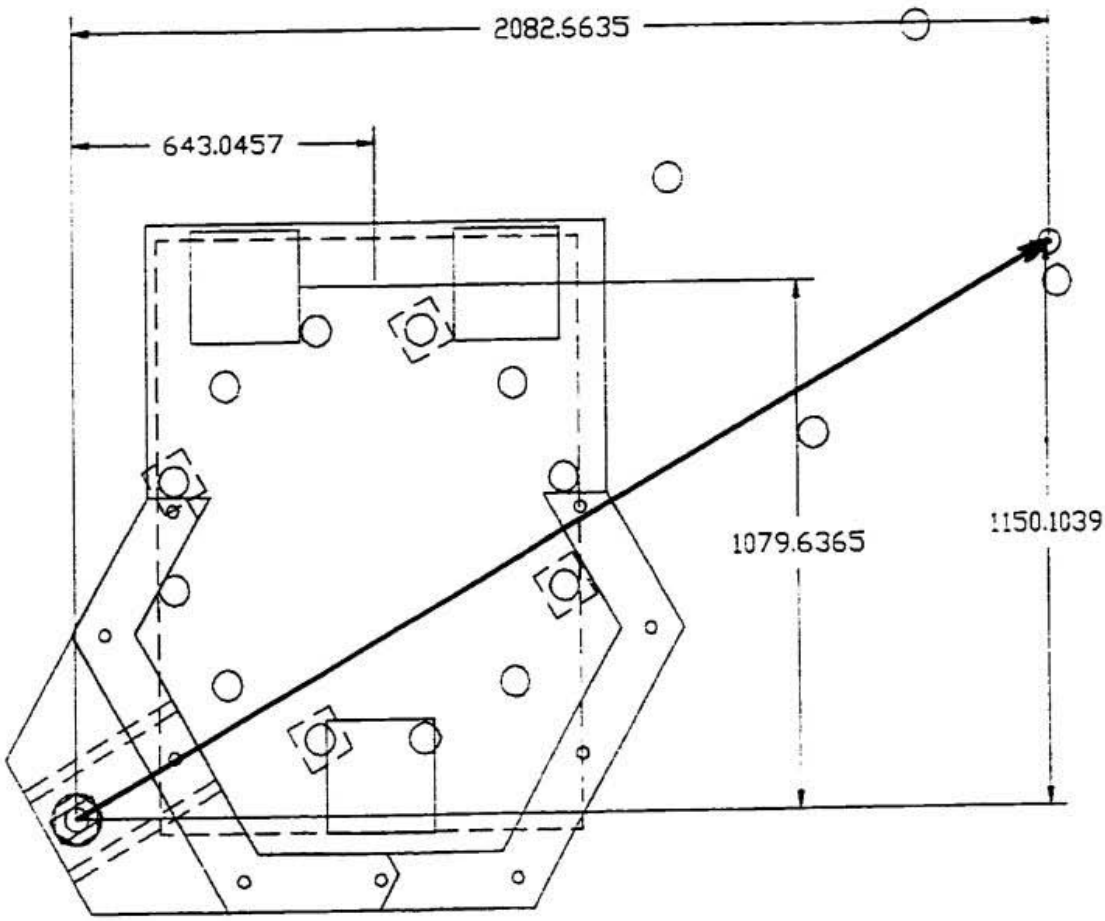

Figure B-70: Direction of Load Application - Orientation 10

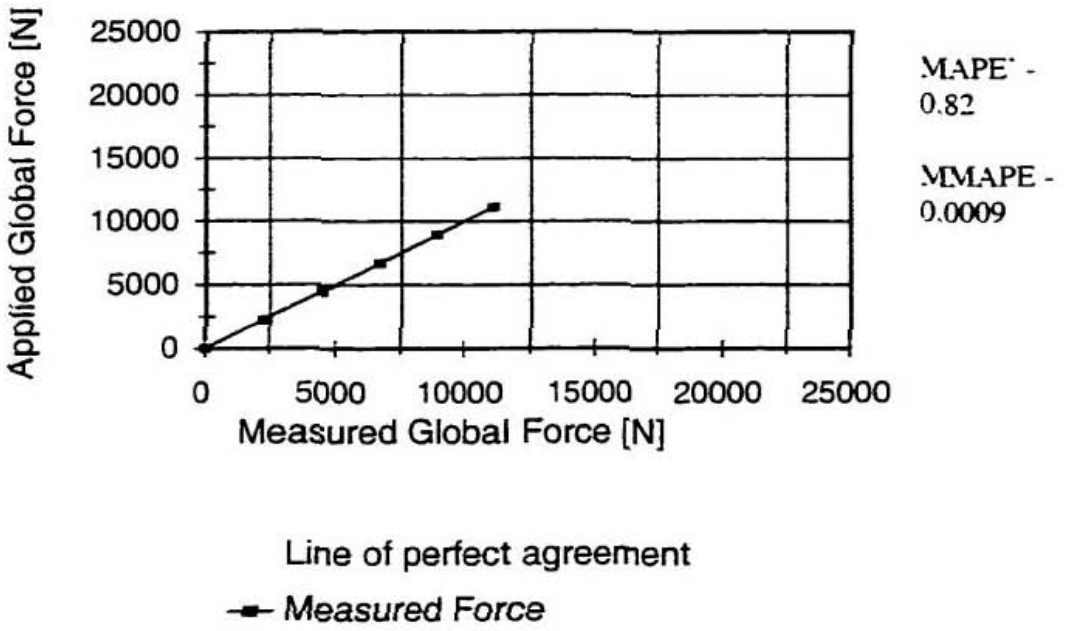

Figure B-71: Global Force Comparison - Orientation 10

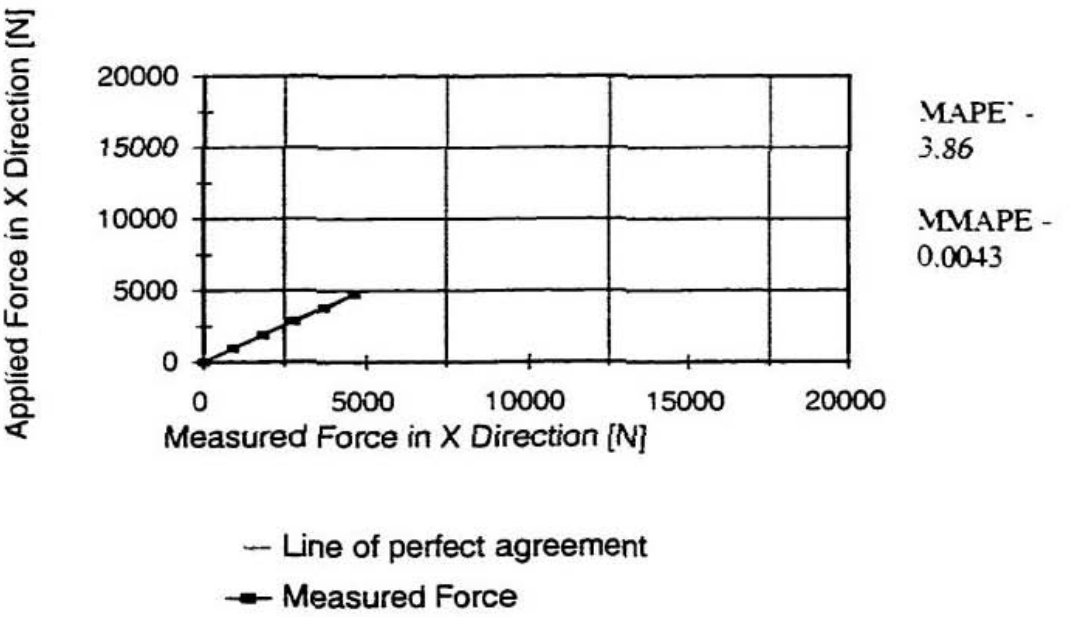

Figure B-72: Comparison of Forces in X Direction - Orientation 10

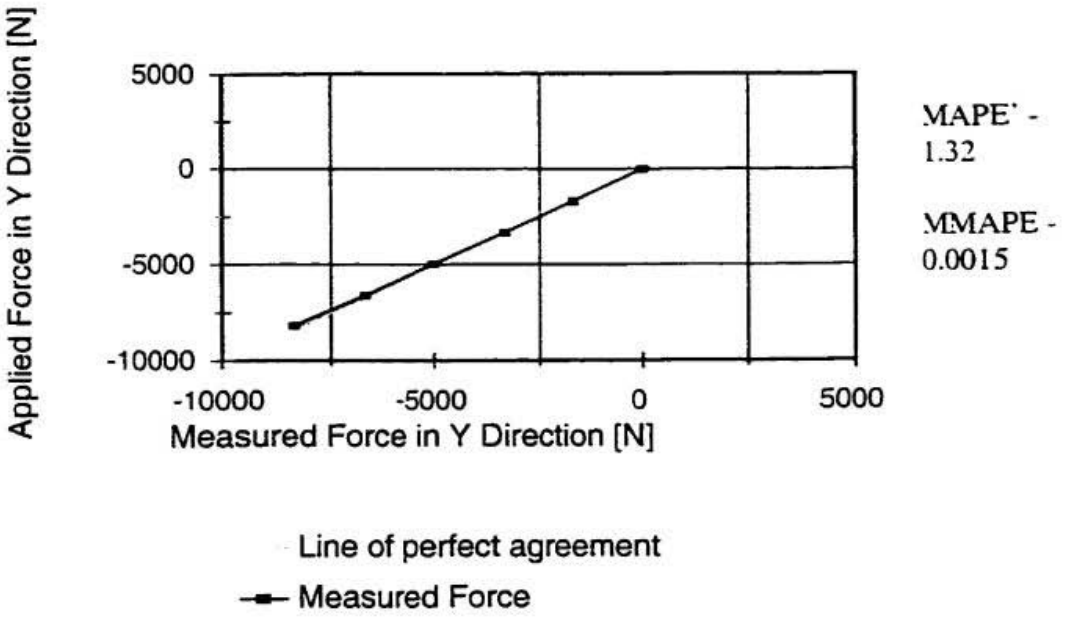

Figure B-73: Comparison of Forces in Y Direction - Orientation 10

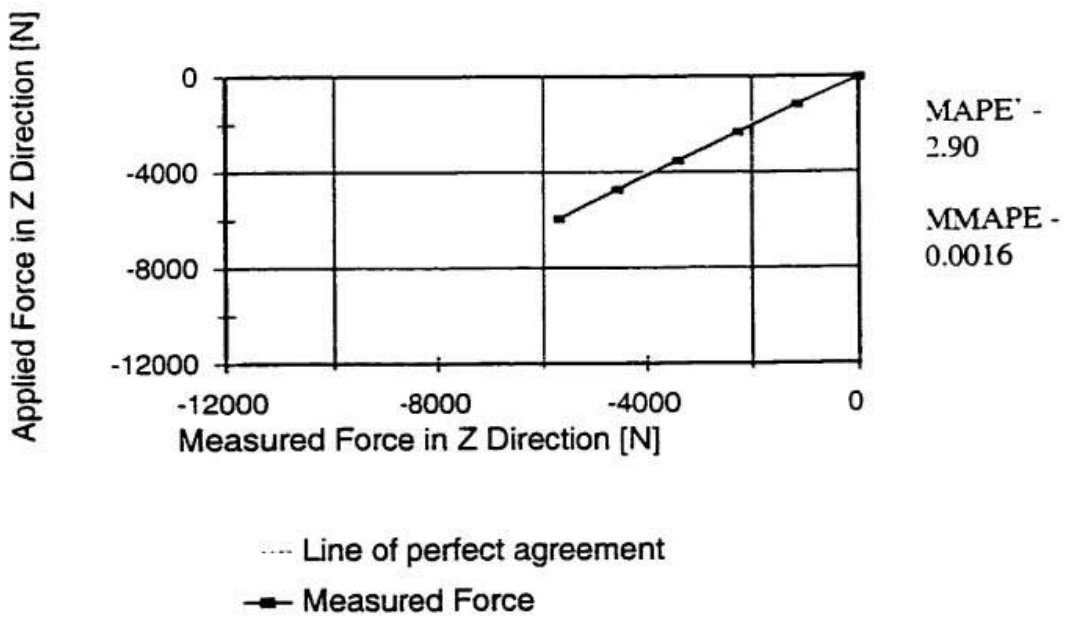

Figure B-74: Comparison of Forces in Z Direction - Orientation 10

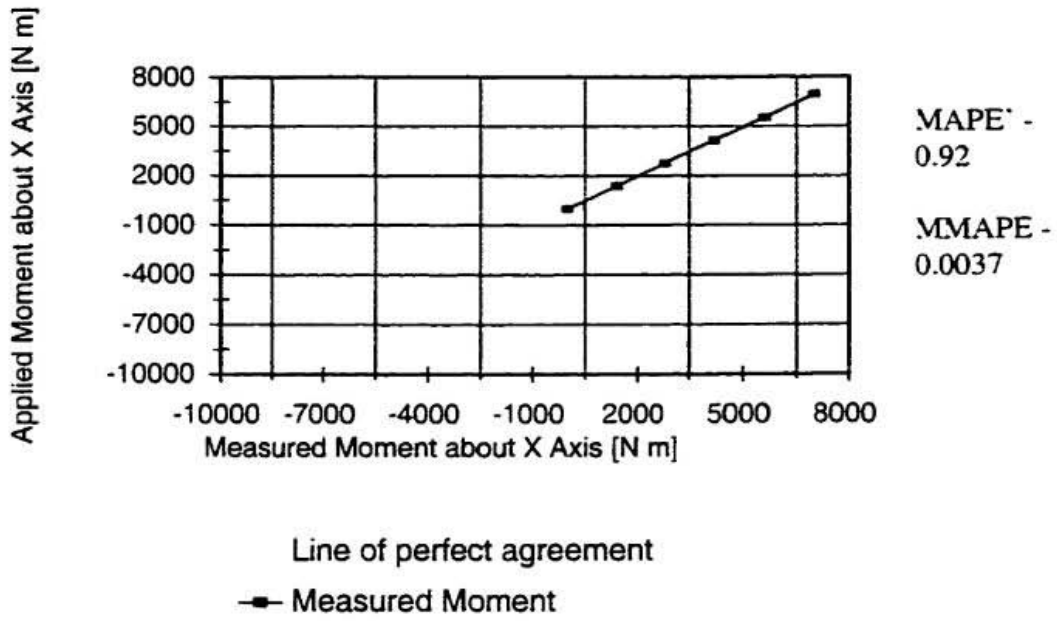

Figure B-75: Comparison of Moments About X Axis - Orientation 10

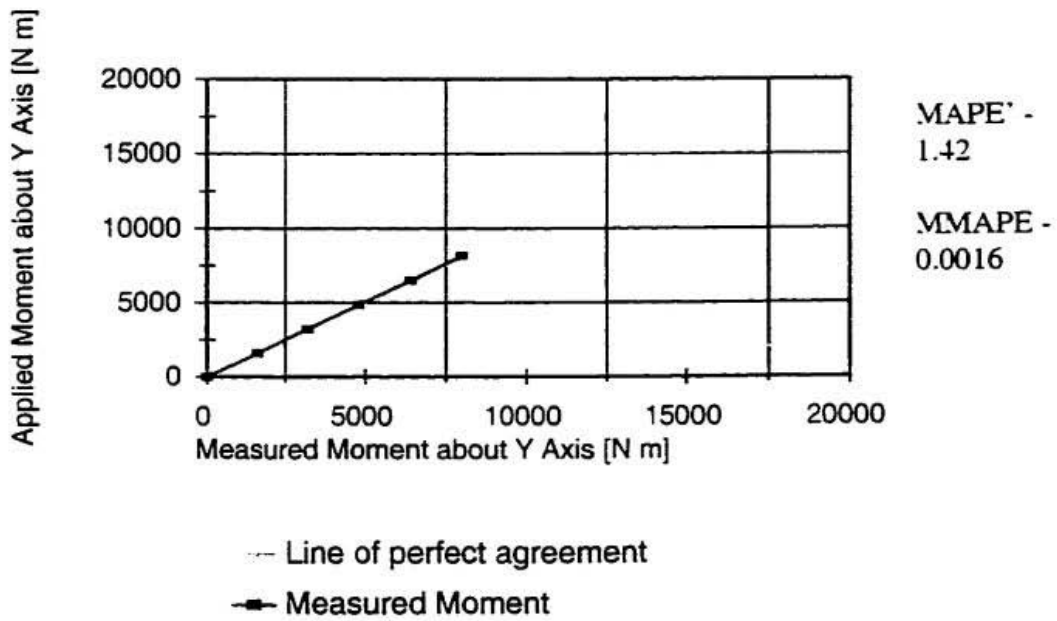

Figure B-76: Comparison of Moments about Y Axis - Orientation 10

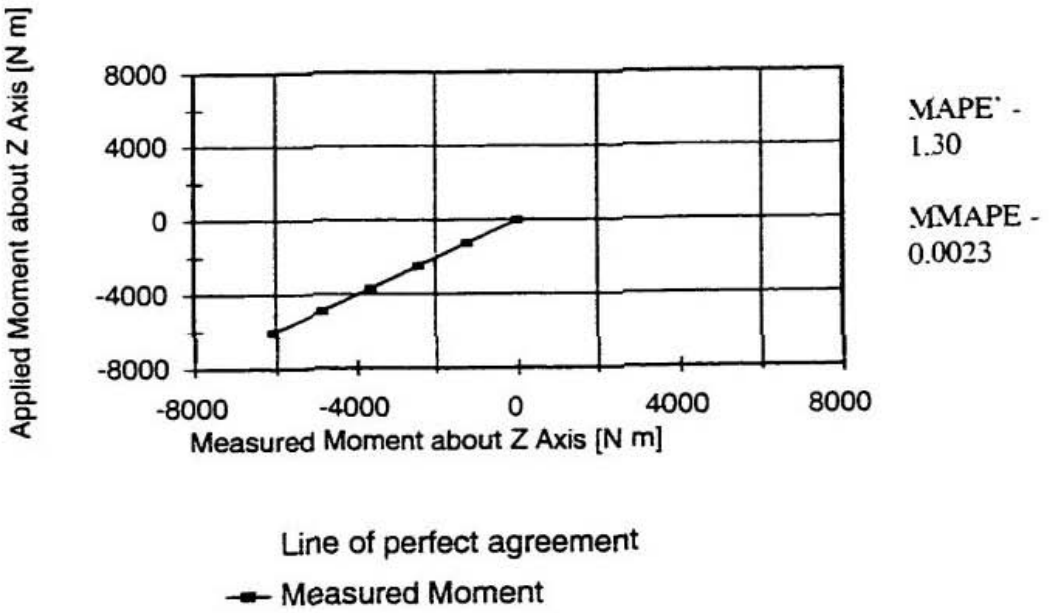

Figure B-77: Comparison of Moments About Z Axis - Orientation 10

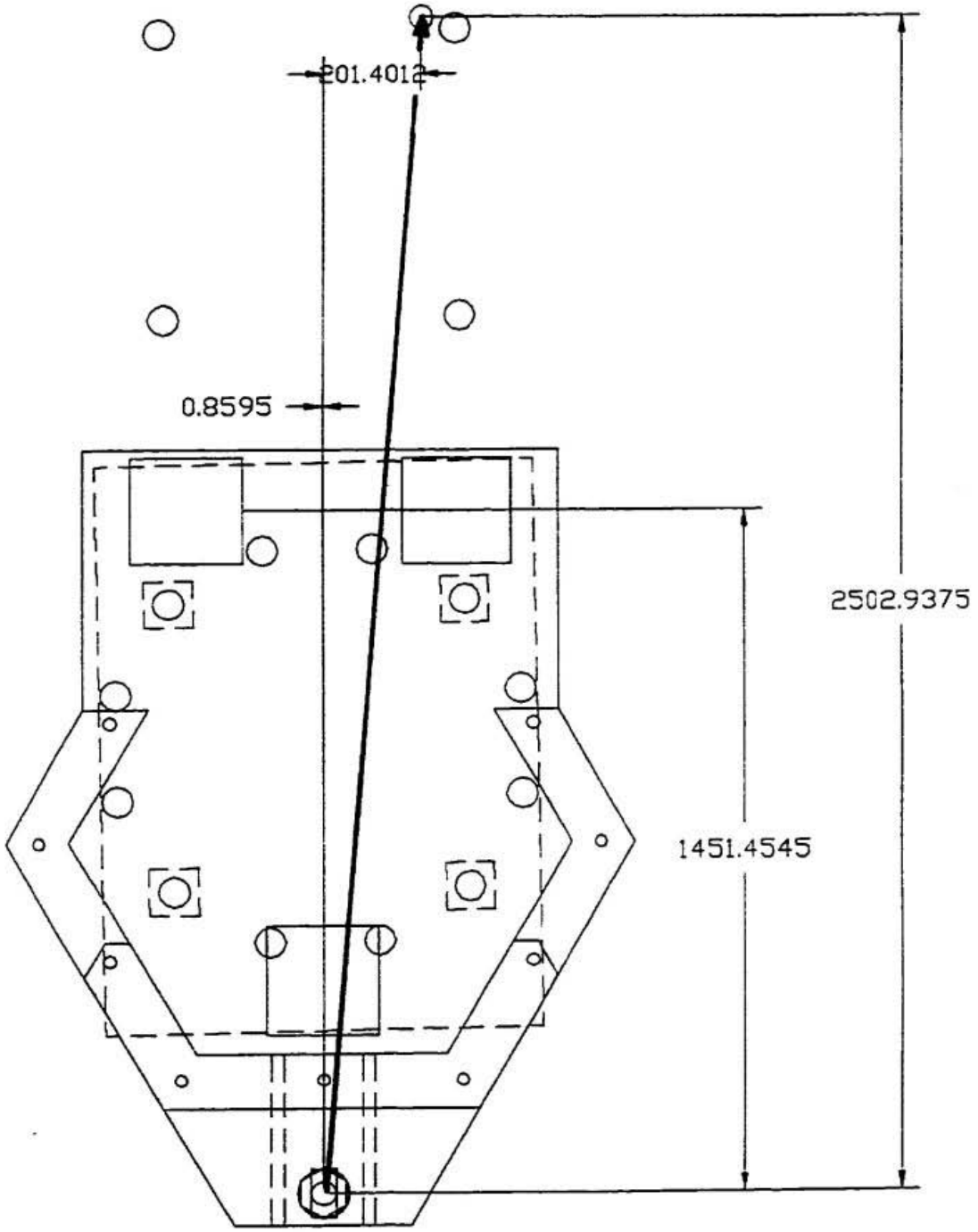

Figure B-78: Direction of Load Application - Orientation 11

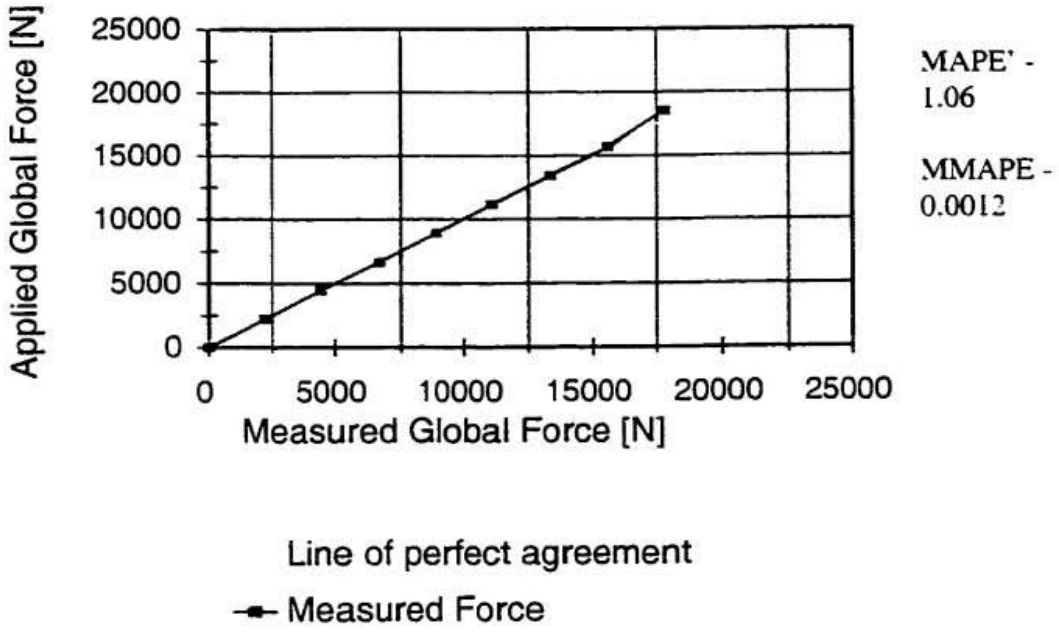

Figure B-79: Global Force Comparison - Orientation 11

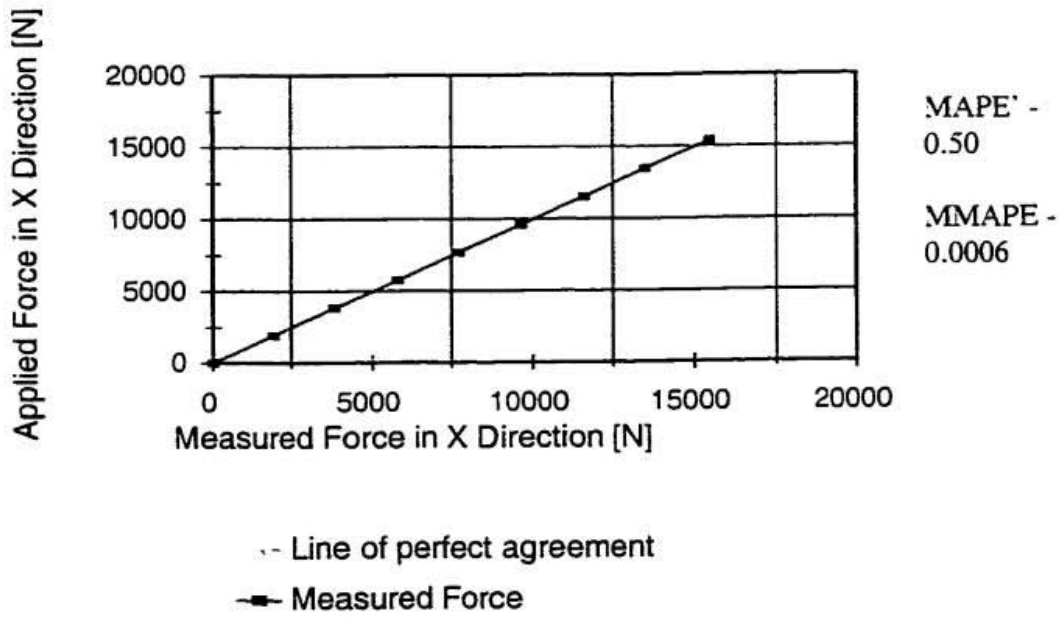

Figure B-80: Comparison of Forces in X Direction - Orientation 11

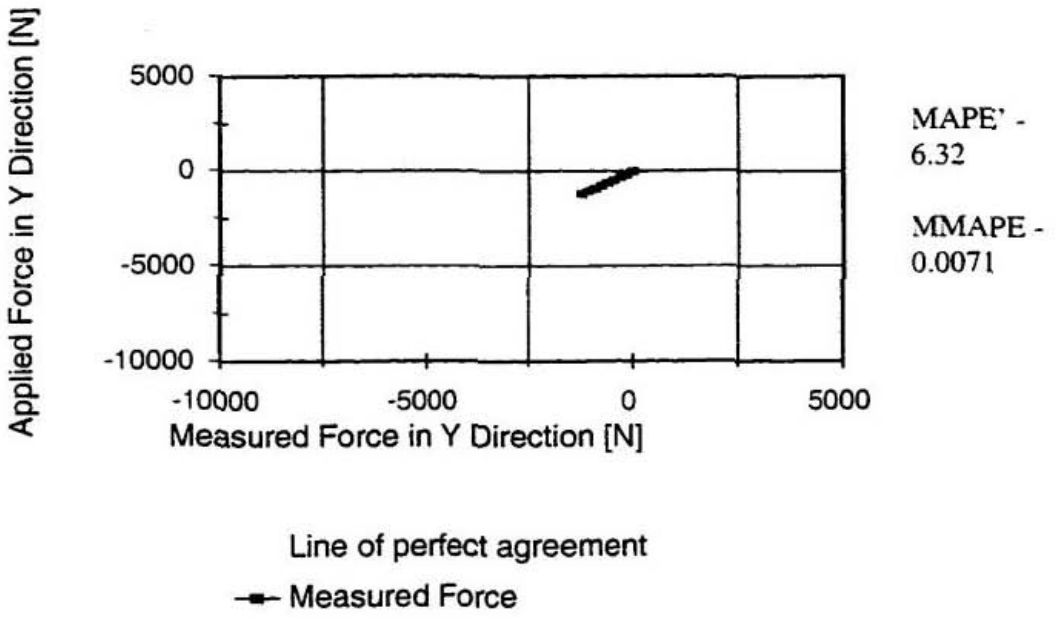

Figure B-81: Comparison of Forces in Y Direction - Orientation 11

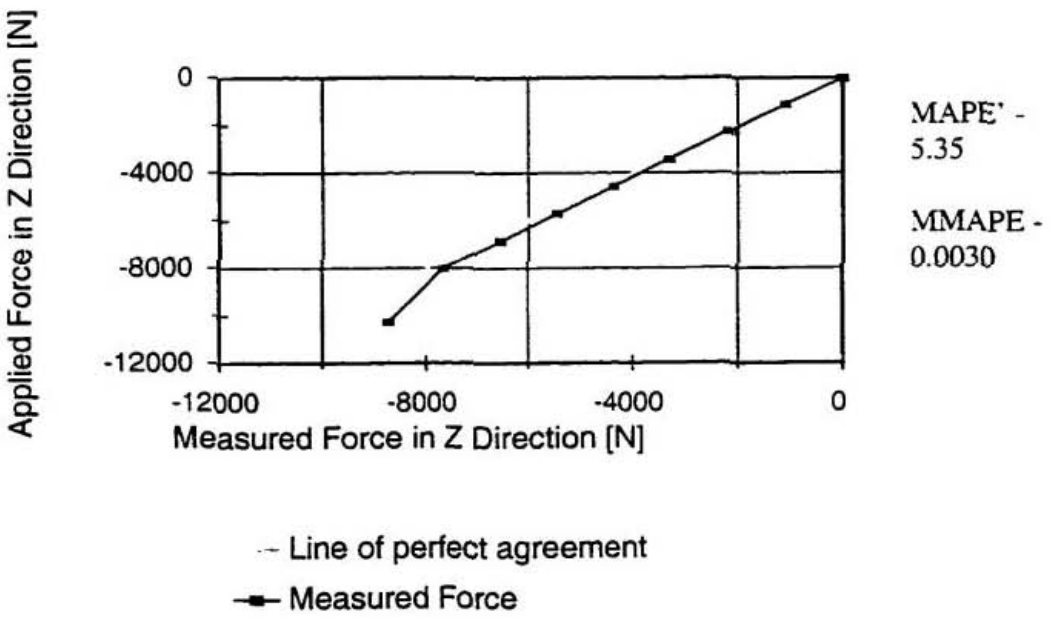

Figure B-82: Comparison of Forces in Z Direction - Orientation 11

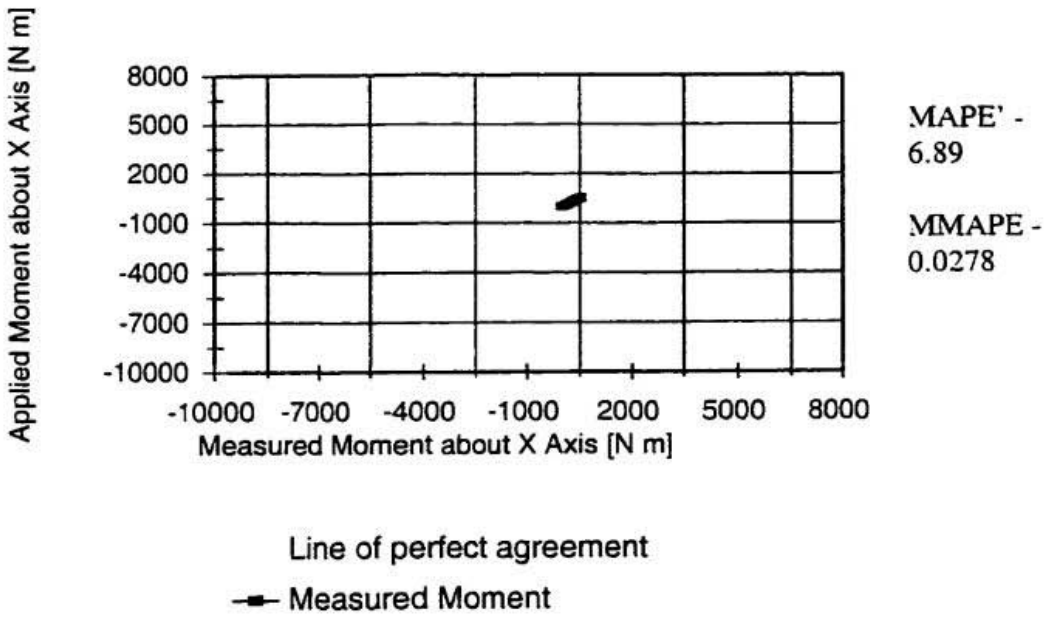

Figure B-83: Comparison of Moments About X Axis - Orientation 11

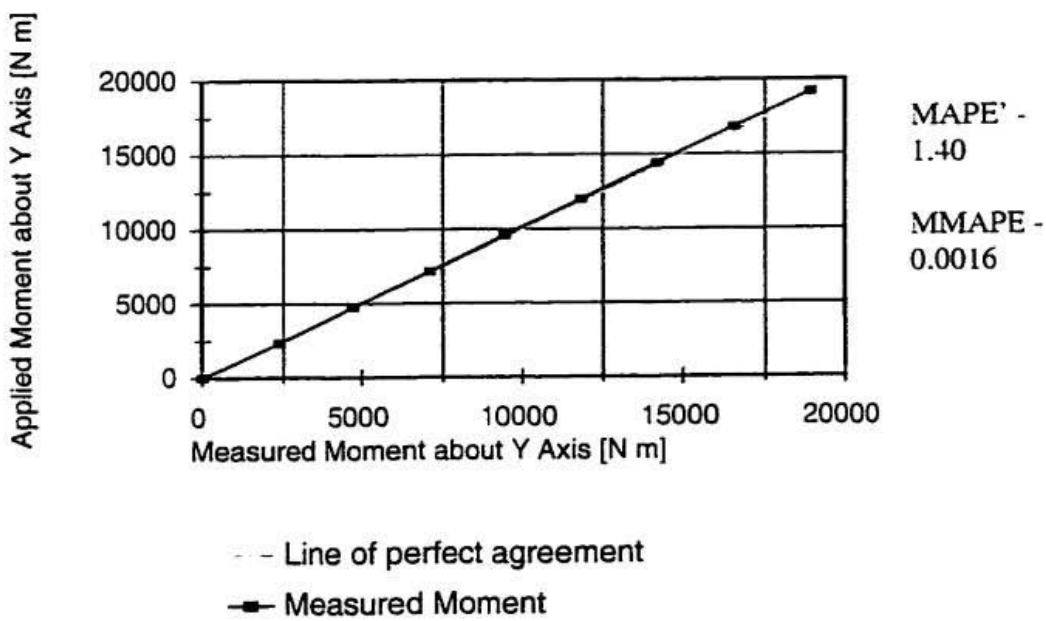

Figure B-84: Comparison of Moments about Y Axis - Orientation 11

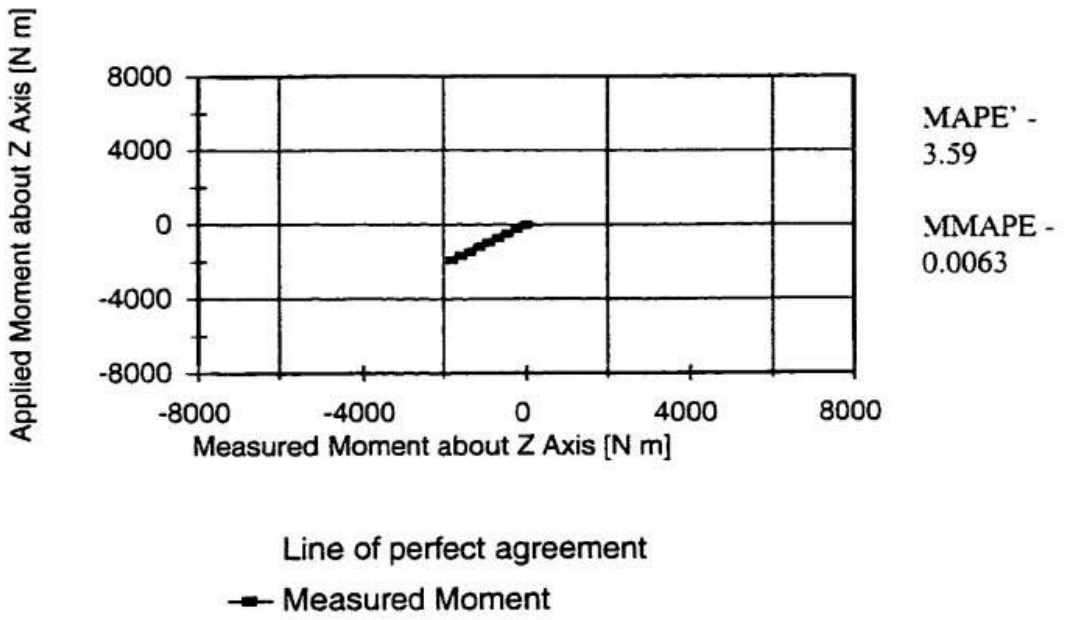

Figure B-85: Comparison of Moments About Z Axis - Orientation 11

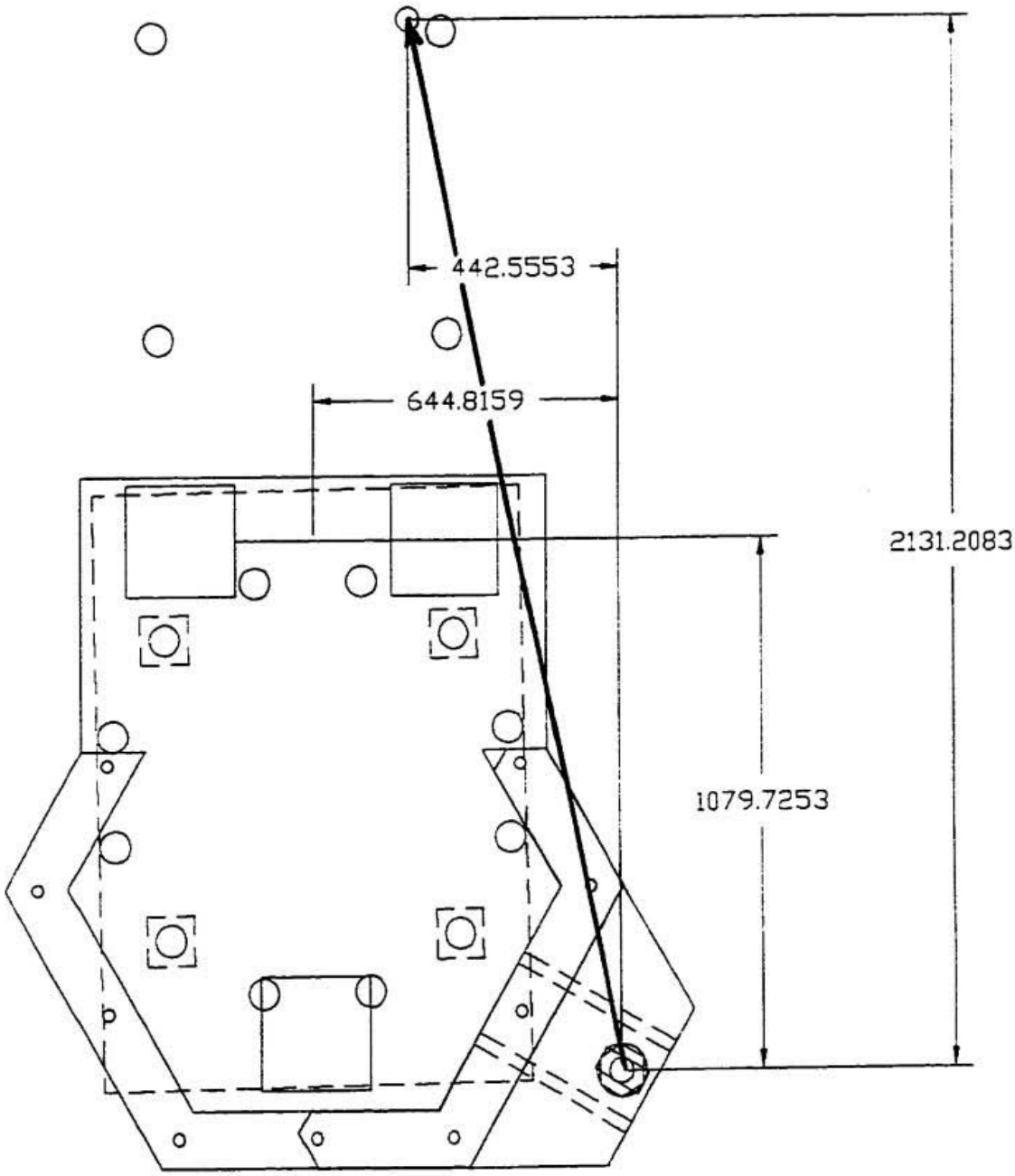

Figure B-86: Direction of Load Application - Orientation 12

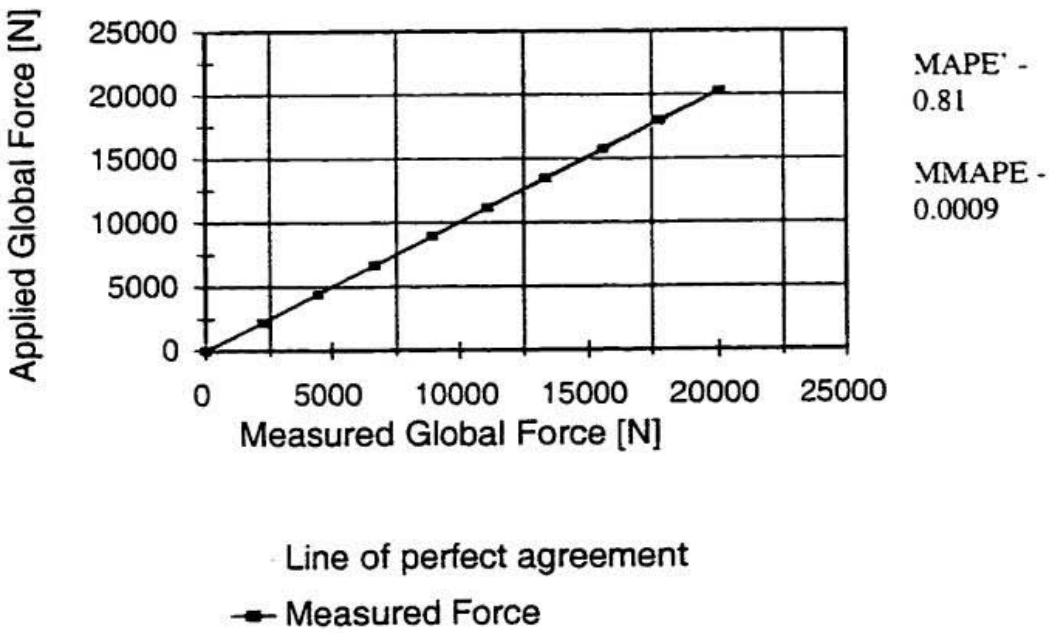

Figure B-87: Global Force Comparison - Orientation 12

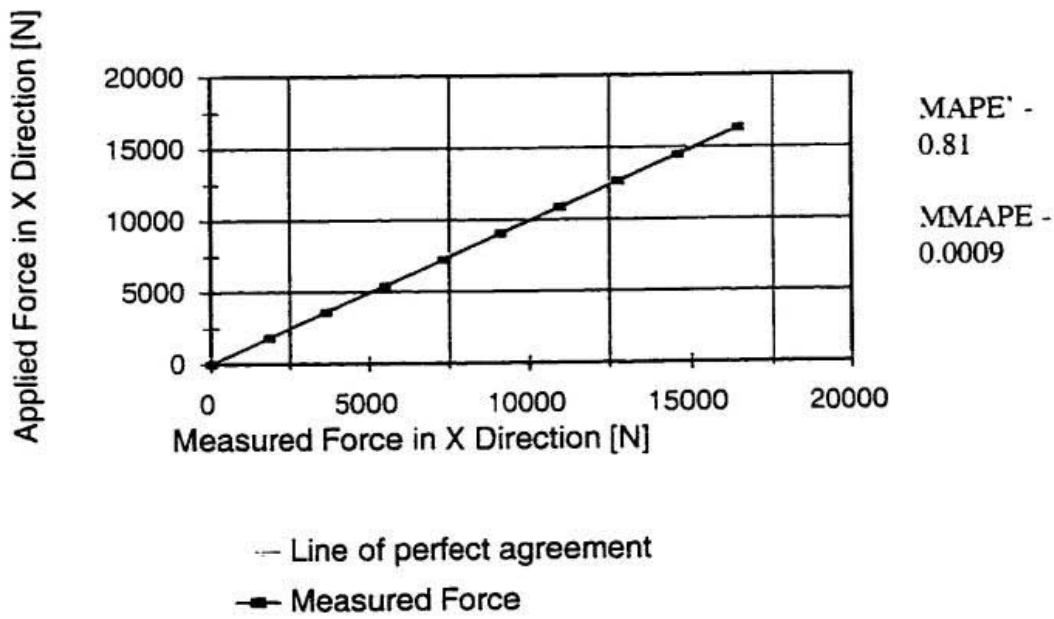

Figure B-88: Comparison of Forces in X Direction - Orientation 12

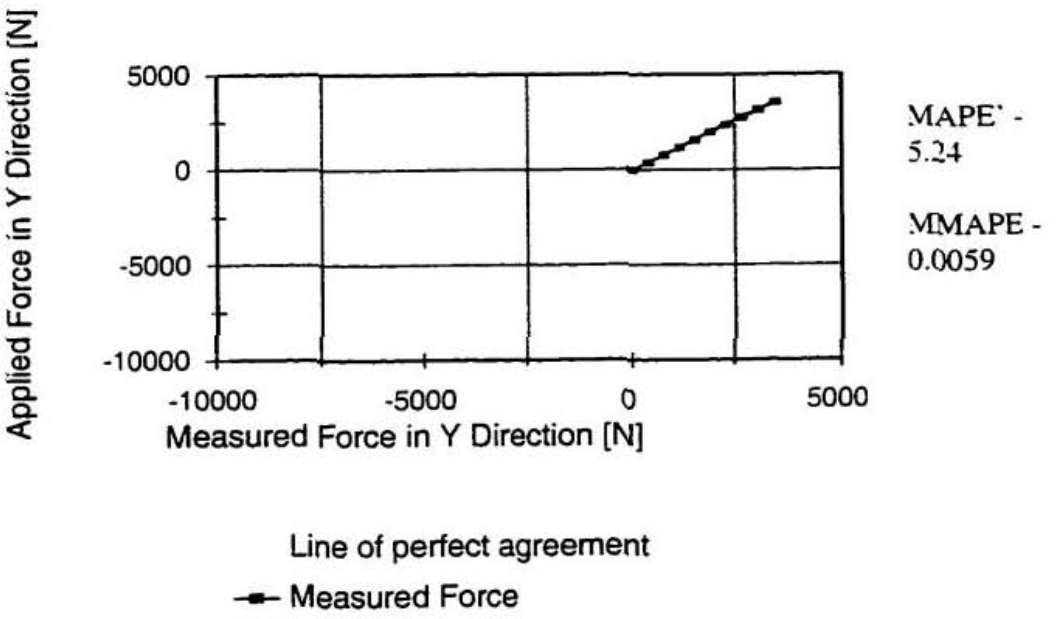

Figure B-89: Comparison of Forces in Y Direction - Orientation 12

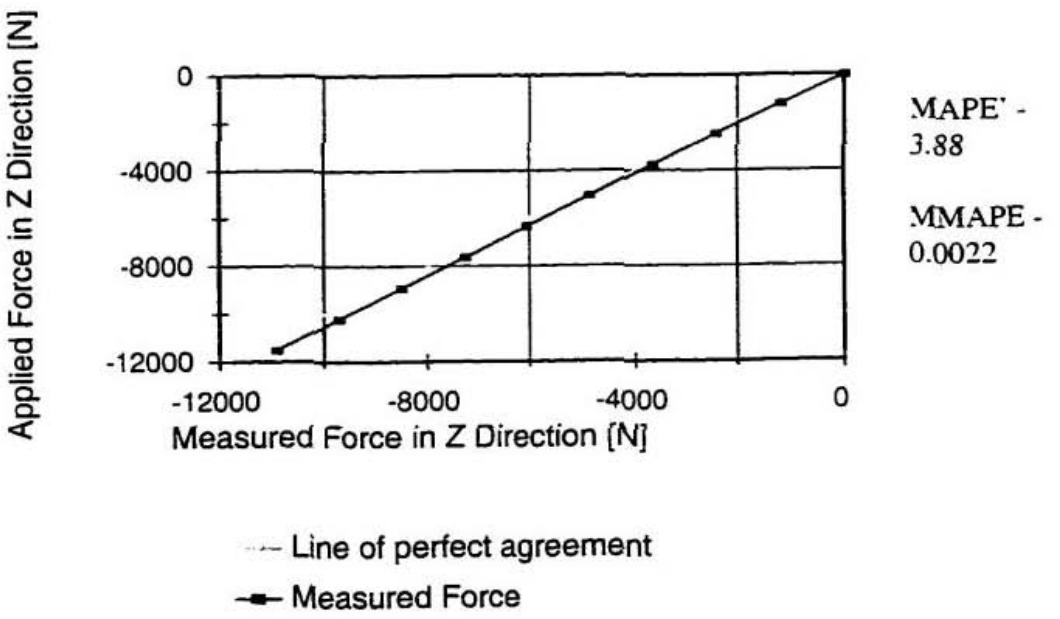

Figure B-90: *Comparison* of Forces in Z Direction - Orientation 12

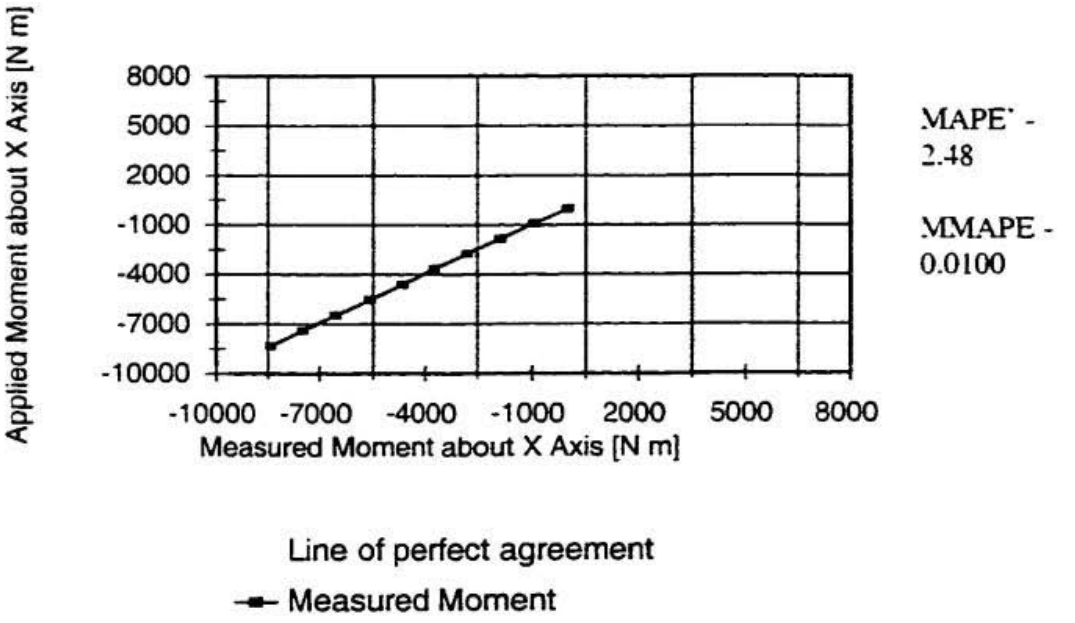

Figure B-91: Comparison of Moments About X Axis - Orientation 12

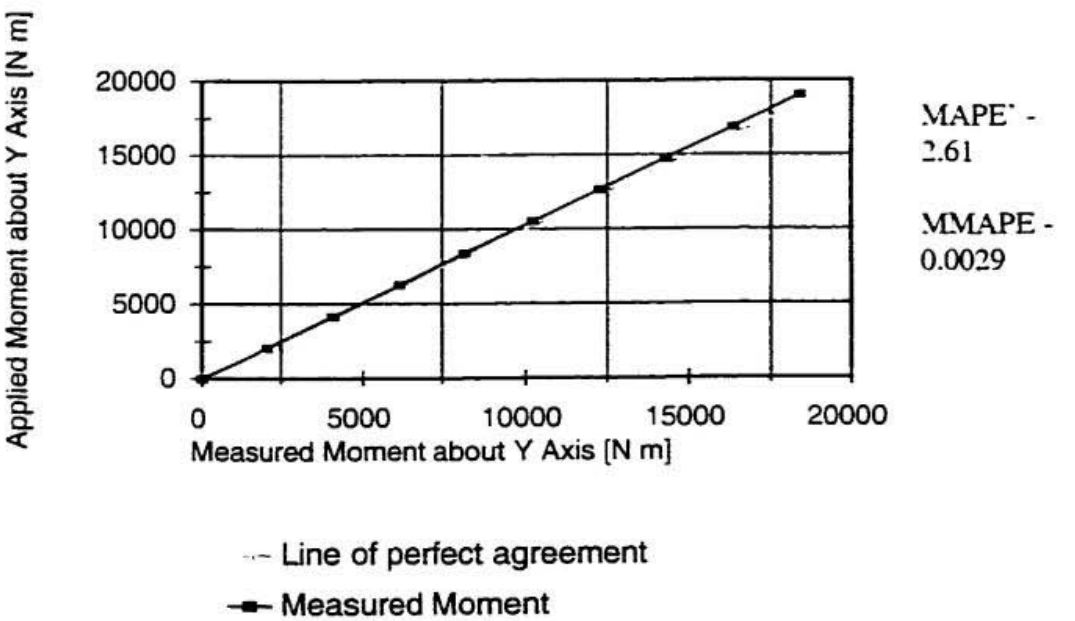

Figure B-92: Comparison of Moments about Y Axis - Orientation 12

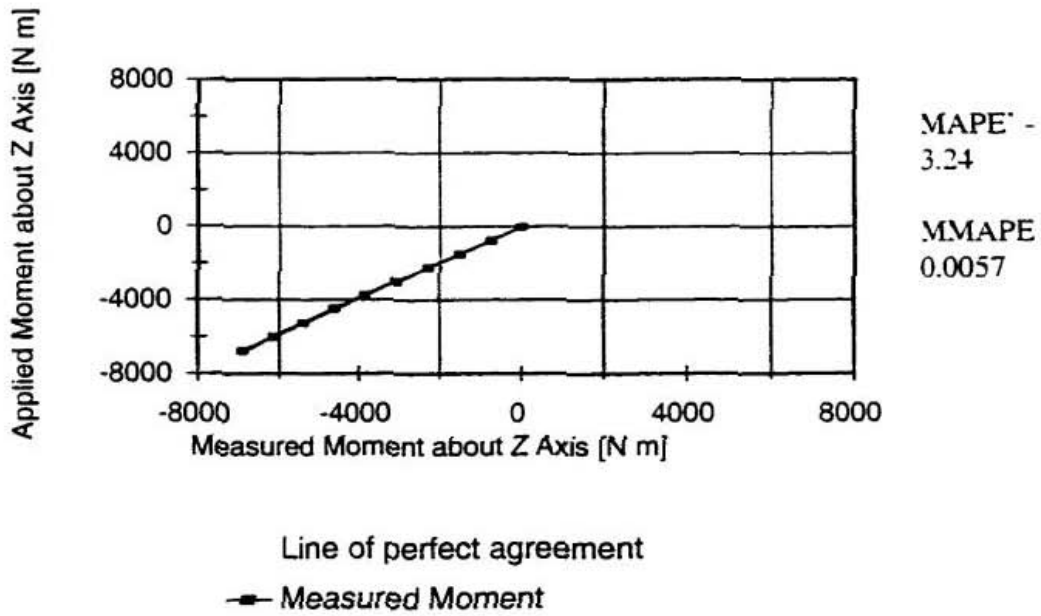

Figure B-93: Comparison of Moments About Z Axis - Orientation 12

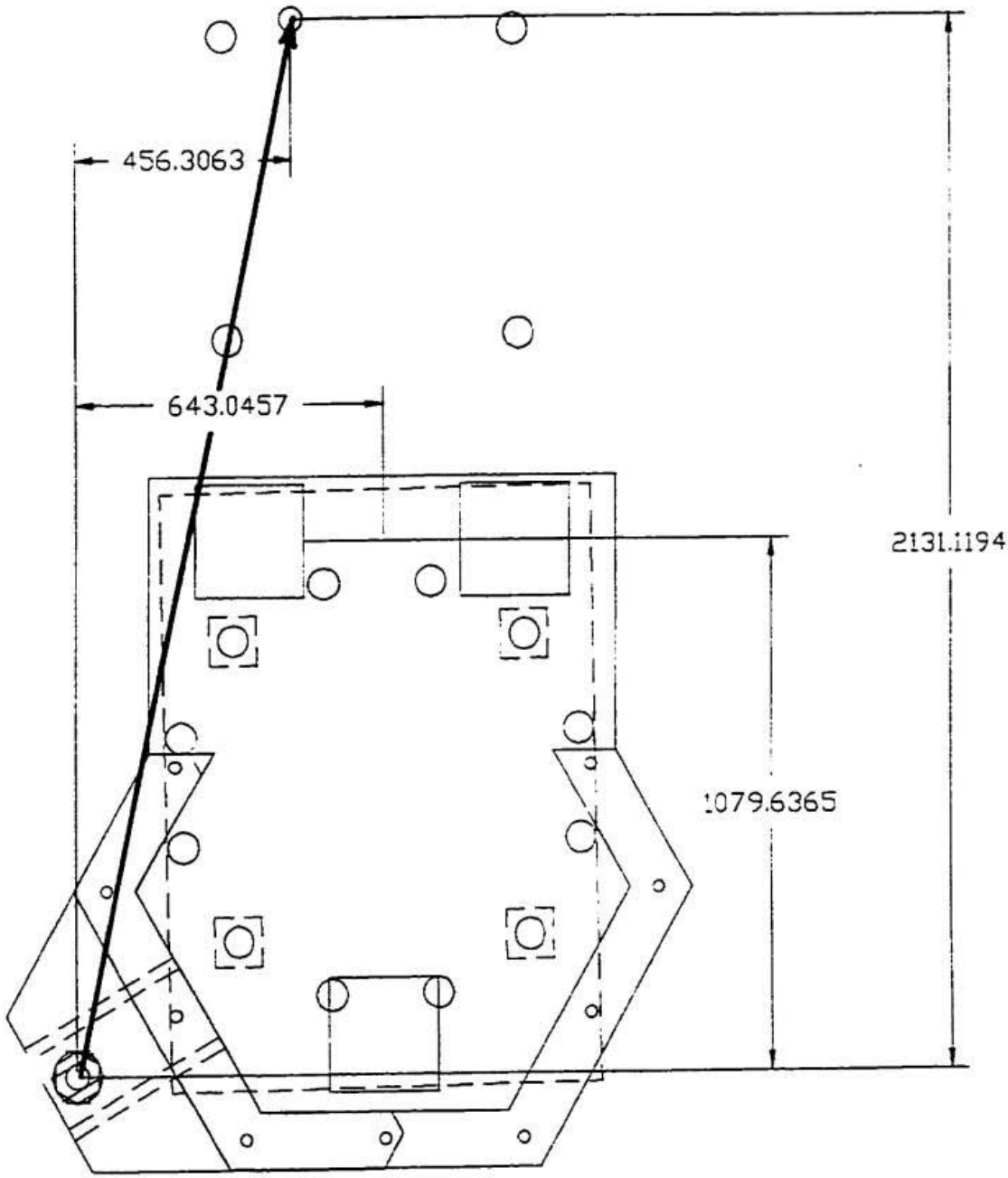

Figure B-94: Direction of Load Application - Orientation 13

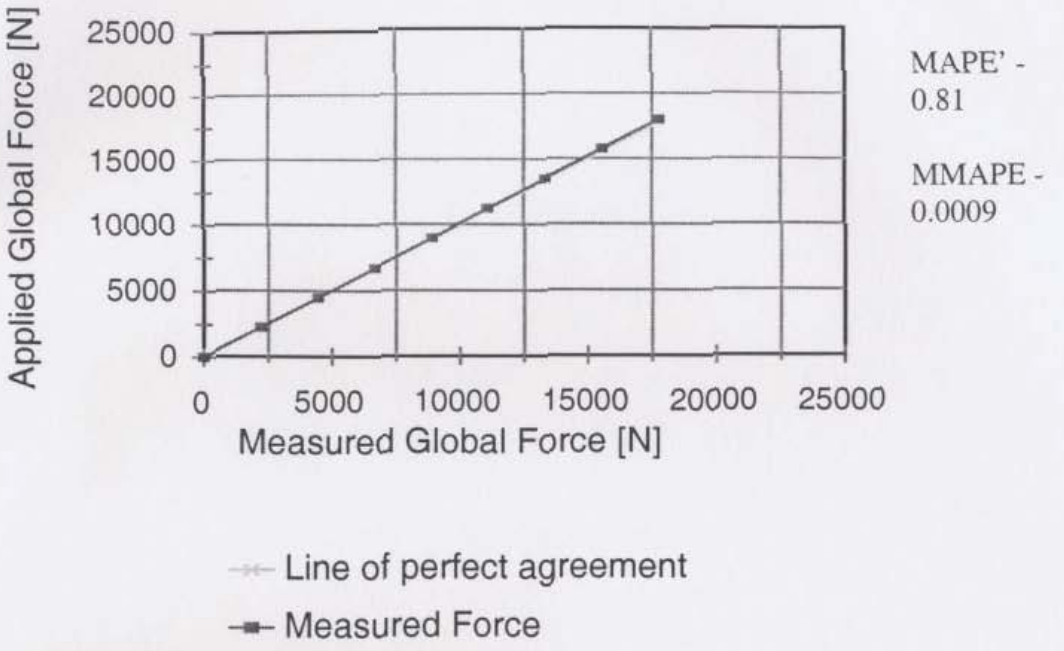

Figure B-95: Global Force Comparison - Orientation 13

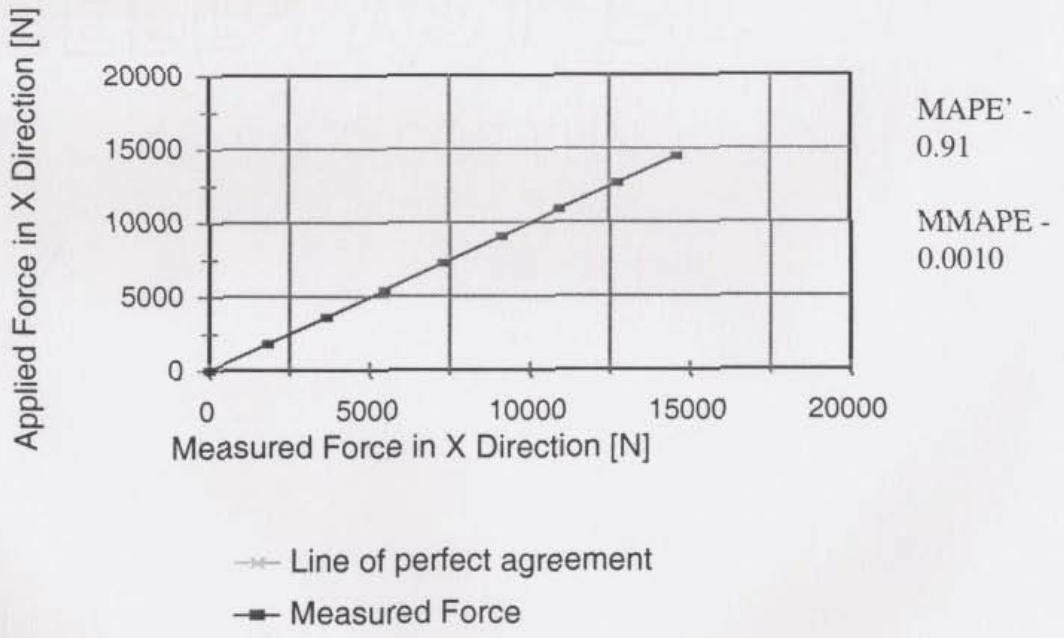

Figure B-96: Comparison of Forces in X Direction - Orientation 13

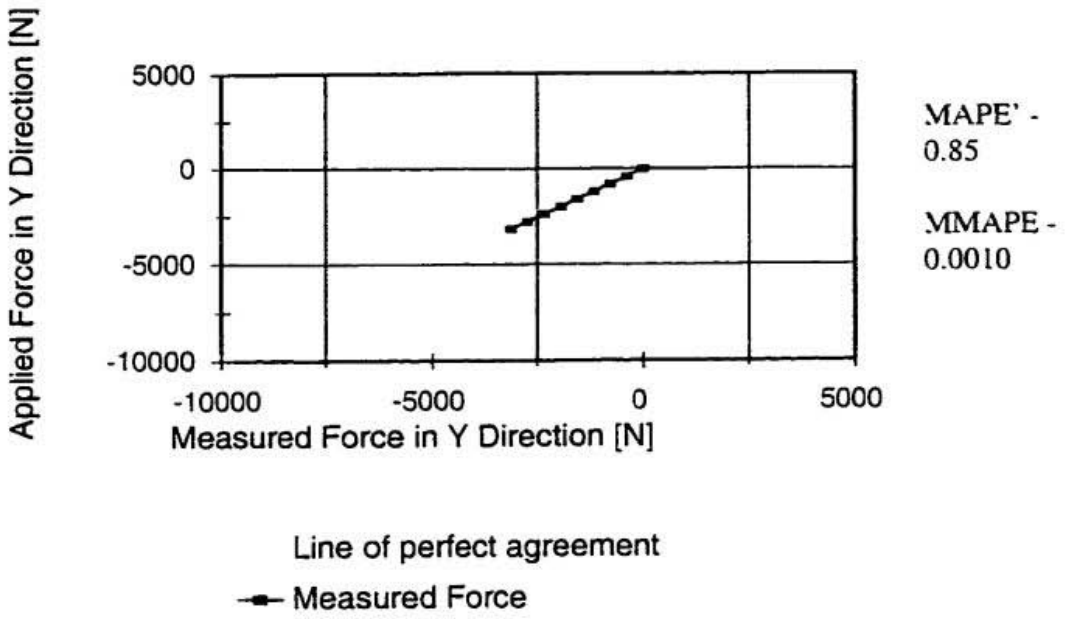

Figure B-97: Comparison of Forces in Y Direction - Orientation 13

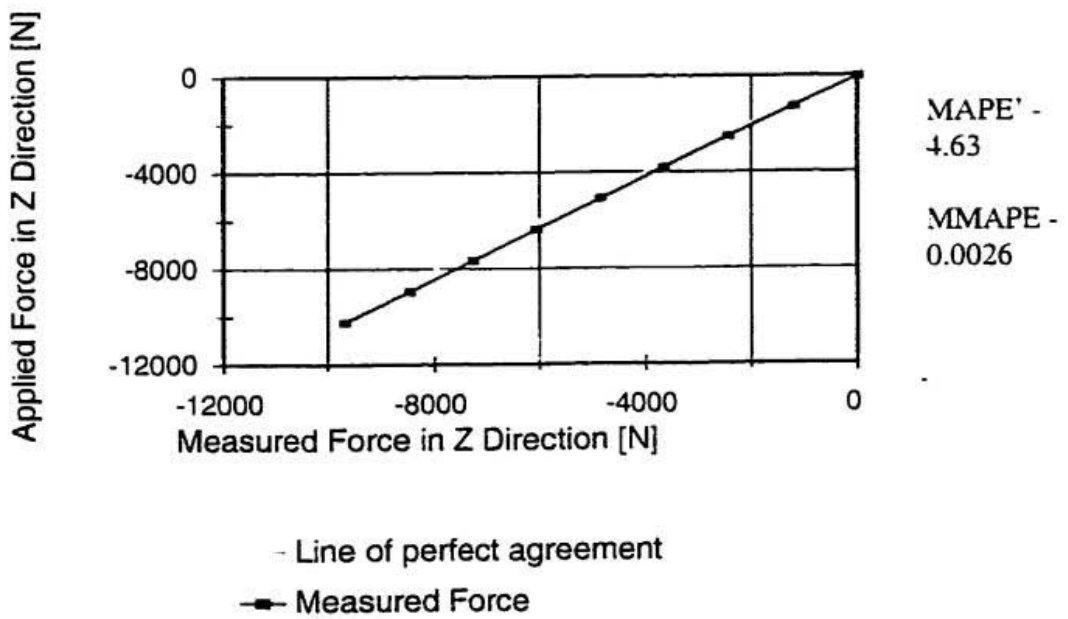

Figure B-98: Comparison of Forces in Z Direction - Orientation 13

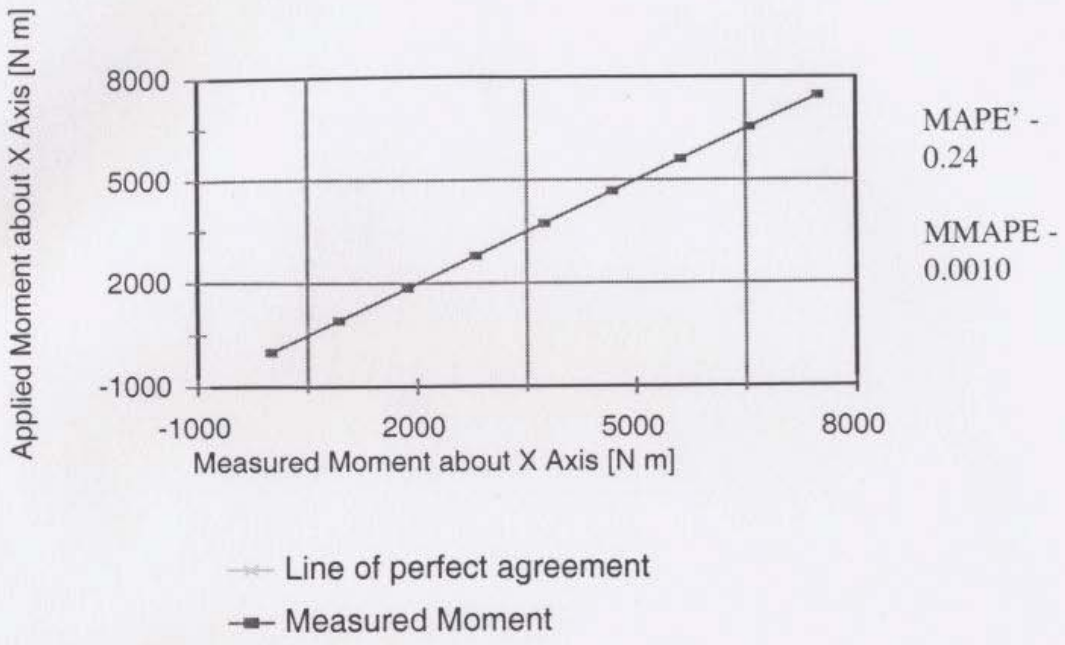

Figure B-99: Comparison of Moments About X Axis - Orientation 13

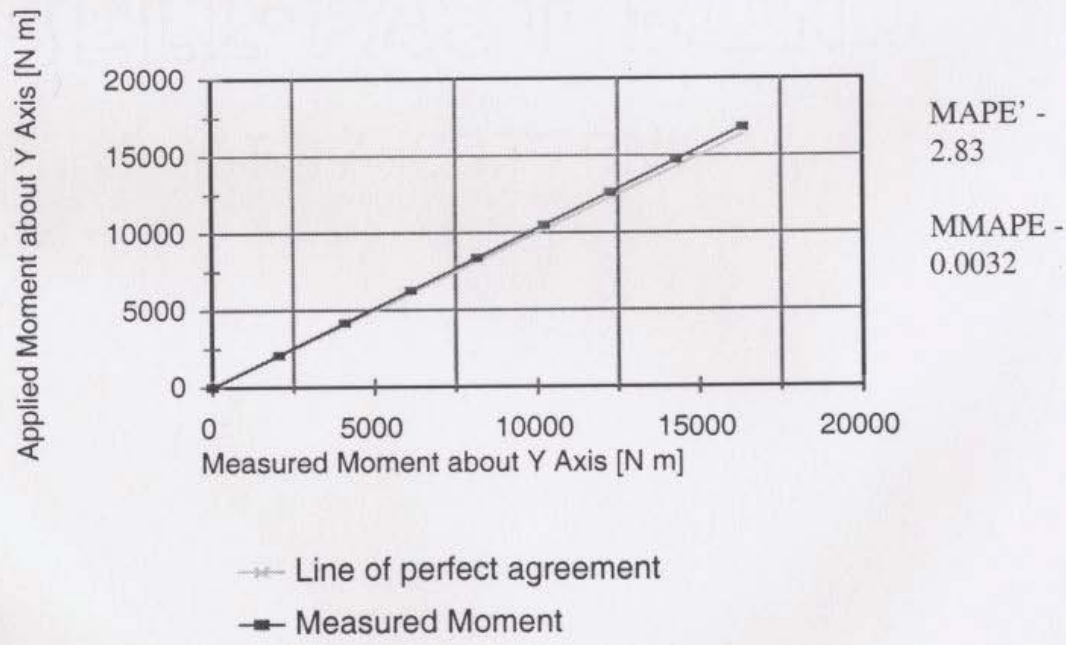

Figure B-100: Comparison of Moments about Y Axis - Orientation 13

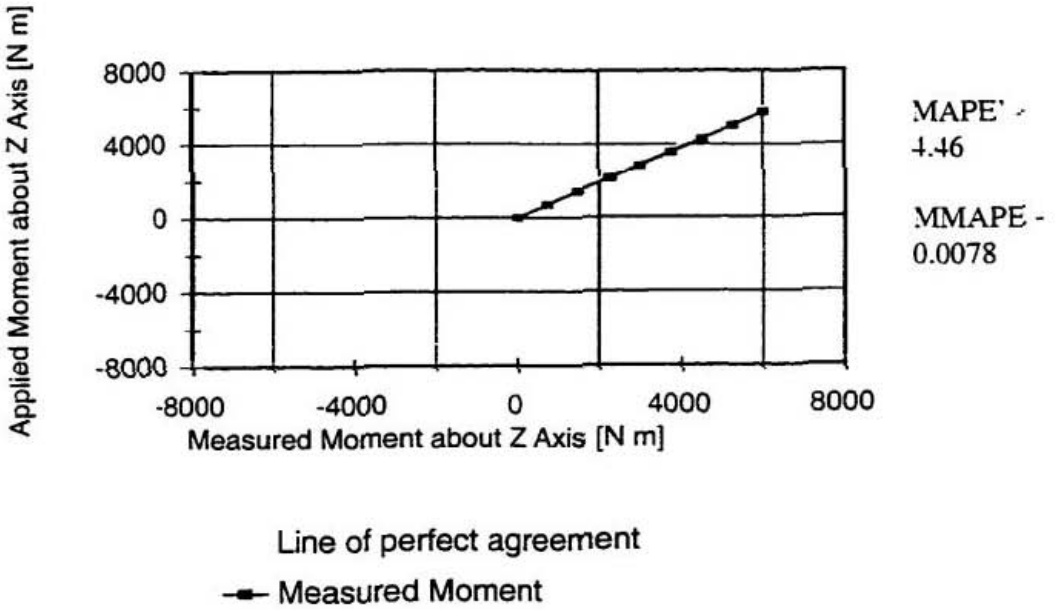

Figure B-101: Comparison of Moments About Z Axis - Orientation 13

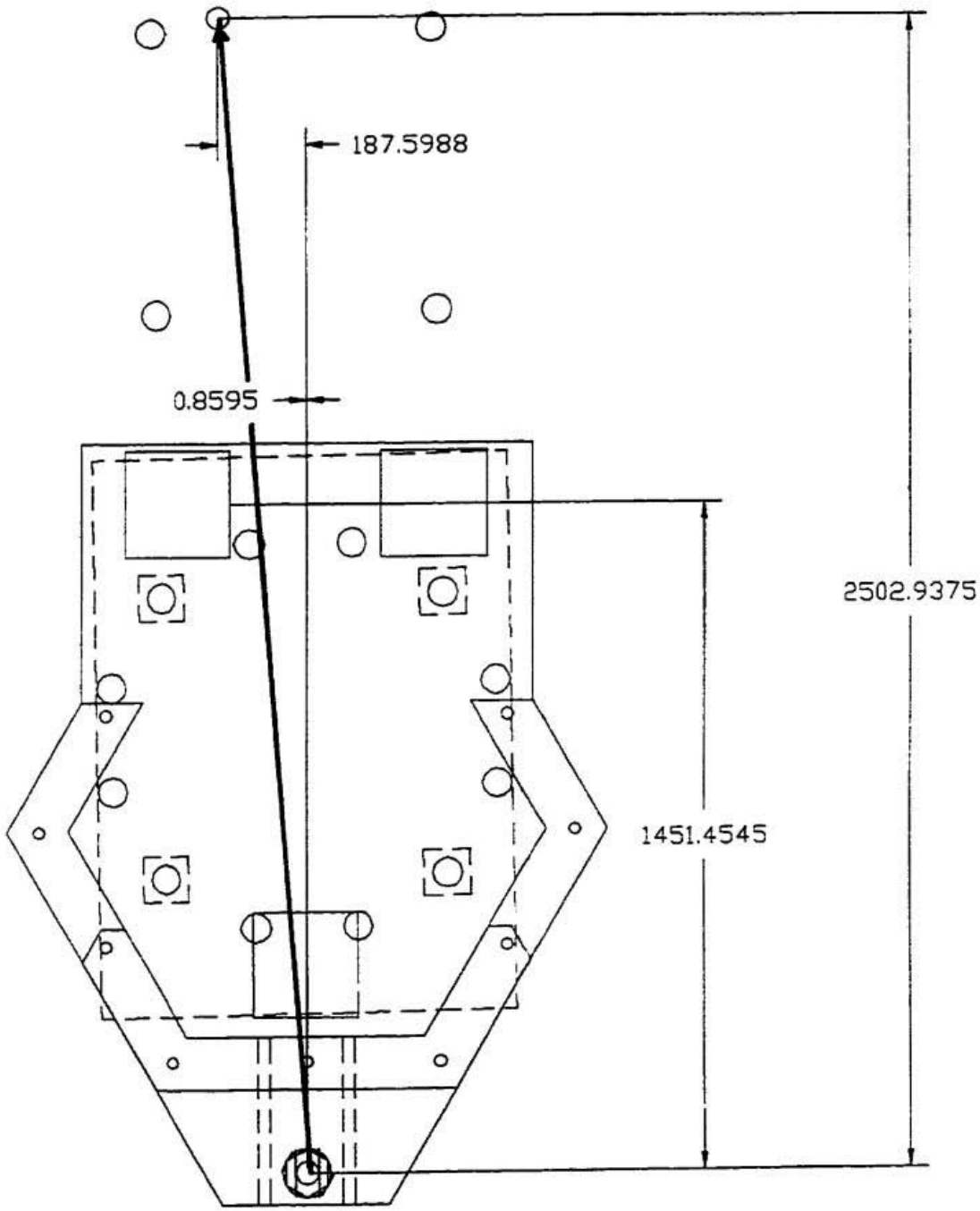

Figure B-102: Direction of Load Application - Orientation 14

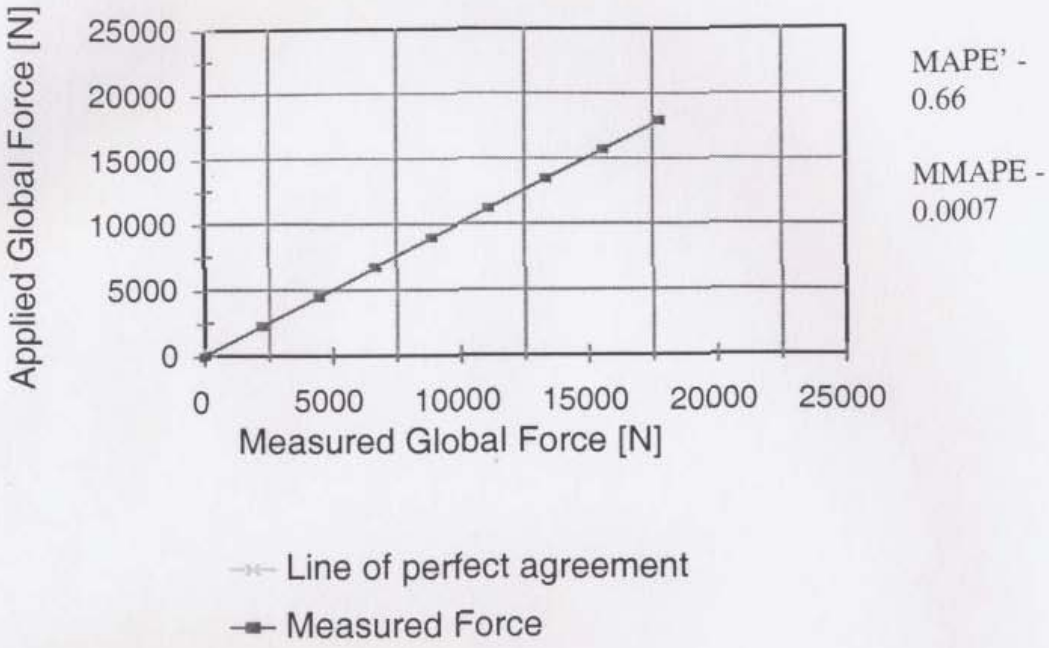

Figure B-103: Global Force Comparison - Orientation 14

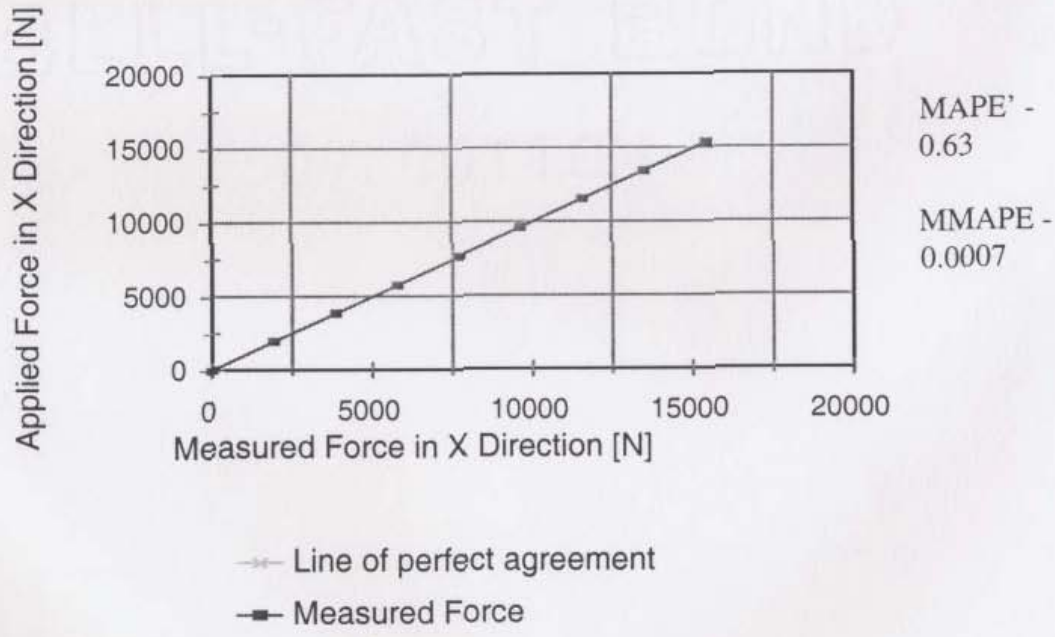

Figure B-104: Comparison of Forces in X Direction - Orientation 14

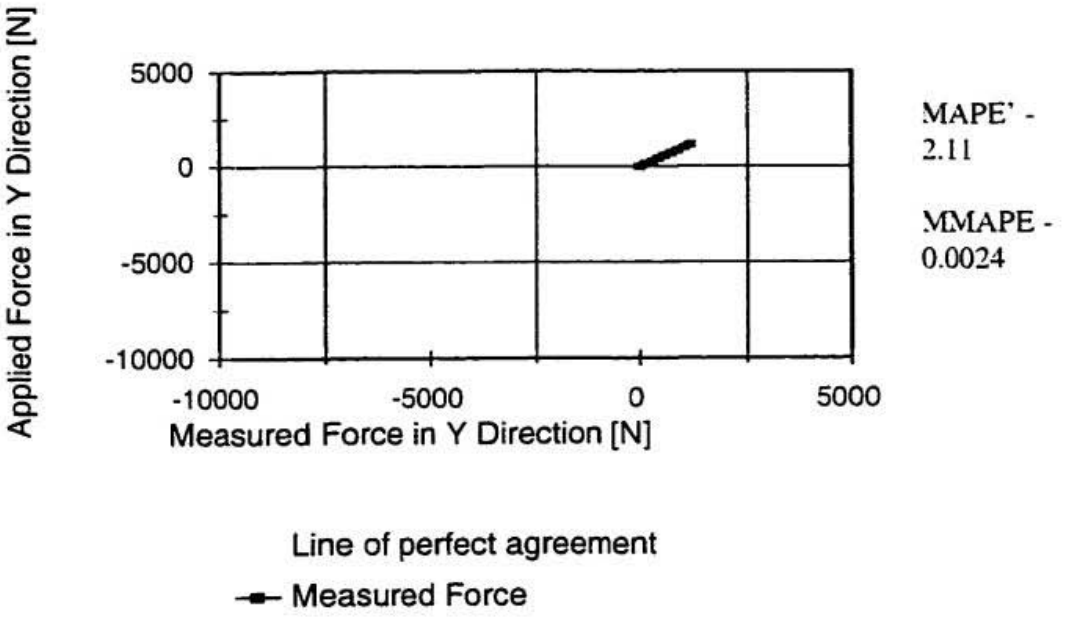

Figure B-105: Comparison of Forces in Y Direction - Orientation 14

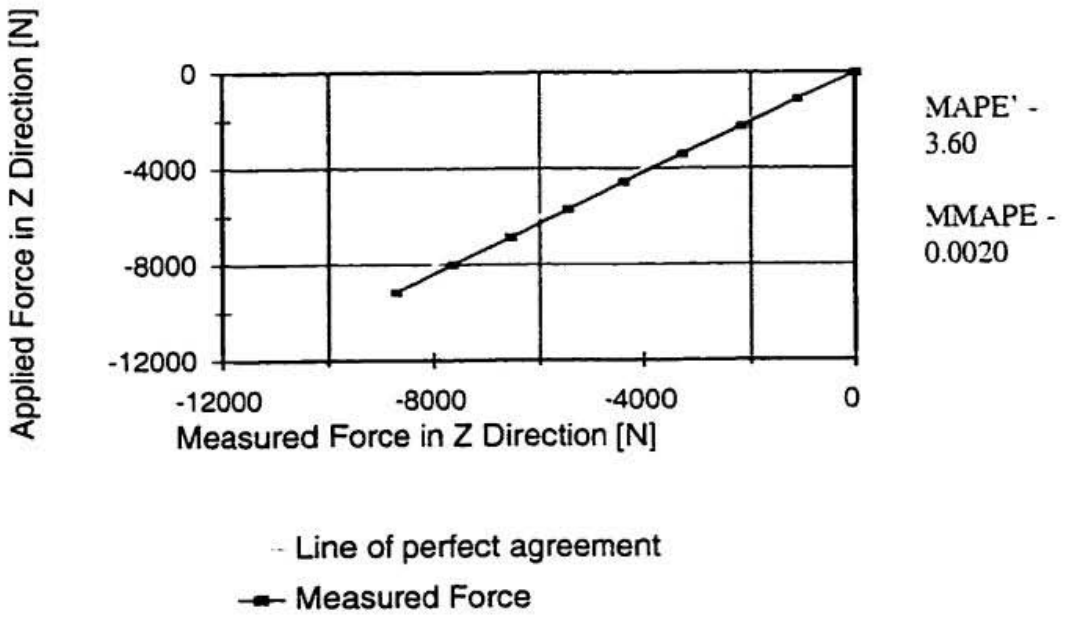

Figure B-106: Comparison of Forces in Z Direction - Orientation 14

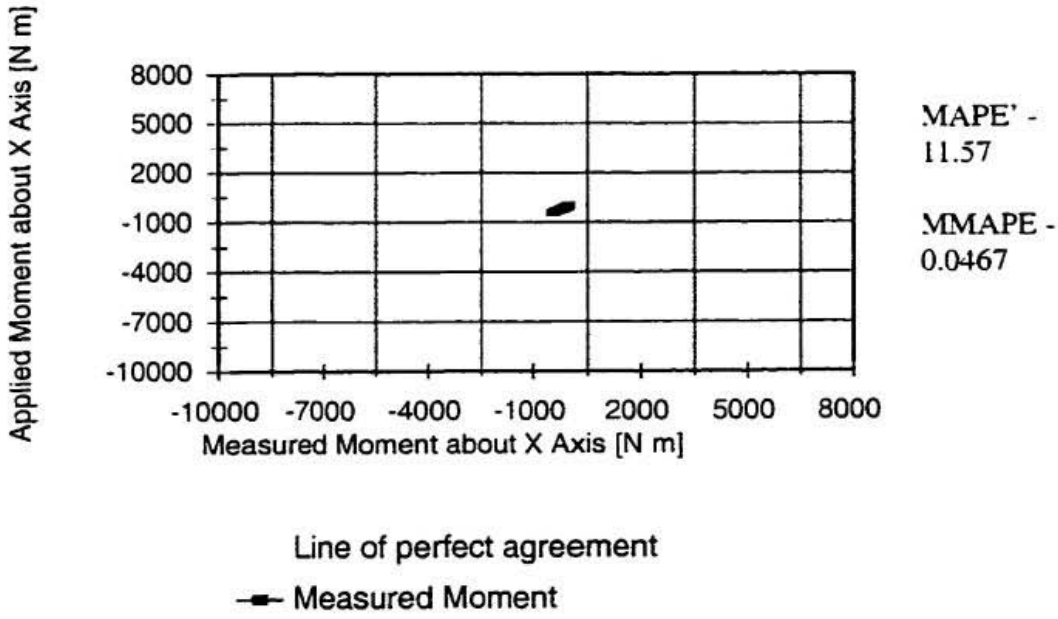

Figure B-107: Comparison of Moments About X Axis - Orientation 14

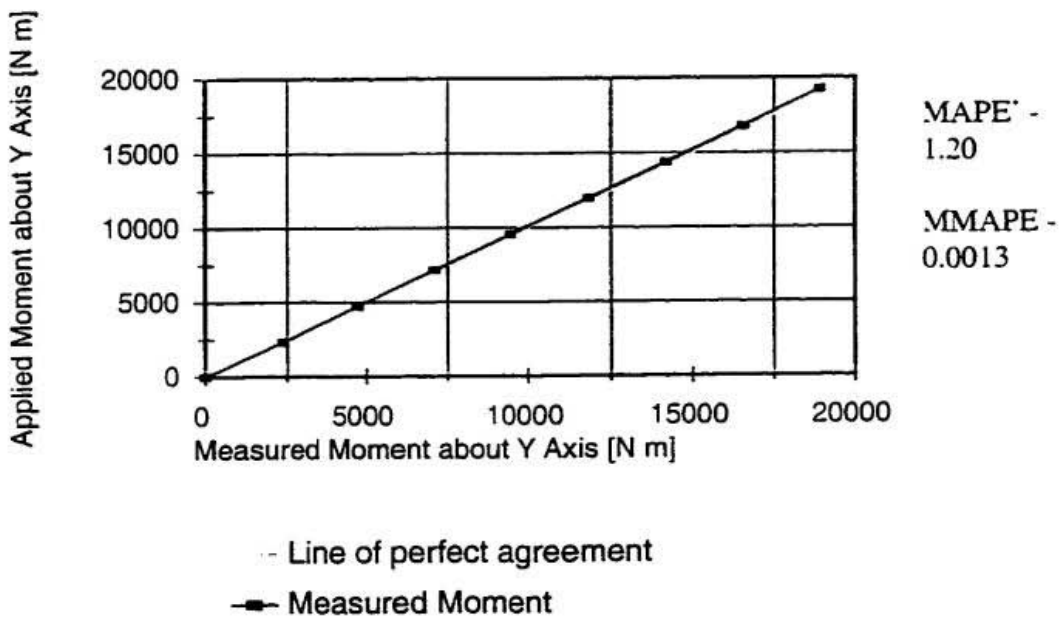

Figure B-108: Comparison of Moments about Y Axis - Orientation 14

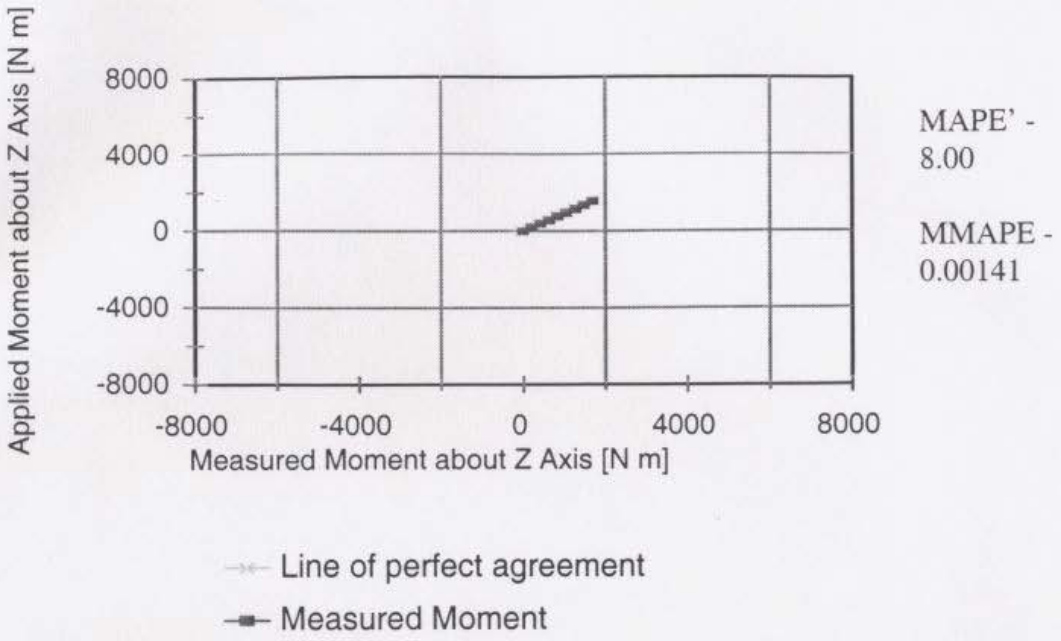

Figure B-109: Comparison of Moments About Z Axis - Orientation 14

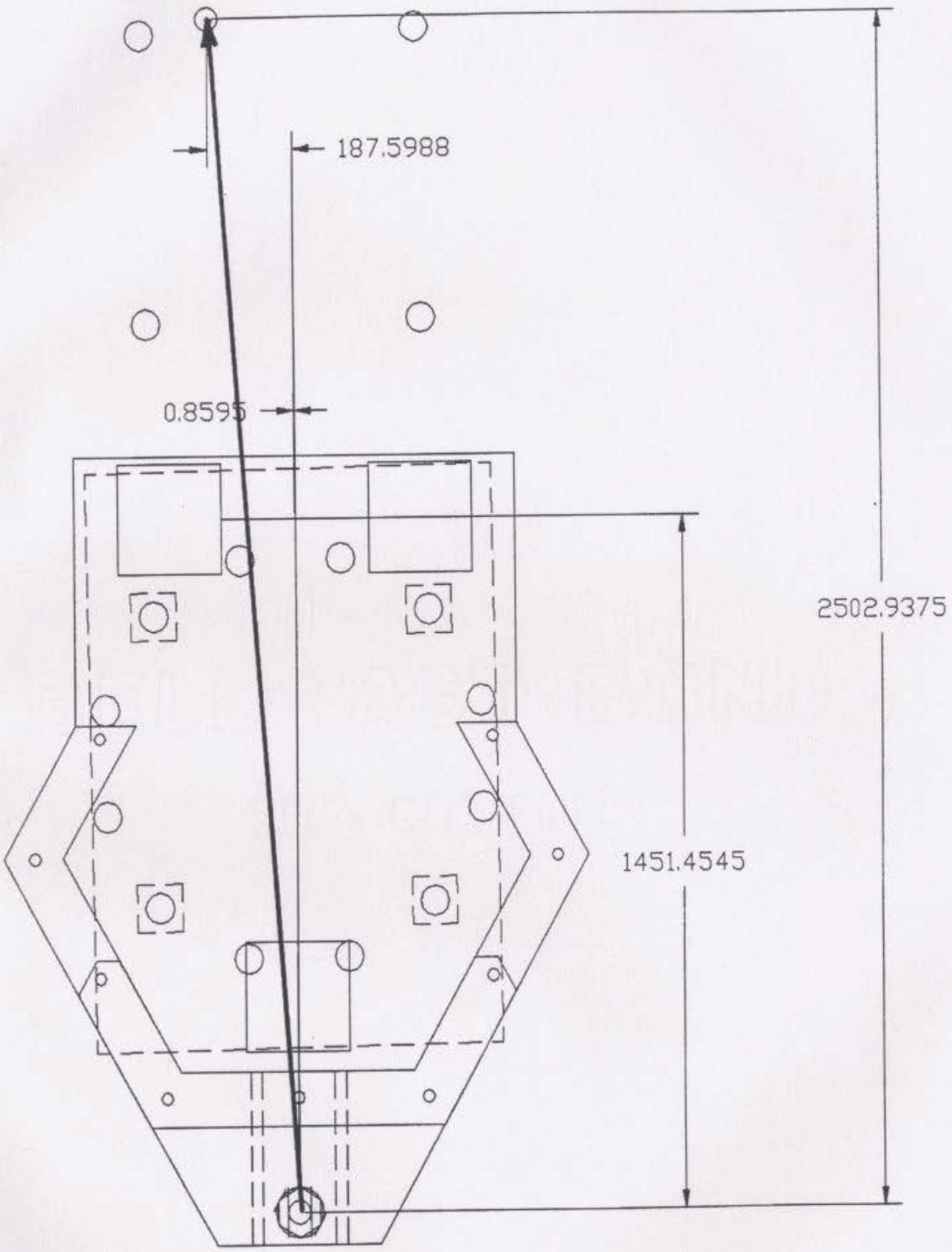

Figure B-110: Direction of Load Application - Ice Test

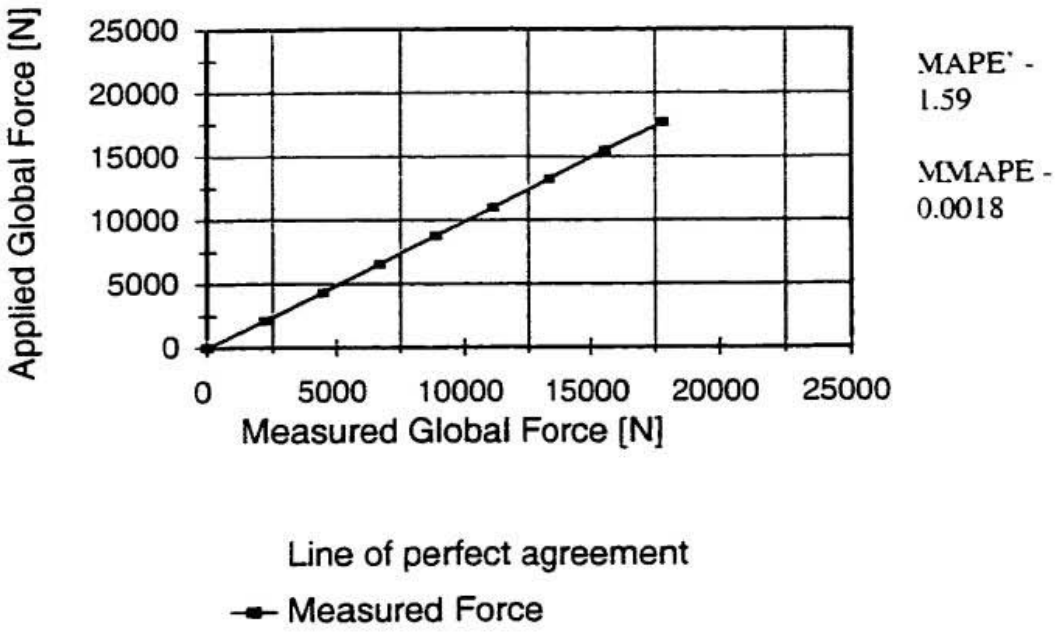

Figure B-111: Global Force Comparison - Ice Test

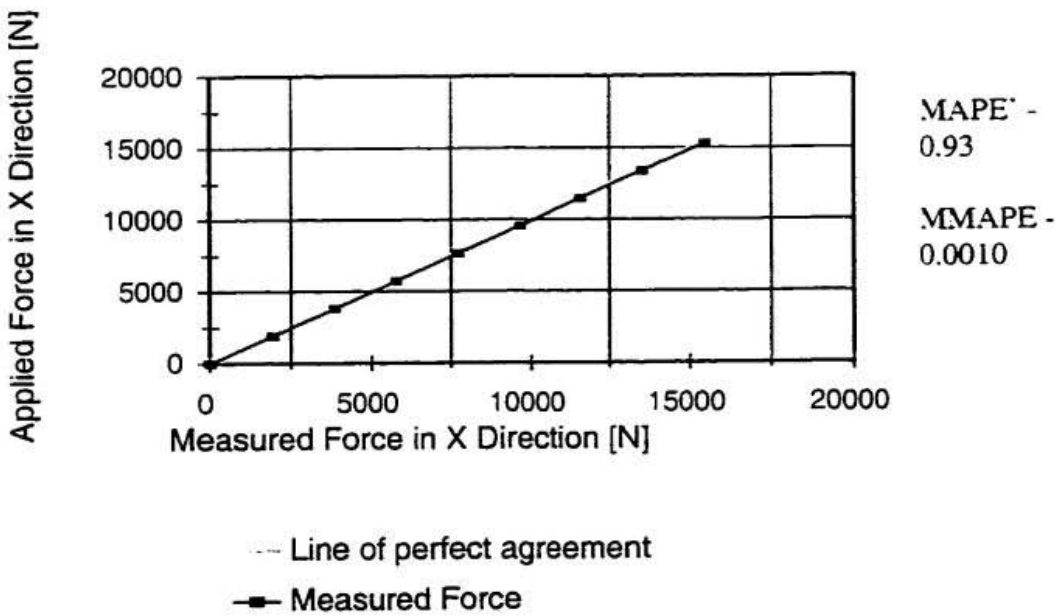

Figure B-112: Comparison of Forces in X Direction - Ice Test

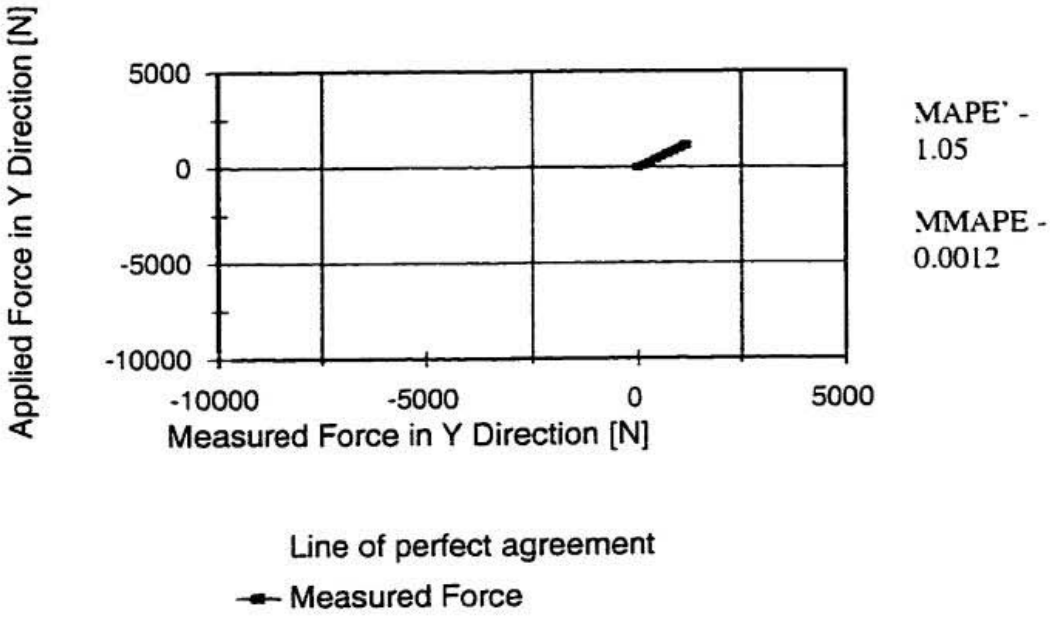

Figure B-113: Comparison of Forces in Y Direction - Ice Test

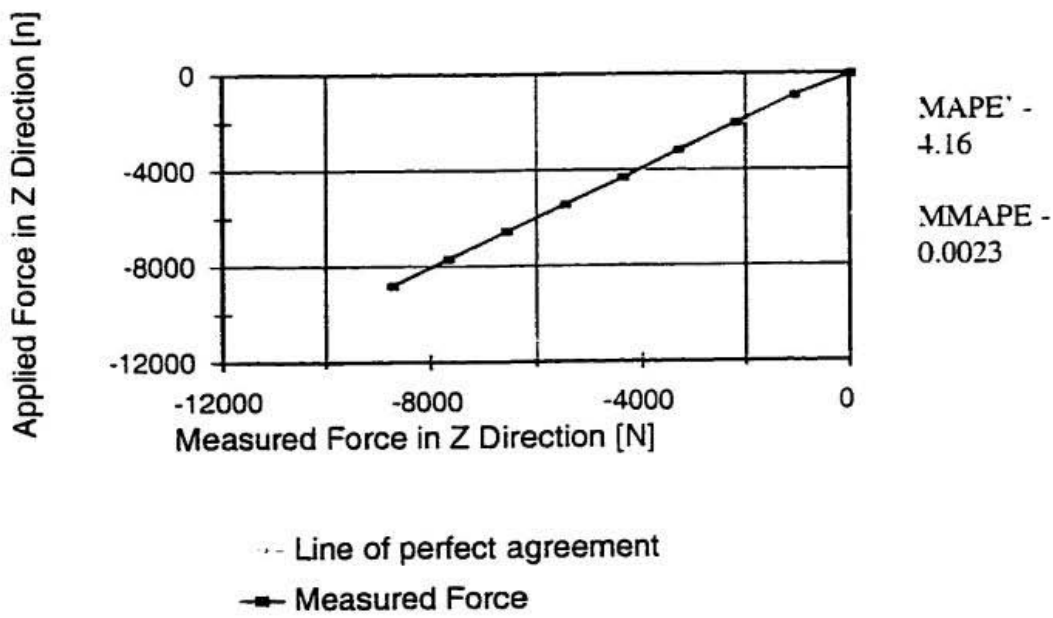

Figure B-114: Comparison of Forces in Z Direction - Ice Test

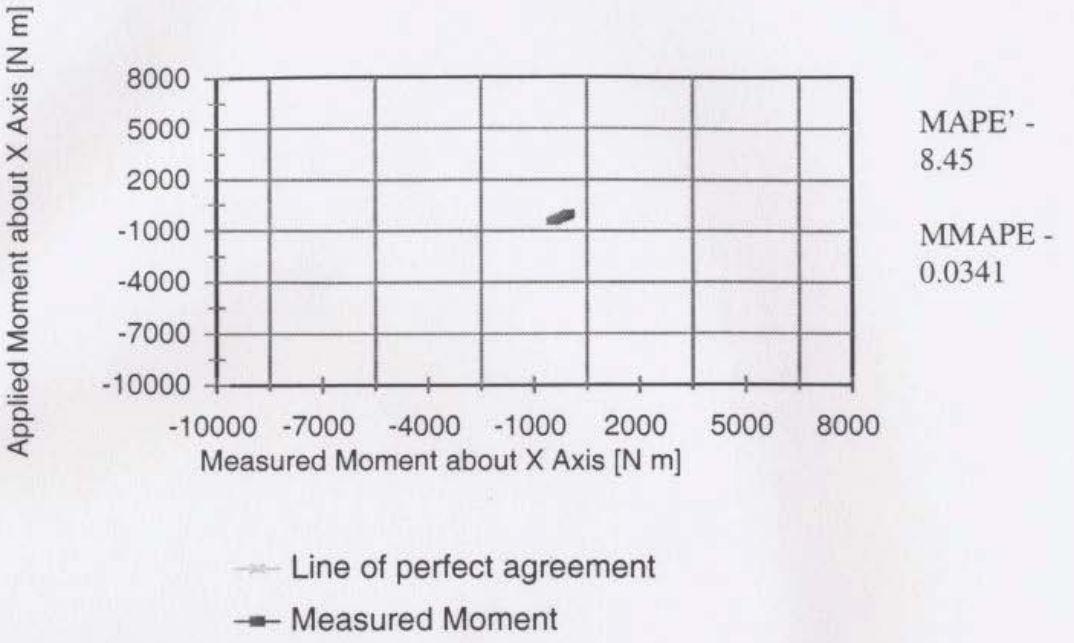

Figure B-115: Comparison of Moments About X Axis - Ice Test

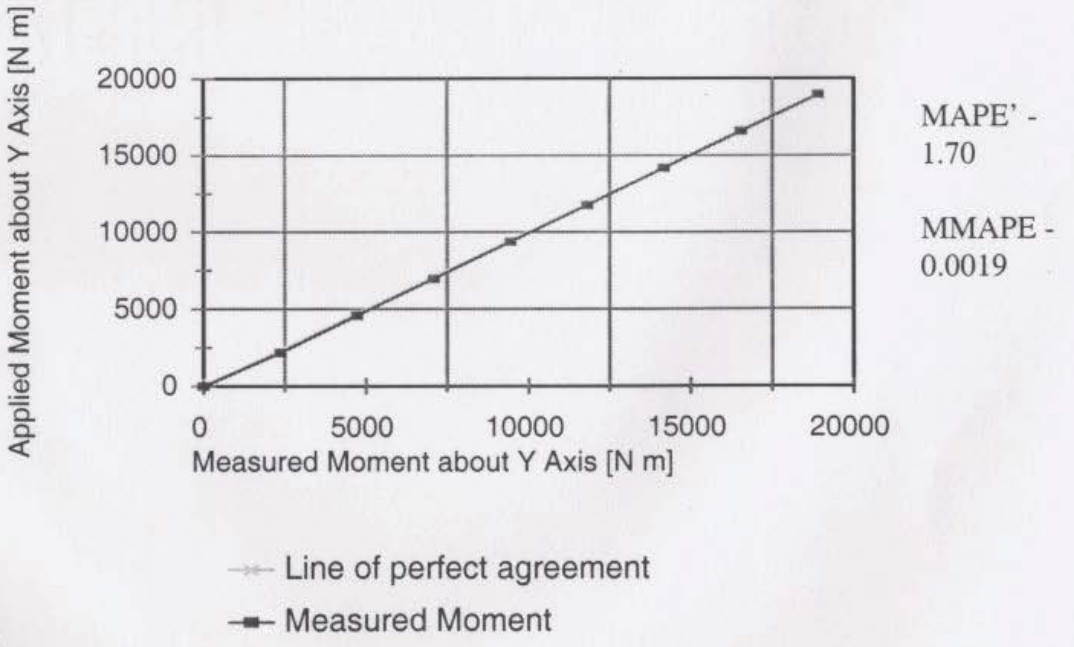

Figure B-116: Comparison of Moments about Y Axis - Ice Test

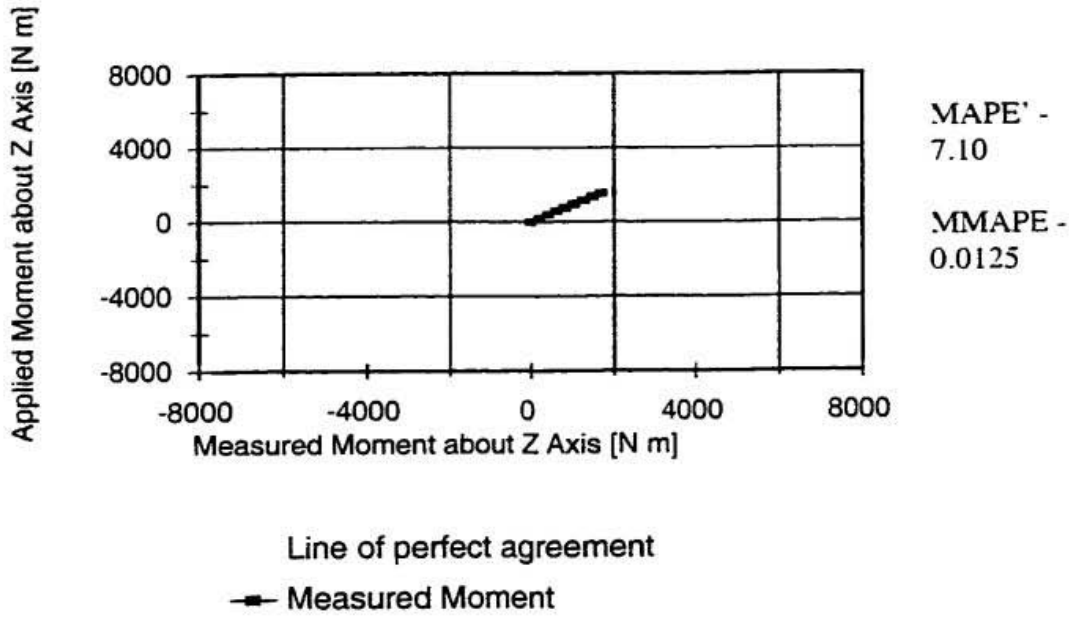

Figure B-117: Comparison of Moments About Z Axis - Ice Test